© Copyright 2019

Diana R. Gergel

Modeling the changing roles of snow and permafrost in mid- and high-latitude climate systems

Diana R. Gergel

A dissertation

submitted in partial fulfillment of the

requirements for the degree of

Doctor of Philosophy

University of Washington

2019

Reading Committee:

Bart Nijssen, Chair

Jessica Lundquist

Martyn P. Clark

Program Authorized to Offer Degree:

Civil and Environmental Engineering

University of Washington

Abstract

Modeling the changing roles of snow and permafrost
in mid- and high-latitude climate systems

Diana R. Gergel

Chair of the Supervisory Committee:
Professor WOT Bart Nijssen
Civil and Environmental Engineering

The land surface plays a key role in local and regional climates at mid- and high-latitudes as well as in the global climate system. Consequently, changes in snow and permafrost affect other parts of the climate system. In this dissertation, we explore the role of the land surface in the cryosphere, with a particular focus on high latitudes, using a hierarchy of standalone land surface models (LSMs), fully-coupled regional climate models (RCMs) and global climate models (GCMs). In Chapter 2, I describe simulated changes in snowpack and fire potential in the western US using the Variable Infiltration Capacity (VIC) hydrology model under future climate projections for an ensemble of GCMs from the Coupled Model Intercomparison Project (CMIP5) archive for two Representative Concentration Pathways (RCPs), RCP4.5 and RCP 8.5. Large losses of snowpack and increases in fire potential are projected to occur in the mountainous parts of the western US in the 21st century, whereas increases in fire potential are much more uncertain in lowland regions due to large uncertainty in precipitation projections.

In Chapter 3, I draw on two modeling ensembles, the Community Earth System Large Ensemble (CESM-LE) and the CESM Low Warming Ensemble (CESM-LWE), to understand projected changes in snow and how these changes will affect soil thermal regimes and permafrost in the 21st century over the circumpolar Arctic for three levels of warming: 1.5°C, 2°C and RCP 8.5. Even for the lower emissions scenarios represented by the 1.5°C and 2°C global-mean warming pathways, the majority of the Arctic is projected to experience significant decreases in Snow Water Equivalent (SWE), while parts of Eurasia will experience substantial increases. Large losses of permafrost are projected due to a significant warming of the soil column by the end of the 21st century. Soil organic carbon (SOC) stocks are highly vulnerable and loss of permafrost could result in potentially large losses of carbon to the atmosphere.

In Chapter 4, I describe the process of designing a new parameter set for application over a pan-Arctic domain in version 5 of the VIC hydrology model (VIC-5) and in the Regional Arctic System Model (RASM), a fully-coupled regional climate model. Simulated streamflow in RASM simulations is significantly higher than in standalone VIC-5 simulations and much more closely matches observations, while simulated permafrost in standalone VIC-5 simulations more closely approximates observed permafrost extent, illustrating the difficulties of designing land surface parameters for application in a land surface model that is used in both standalone and fully-coupled modeling contexts.

TABLE OF CONTENTS

LIST OF FIGURES

LIST OF TABLES

Acknowledgements

First and foremost, I would like to thank my Ph.D. advisor, Dr. Bart Nijssen, for his support, guidance, teaching and mentorship. I have learned so much from him over the past five years and would not have been able to succeed in graduate school without his tireless encouragement. Perhaps the most important thing I have learned from Dr. Nijssen is how to be an ethical scientist, and I plan to make this the foundation of my future work. The Computational Hydrology group has been a bedrock (pun intended) of collegial research support over the past five years and has made it possible for me to develop the skillset I needed for graduate school. In particular, I would like to thank Joe Hamman for being such a supportive colleague at every step of the way and someone I could always look to for advice as I navigated supercomputers, graduate school and ultimately job searching as well. I would like to thank the members of my dissertation committee: Dr. Jessica Lundquist, Dr. Martyn Clark, Dr. Abigail Swann and Dr. Cecilia Bitz for their support and encouragement of my work.

For the past four years of my Ph.D. studies, I have been part of the Regional Arctic System Model (RASM) team, led by Dr. Wieslaw Maslowski (PI), Dr. John Cassano (co-PI), Dr. Bart Nijssen (co-PI), and others. Through our biannual in-person project meetings and frequent discussions, I was able to participate in invaluable conversations about the Arctic climate system and develop my skills as a climate scientist. In particular I would like to thank Dr. Andrew Roberts, a former member of the RASM team and now a scientist at the Los Alamos National Laboratory (LANL), for his support over the years and in my job search. Overall, my experience with the RASM team was formative in my decision to pursue a career in climate science research after graduating and I am extremely grateful to have been part of the team.

Through my participation in the UW Program on Climate Change and work in science communication, I had the privilege to work with a number of scientists in other fields at the UW. Dr. Eric Salathé and Dr. Lisa Hayward Watts (director and communications manager of the former Northwest Climate Science Center, respectively) were always a pleasure to work with and much of what I learned about science communication I owe to them. They provided me with the opportunity to attend several week-long workshops on climate communication that proved invaluable for putting my research in context and figuring out how to better communicate it to other scientists and to the public. The interdisciplinary conversations and retreats that I've been able to be a part of through the UW Program on Climate Change are due to the endless work of Miriam Bertram, who cheered me on at various points and was always keen to hold me to my word, even when I faltered. The UW Program on Climate Change was crucial for me in enabling interactions with scientists working on climate research and/or polar science in other departments and labs.

I would be remiss if I did not thank the professors I had before my Ph.D. studies who encouraged me and supported me in getting to that point. I was fortunate as an undergraduate to have a fantastic research advisor, Dr. Christopher Lee, who would go on to become one of my most important mentors as well as a close friend. My thesis advisor, Dr. Christopher Browning, was also extremely important in my decision to go to graduate school. Later on, once I decided to switch fields from history to computational sciences while a Ph.D. student in history at UC Berkeley, Dr. Wayne Getz and Dr. Zack Powell agreed to let me take their ecological modeling class without me knowing how to code or even knowing what coding really was. They believed in me when I didn't believe in myself and answered my endless questions with patience and kindness. Without them and their class, I might have given up on becoming a scientist.

My friends have been a mainstay for me throughout my time in graduate school, reminding me what really matters and bringing much-needed perspective and humor to my life. I am eternally grateful and cannot thank you all enough. Komal Desai, who has been one of my closest friends since we were suitemates in college my freshman year, has been a rock for me and someone I can always count on no matter what. Jason Pollens has been as well and is always ready with a joke to put things into perspective. Sima Bouzid and I have supported each other through graduate school, job searching and so much more, and I am so grateful to her for being there for me through thick and thin. Irina Erofeeva's deep insights have sustained me, and I've had a reminder of her wise words above my desk for the last year. I am grateful for the friendship I have with Ana Ordonez and Jon Moen, and for their support, perspective and constant snarky humor and stream[flow] of puns. For all other friends whom I haven't mentioned, thank you so much as well.

There are a number of other very important people in my life who have been there for me in all kinds of ways. My sister, Elizabeth Gergel, is always there to lend an ear if things are stressful and to distract me by sharing stories about her professional life in music, which is so far from my own. She has been a key part of my support system and I am so grateful to her for everything over the years. I would like to thank my grandmothers, Meri Gergel and Suzanne Lowenstein, for encouraging me so much along the way. Grandma Meri believed that working hard and getting an education was a ticket out, and she instilled that in me from a young age. And last but definitely not least, I would like to thank my boyfriend, Joe Mash, for being endlessly patient, supportive, and thoughtful. I am grateful to him beyond words for everything that he brings to my life and the maturity with which he has approached my dissertation stress.

His undying enthusiasm is contagious and has been a bastion from long days and weekends of dissertation writing.

Lastly, I have a number of generous funding sources for which I would like to express my gratitude. My graduate school research has been funded in part by the U.S. Department of Energy grants DE-FG02-07ER64460 and DE-SC0006856 to the University of Washington. It was also supported in part by the Regional and Global Model Analysis (RGMA) component of the Earth and Environmental System Modeling (EESM) program of the U.S. Department of Energy's Office of Science, as a contribution to the HiLAT-RASM project. Supercomputing resources, which I have used extensively for my doctoral research, were provided by the Department of Defense (DoD) High Performance Computing Modernization Program at the Air Force Research Laboratory (AFRL), Engineer Research and Development Center (ERDC) and the Navy. For the 2014-2015 academic year, I was fortunate to receive a Valle Fellowship through the Department of Civil and Environmental Engineering at the University of Washington.

Chapter 1

INTRODUCTION

1.1 Background

Terrestrial processes play a key role in the middle and high latitudes as well as in the global climate system. In the western US, snow is the largest source of water storage. Most of the precipitation occurs during the winter and spring months, and in the summer it is either released as streamflow (at higher elevations) or returned to the atmosphere via evapotranspiration (at lower elevations). Consequently, snow is a key driver of the hydrologic cycle in both mountainous and lowland areas (Barnett et al., 2005). In the Arctic, precipitation is the major input flux to the terrestrial freshwater system, much of which falls and is stored as snow. The two major fluxes out of the freshwater system are: 1) evapotranspiration, which is a key link between water and energy cycles and land-atmosphere exchange, and 2) runoff, which is driven by snowmelt and soil moisture and which comprises a key link between terrestrial and ocean processes (Bring et al., 2016). Runoff is the primary freshwater source into the Arctic Ocean, hence it is a significant driver of ocean salinity, sea ice conditions, and even global thermohaline circulation (Serreze et al., 2002). Taken together, the freshwater system is comprised of important feedbacks between terrestrial hydrology, ocean processes, the atmosphere and ecosystem-level dynamics (Hinzman et al., 2013).

However, the mid- and high latitudes are undergoing rapid and unprecedented changes due to climate change. These changes strongly affect the hydrologic cycle and the freshwater budget, which in turn impact the terrestrial carbon cycle, fire potential, global ocean circulation, and future sea level rise. Changes that have already been observed are expected to increase and intensify in the future as temperatures warm and precipitation changes continue in response to rising greenhouse gas emissions in the atmosphere (Lique et al., 2016). Mote et al., (2018) found

declining trends in snowpack at over 90% of snow monitoring sites in the western US, of which 33% were statistically significant. Decreases in snowpack and resultant decreases in soil moisture, in conjunction with warming temperatures, create atmospheric and ground conditions conducive to fire occurrence. Abatzoglou and Williams (2016) showed how forest fire activity nearly doubled since 1984 in the western US. These dramatic changes in the land surface in the western US are projected to continue into the future. Fyfe et al. (2017) used an ensemble of historical and future simulations with CanESM2, a fully-coupled GCM, in conjunction with reanalysis data, to show that continued losses of snowpack are projected, with losses of up to 60% over the next 30 years. Barbero et al. (2015) showed that the potential for very large fires (VLFs) is projected to increase throughout the mountainous western US.

Similarly dramatic changes are projected to occur in the Arctic. Bintanja and Andry (2017) analyzed 37 climate models from the Coupled Model Intercomparison Project, phase 5 (CMIP5; Taylor et al., 2011) and found that rain was projected to become the dominant form of precipitation in the Arctic by the end of the 21st century. In colder parts of the Arctic, such as the Siberian and Eurasian tundra and taiga, snowfall is projected to increase, which has been closely tied to Arctic sea ice loss (Ghatak et al., 2012; Deser et al., 2010). Permafrost is projected to change dramatically, with CMIP5 models projecting a range of possible permafrost losses for the Representative Concentration Pathways (RCPs), representing different levels of increase in radiative forcing. The range of permafrost losses include 2-6% for RCP 2.6, 15-87% for RCP 4.5, and 30-99% for RCP 8.5 (Koven et al., 2012). These permafrost soils are extremely rich in carbon, containing around 1700 Pg, which is nearly double the amount of carbon currently in the atmosphere. Thawing permafrost makes this carbon highly vulnerable to being released into the atmosphere, a phenomenon called the carbon-climate feedback (MacDougall et al., 2012).

To better understand these complex changes in the mid- and high latitudes that are already underway and projected to intensify in the future, a hierarchy of models has been used to represent terrestrial freshwater systems and the climate system as a whole. Studying the cryosphere is challenging due to the scarcity of observations with which to characterize the system, thus models take on particular importance (Lique et al., 2016). Component models of a single part of the earth system, such as the land surface, have often been used to represent the Arctic freshwater system (Lettenmaier and Su, 2012). However, these models do not have a way of representing the land-atmosphere and ocean-atmosphere-land exchanges of water and energy fluxes which are important for understanding the dynamic processes inherent to the climate system. Moreover, allowing for dynamic interactions between earth system components enables feedbacks to occur. Regional and global climate models (RCMs and GCMs, respectively) have been widely used to characterize the nature of these feedbacks, and the Regional Arctic System Model (RASM) was specifically designed for this application in the Arctic (Maslowski et al., 2012).

1.2 Objectives and Research Questions

The overarching goal of this dissertation is to use a hierarchy of models to better understand projected impacts of climate change in the cryosphere in the middle and high latitudes. The second chapter looks at the projected impacts of climate change on snowpack and fire potential in the western United States by using a suite of GCMs from CMIP5 and the Variable Infiltration Capacity (VIC; Liang et al., 1994) hydrologic model. Chapter 3 draws upon two climate model ensembles, the Community Earth System Model Large Ensemble (CESM-LE; Kay et al., 2014) and the CESM Low Warming Ensemble (CESM-LWE; Sanderson et al., 2017),

to understand the mechanistic interactions between changing snowpack and permafrost and their implications for the release of carbon from thawing permafrost by the end of the twenty-first century. Chapter 4 describes the development of a new hydrologic model parameter set for application in the VIC-5 hydrology model, both as a standalone model and as the land surface model component in RASM, and delves into the challenges involved with calibrating parameters in the Arctic and designing a parameter set that performs well in standalone simulations as well as RASM simulations. Chapter 5 describes our overall conclusions as well as recommendations for future research that would extend the work of the third and fourth chapters.

Overall, the chapters are intended to answer the following overarching questions:

1) How will climate change impact the cryosphere in the middle and high latitudes over the course of the twenty-first century? In particular, how will projected changes in temperature and precipitation reinforce or counter each other?
2) What is the role of the land surface in the coupled climate system?
3) How can we use a hierarchy of models – land surface models, regional climate models and global climate models – to advance our understanding of the coupled interactions between components in the Arctic climate system?
4) How should land surface model parameters be designed – specifically VIC-5 parameters – for application in both standalone modeling as well as fully-coupled modeling with the Regional Arctic System Model (RASM) and what are the modeling tradeoffs involved?

Several important themes undergird and link the three chapters. Firstly, in the three core chapters of this work, I use a hierarchy of different models with differing levels of complexity and geographical scope and compare to available observations when available. The usage of

different kinds of models is intended to shed light on how models are crucial tools in answering scientific questions relating to the effects of climate change on terrestrial hydrology. It is also intended to reveal differences in land surface modeling with standalone models versus fully-coupled climate models, which is the focus of Chapter 4. A key theme undergirding chapters 2-3 is the balance between warming temperatures and changes in precipitation which characterize current and future climate change. Earlier work on climate change impacts on precipitation pointed to a "wet gets wetter, dry gets drier" paradigm (e.g. Held & Soden, 2006), but since then that paradigm has been brought into question. My second chapter differentiates between lowland and upland regions in the western US and shows the extent to which temperatures increase and precipitation changes – and the balance between the two – leads to either increases or decreases in fire potential. In my third chapter, a conceptually similar pattern plays out in understanding how changes in snow impact soil thermal regimes. In areas where snowfall increases but temperatures increase relatively less, permafrost is relatively less affected, as increased snowpack serves as an insulator. In areas where temperatures increase more relative to colder parts of the domain and precipitation increases but falls as rain, the soil thermal regime shifts dramatically.

1.3 References

Abatzoglou, J. T., & Williams, A. P. (2016). Impact of anthropogenic climate change on wildfire across western US forests. *Proceedings of the National Academy of Sciences*, *113*(42), 11770–11775. https://doi.org/10.1073/pnas.1607171113

Barbero, R., Abatzoglou, J. T., Larkin, N. K., Kolden, C. A., & Stocks, B. (2015). Climate change presents increased potential for very large fires in the contiguous United States.

International Journal of Wildland Fire, *24*(7), 892–899. https://doi.org/10.1071/WF15083

Barnett, T. P., Adam, J. C., & Lettenmaier, D. P. (2005). Potential impacts of a warming climate on water availability in snow-dominated regions. *Nature*, *438*(7066), 303–309. https://doi.org/10.1038/nature04141

Bintanja, R., & Andry, O. (2017). Towards a rain-dominated Arctic. *Nature Climate Change*, *7*(4), 263–267. https://doi.org/10.1038/nclimate3240

Bring, A., Fedorova, I., Dibike, Y., Hinzman, L., Mård, J., Mernild, S. H., … Woo, M.-K. (2016). Arctic terrestrial hydrology: A synthesis of processes, regional effects, and research challenges. *Journal of Geophysical Research: Biogeosciences*, *121*(3), 621–649. https://doi.org/10.1002/2015JG003131

Deser, C., Tomas, R., Alexander, M., & Lawrence, D. (2010). The Seasonal Atmospheric Response to Projected Arctic Sea Ice Loss in the Late Twenty-First Century. *Journal of Climate*, *23*(2), 333–351. https://doi.org/10.1175/2009JCLI3053.1

Fyfe, J. C., Derksen, C., Mudryk, L., Flato, G. M., Santer, B. D., Swart, N. C., … Jiao, Y. (2017). Large near-term projected snowpack loss over the western United States. *Nature Communications*, *8*(1), 1–7. https://doi.org/10.1038/ncomms14996

Ghatak, D., Deser, C., Frei, A., Gong, G., Phillips, A., Robinson, D. A., & Stroeve, J. (2012). Simulated Siberian snow cover response to observed Arctic sea ice loss, 1979–2008. *Journal of Geophysical Research: Atmospheres*, *117*(D23). https://doi.org/10.1029/2012JD018047

Held, I. M., & Soden, B. J. (2006). Robust Responses of the Hydrological Cycle to Global Warming. *Journal of Climate*, *19*(21), 5686–5699. https://doi.org/10.1175/JCLI3990.1

Hinzman, L. D., Deal, C. J., McGuire, A. D., Mernild, S. H., Polyakov, I. V., & Walsh, J. E. (2013). Trajectory of the Arctic as an integrated system. *Ecological Applications*, *23*(8), 1837–1868. https://doi.org/10.1890/11-1498.1

Kay, J. E., Deser, C., Phillips, A., Mai, A., Hannay, C., Strand, G., … Vertenstein, M. (2014). The Community Earth System Model (CESM) Large Ensemble Project: A Community Resource for Studying Climate Change in the Presence of Internal Climate Variability. *Bulletin of the American Meteorological Society*, *96*(8), 1333–1349. https://doi.org/10.1175/BAMS-D-13-00255.1

Koven, C. D., Riley, W. J., & Stern, A. (2012). Analysis of Permafrost Thermal Dynamics and Response to Climate Change in the CMIP5 Earth System Models. *Journal of Climate*, *26*(6), 1877–1900. https://doi.org/10.1175/JCLI-D-12-00228.1

Lettenmaier, D. P., & Su, F. (2012). Progress in Hydrological Modeling over High Latitudes: Under Arctic Climate System Study (ACSYS). In P. Lemke & H.-W. Jacobi (Eds.), *Arctic Climate Change: The ACSYS Decade and Beyond* (pp. 357–380). https://doi.org/10.1007/978-94-007-2027-5_9

Liang, X., Lettenmaier, D. P., Wood, E. F., & Burges, S. J. (1994). A simple hydrologically based model of land surface water and energy fluxes for general circulation models. *Journal of Geophysical Research: Atmospheres*, *99*(D7), 14415–14428. https://doi.org/10.1029/94JD00483

Lique, C., Holland, M. M., Dibike, Y. B., Lawrence, D. M., & Screen, J. A. (2016). Modeling the Arctic freshwater system and its integration in the global system: Lessons learned and future challenges. *Journal of Geophysical Research: Biogeosciences*, *121*(3), 540–566. https://doi.org/10.1002/2015JG003120

MacDougall, A. H., Avis, C. A., & Weaver, A. J. (2012). Significant contribution to climate warming from the permafrost carbon feedback. *Nature Geoscience*, *5*(10), 719–721. https://doi.org/10.1038/ngeo1573

Maslowski, W., Clement Kinney, J., Higgins, M., & Roberts, A. (2012). The Future of Arctic Sea Ice. *Annual Review of Earth and Planetary Sciences*, *40*(1), 625–654. https://doi.org/10.1146/annurev-earth-042711-105345

Mote, P. W., Li, S., Lettenmaier, D. P., Xiao, M., & Engel, R. (2018). Dramatic declines in snowpack in the western US. *Npj Climate and Atmospheric Science*, *1*(1), 1–6. https://doi.org/10.1038/s41612-018-0012-1

Sanderson, B. M., Xu, Y., Tebaldi, C., Wehner, M., O'Neill, B. C., Jahn, A., … Lamarque, J. F. (2017). Community climate simulations to assess avoided impacts in 1.5 and 2°C futures. *Earth System Dynamics*, *8*(3), 827–847. https://doi.org/10.3929/ethz-b-000191578

Serreze, M. C., Bromwich, D. H., Clark, M. P., Etringer, A. J., Zhang, T., & Lammers, R. (2002). Large-scale hydro-climatology of the terrestrial Arctic drainage system. *Journal of Geophysical Research: Atmospheres*, *107*(D2), ALT 1-1-ALT 1-28. https://doi.org/10.1029/2001JD000919

Taylor, K. E., Stouffer, R. J., & Meehl, G. A. (2011). An Overview of CMIP5 and the Experiment Design. *Bulletin of the American Meteorological Society*, *93*(4), 485–498. https://doi.org/10.1175/BAMS-D-11-00094.1

Chapter 2

EFFECTS OF CLIMATE CHANGE ON SNOWPACK AND FIRE POTENTIAL IN THE WESTERN USA

This chapter has been published in its current form in the journal *Climatic Change.* Used with permission. The supplemental material for this chapter is provided in appendix A.

D.R. Gergel, B. Nijssen, J. T. Abatzoglou, D.P. Lettenmaier, M.R. Stumbaugh (2017) Effects of climate change on snowpack and fire potential in the western USA. *Climatic Change* 141: 287-299, doi: 10.1007/s10584-017-1899-y.

Abstract

We evaluate the implications of ten twenty-first century climate scenarios for snow, soil moisture, and fuel moisture across the conterminous western USA using the Variable Infiltration Capacity (VIC) hydrology model. A decline in mountain snowpack, an advance in the timing of spring melt, and a reduction in snow season are projected for five mountain ranges in the region. For the southernmost range (the White Mountains), spring snow at most elevations will disappear by the end of the twenty-first century. We investigate soil and fuel moisture changes for the five mountain ranges and for six lowland regions. The accelerated depletion of mountain snowpack due to warming leads to reduced summer soil moisture across mountain environments. Similarly, warmer and drier summers lead to decreases of up to 25% in dead fuel moisture across all mountain ranges. Collective declines in spring mountain snowpack, summer soil moisture, and fuel moisture across western mountain ranges will increase fire potential in flammability-limited forested systems where fuels are not limiting. Projected changes in fire potential in predominately fuel-limited systems at lower elevations are more uncertain given the confounding signals between projected changes in soil moisture and fuel moisture.

2.1 Introduction

In the western US, snow is the primary source of water storage (Cayan, 1996). Most of the annual precipitation occurs during the cool season and is returned to the atmosphere in the spring and early summer through evapotranspiration, except at the highest elevations and northern coastal areas, where it is predominantly released as runoff and streamflow (Barnett et al., 2005). This annual cycle makes the region particularly vulnerable to changes in climate, which alter the timing and duration of the snow season, and subsequent water availability throughout the dry summer months. Widespread declines in April 1 snow water equivalent (SWE) have been seen at snow course sites across mountains of the western USA over the past 50 years (e.g. Mote, 2006); Hamlet et al., 2005). Declines in snowpack were more pronounced in temperate ranges than the colder, interior ranges, suggesting that the loss in spring snowpack was a result of warming temperatures (Mote et al., 2005). Spring runoff in snowmelt-dominated rivers in the western USA has shifted earlier by 1 to 3 weeks over the past 50 years, which has been attributed to warming temperatures (Stewart et al., 2005) and to decreased mountain precipitation (Kormos et al., 2016).

Projected changes in climate unanimously show continued and accelerated increases in temperature across the western USA through the twenty-first century (Sillmann et al., 2013). Regional changes in precipitation, by contrast, are more uncertain and differ substantially (even by sign) among global climate models (Kharin et al., 2013). Luce et al. (2013) suggested that declines in streamflow in the northwestern USA since 1950 could be attributed to declines in orographic precipitation associated with a reduction in the strength of lower-tropospheric winter westerlies. Lute et al. (2015) found that annual snowfall water equivalent was projected to

decline across the western USA by the mid-twenty-first century and that low-snowfall years would become more frequent.

Stewart et al (2004) among others (e.g. Wood et al., 2004; Lundquist & Flint, 2006) have projected that spring runoff timing could shift earlier by more than a month by the end of the twenty-first century, which has strong implications for summer soil moisture. Soil moisture integrates non-linear impacts of temperature, precipitation, vapor pressure deficit, and wind into the moisture content of vegetation and thus may be a proxy for vegetation and duff dryness, making it an important indicator of ecosystem function (e.g., Littell et al., 2008) and of fire potential in flammability-limited forested regimes. Higuera et al. (2015) showed that summer soil moisture explained over 60% of interannual variability in area burned across the Northern Rocky Mountains. Fluctuations in winter snowpack can have a strong impact on the occurrence of large fires (Westerling et al., 2006) in the western USA, as spring snowpack influences soil moisture in the subsequent summer. Similarly, fuel moisture is an important proxy for potential ignition and fire spread and strongly correlates with the amount of area burned (Flannigan et al., 2005; Abatzoglou and Kolden, 2013).

The frequency of large fires and area burned in wildland fires over the western USA have increased markedly over the past several decades (Westerling et al., 2006; Dennison et al., 2014; Littell et al., 2009). These trends are projected to continue, with widespread increases in large fire frequency (Westerling et al., 2011a; Stavros et al., 2014) and area burned (Westerling et al., 2011b; Littell et al., 2010; Turner et al., 2017). Although projected changes in wildfire activity across the western USA have been estimated using contemporary climate-fire relationships, it is likely that contemporary climate-fire relationships may be non-stationary under a changing climate (McKenzie & Littell, 2017). Past studies (e.g., Littell et al., 2009; Littell and Gwozdz,

2011; Abatzoglou & Kolden, 2013) have defined two general climate-fire regimes that are applicable to the western USA. Wildfires in primarily lower-elevation rangelands are associated with years of higher fuel abundance that result from increased moisture availability, while wildfires in primarily higher-elevation forested areas are associated with moisture deficits that result in increased fuel aridity (Abatzoglou & Kolden, 2013). A long history of fire suppression across parts of the western USA complicates these climate-fire relationships. Despite historical differences in fire suppression and different climate-fire relationships, prior studies have not distinguished between projected changes in fire potential between upland and lowland areas over a domain as large as the western USA.

In this study, our objective is to understand how future changes in climate will affect snowpack, soil moisture, and fuel moisture in upland and lowland regions of the western USA. We focus on the links between hydrologic changes in snowpack and soil moisture, associated both with changing snow processes in the uplands and precipitation changes in the lowlands, and changes in fuel moisture. We also evaluate their combined implications for summer aridity and fire potential. Using an ensemble of ten GCMs allows us to evaluate a broader range of possible outcomes and highlight where projections are consistent (or not) among models. Our intention is not to model changes in fire activity (e.g., burned area, fire frequency), but rather to examine projected changes in fuel aridity metrics that are proximate drivers of interannual variability in fire activity across parts of the region (e.g., Higuera et al., 2015). By the term fire potential, we mean the potential for fire to occur. The vulnerability components of fire risk are beyond the scope of our study.

2.2 Approach

2.2.1 Domain

Our domain consists of five mountain regions and six lowland regions in the western USA. The mountain ranges include the Sierra Nevada mountains, Cascades, Northern and Southern Rockies, and White Mountains (Fig. 2.1). The lowland regions consist of the Great Basin, Coastal North, Coastal South, Northwest Interior, Missouri, and Lower Colorado (Fig. 2.1). The Missouri, Lower Colorado, and Great Basin regions are defined by USGS Hydrologic Unit Code (HUC) 02 boundaries (Watershed Boundary Dataset for HUC-02s 2015). For Missouri HUC-02, only the area west of 103° is included. The mountain regions were defined as consisting of the 1/16° latitude-longitude grid cells for which the historical (1970–1999) model-simulated mean April 1 SWE exceeded 10 mm.

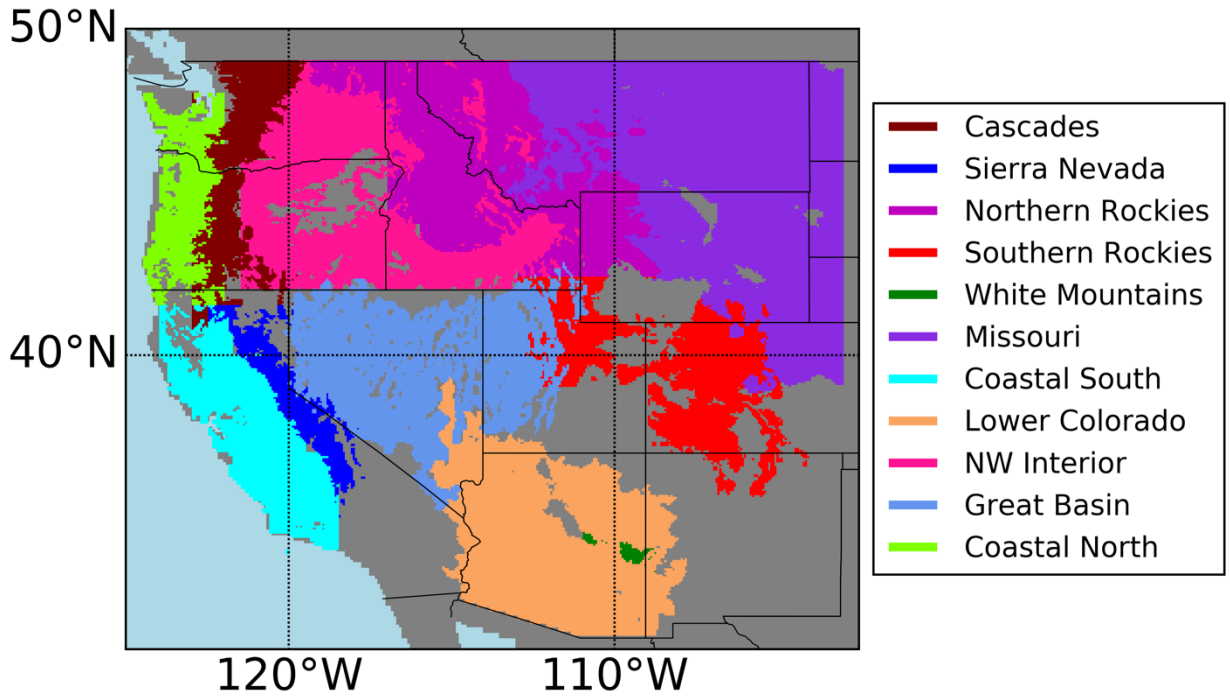

Figure 2.1. Map of mountain ranges and lowlands in the western US included in this study.

2.2.2 Climate forcing datasets and downscaling

We used meteorological inputs from Livneh et al. (2013) for historical Variable Infiltration Capacity (VIC) model simulations, which we compared to SNOTEL observations (Figure A3.1) and which were also used to define the April 1 SWE threshold for mountain ranges. Our comparison to SNOTEL observations served as a validation for modeled SWE (see Figure A3.1 and Appendix A). Hydrologic simulations were driven by precipitation, maximum and minimum temperature, and wind speed outputs downscaled using the Multivariate Adaptive Constructive Analogues (MACA) statistical downscaling approach (Abatzoglou and Brown 2012). Meteorological inputs used as the training dataset for the MACA downscaling were taken from Livneh et al. (2013) from 1950 to 2011. We used ten GCMs (Table A3.1), selected from the Coupled Model Intercomparison Project 5 (CMIP5) archive (Taylor et al., 2011) based on their ability to simulate the historical climate in the western USA (Rupp et al., 2013). For each GCM, we used downscaled climate taken from the control forcing (1960–2005) and future forcing (2006–2099) experiments, with the latter including both Representative Concentration Pathways (RCPs) 4.5 and 8.5.

Since Livneh et al. (2013) used a standard lapse rate of −6.5 °C/km over the western USA, this may have introduced biases into our meteorological forcings, particularly over topographically complex regions that have heterogeneous lapse rates, such as on the windward side of the Cascades (Minder et al., 2010), which can significantly impact hydrologic modeling (Mizukami et al., 2013). Behnke et al. (2016) showed, however, that Livneh et al. (2013) is one of the better-performing gridded climate datasets over the contiguous USA (CONUS), despite the lapse rate assumption. While the choice of downscaling approach adds an additional layer of uncertainty (Gutmann et al. 2014), Mizukami et al. (2015) found that the choice of downscaling

method resulted in less variability than the choice of hydrologic model. Thus, we expect that the inter-model variation between GCMs in our study is much larger than the spread that would have resulted from using multiple downscaling methods. However, dynamical downscaling methods, in contrast to the statistical downscaling that was used in this study, might have yielded different results.

2.2.3 Hydrological modeling

The VIC model (Liang et al., 1994) Version 4.1.2.l was run in energy balance mode at a 1/16° spatial resolution and a 3-hour time step over the western USA. Model spin-up was accomplished by running the model with gridded historical inputs from Livneh et al. (2013) for 1950–1959 for all simulations for the control period and with 1995–2005 downscaled output from each GCM (and each scenario) for the future runs. Hydrological fluxes and states were then archived at a daily time step. VIC model parameters were taken from Livneh et al. (2013) and were calibrated to observed and/or naturalized flows in Livneh et al. (2013) for multiple large river basins across the western USA. The VIC model output, as well as the MACA-downscaled GCMs, is archived at the University of Idaho Applied Climate Science Lab at http://climate.nkn.uidaho.edu/IntegratedScenarios/ (Northwest Knowledge Network) and is publicly available.

2.2.4 Fuel moisture modeling

The US National Fire Danger Rating system (NFDRS) estimates dead fuel moisture (DFM) for different sized fuel classes (Cohen and Deeming, 1985). We computed 100 and 1000-hour DFM using regression equations for equilibrium moisture content (EMC) developed by

Simard (1968) and used by the NFDRS (Cohen and Deeming 1985; see Appendix A). The 100 and 1000-h DFM correspond to the timescale of exponential decay of DFM with respect to the EMC, with 1000-h fuel representative of larger-diameter fuels that respond more slowly to fluctuations in EMC than 100-h fuels.

2.2.5 Analysis periods

We partitioned the control and future simulations into four 30-year periods: historical (1970– 1999), 2020s (2010–2039), 2050s (2040–2069), and 2080s (2070–2099). We used these periods throughout our study to evaluate projected hydrologic changes during the twenty-first century. We also examined transient changes during the twenty-first century. Climate change results were calculated by comparing future GCM simulations with the control simulation from the same GCM.

2.3 Results

2.3.1 Temperature and precipitation projections

Average winter (November–March) temperature increases in all mountain ranges throughout the twenty-first century (Table A3.2). Warming rates are generally larger over continental areas than maritime areas. For RCP 8.5, temperature increases exceed +4 °C by the 2080s and exceed +5 °C in the Northern and Southern Rockies. The Southern Cascades exhibit the least warming of the five mountain ranges, but still experience an increase of nearly +4 °C in the 2080s.

For most of the mountain ranges and lowland regions, the ensemble mean total winter precipitation increases up to 30% by the 2080s, with the exception of the White Mountains in

Arizona and the Lower Colorado, which are projected to experience reductions in winter precipitation in the ensemble mean (Figure A3.2). The southern part of the Lower Colorado basin, in particular, shows a reduction greater than 30% by the 2080s in RCP 8.5. There are large differences between the 2020s, 2050s, and 2080s for RCPs 4.5 and 8.5, with increases becoming larger in the Missouri basin, the southern part of the Northwest Interior and the northern part of the Great Basin. Spring (March–May) ensemble mean precipitation shows a similar pattern in the Northwest Interior and the Missouri basin but shows decreases in the Great Basin.

2.3.2 Projected changes in snowpack

Shifts in precipitation and temperature impact snowpack across the domain. Figure 2.2 shows the ensemble mean of simulated SWE aggregated by mountain range as well as the full range and the interquartile range of aggregate SWE predicted by the ensemble of GCMs. Although the magnitude of the decline differs among models, decreasing trends are robust across all future simulations for mean April 1 SWE storage (in km^3) between the historical and future periods (Table A3.3). The greatest relative decline in SWE is projected in the White Mountains, which by the end of the twenty-first century are projected to be nearly free of snow (95% reduction, ensemble mean) or entirely snow-free (maximum projected changes). Although the Northern Rockies also show a large decrease for RCP 8.5, it is substantially smaller in relative terms (48%) than for the Cascades, Sierra Nevada, and White Mountains, which have average projected losses of 65, 65, and 95%, respectively (Table A3.3). Much of the differential effects of climate change on SWE can be explained in terms of elevation and thus temperature (see Figure A3.5 and Figure A3.6).

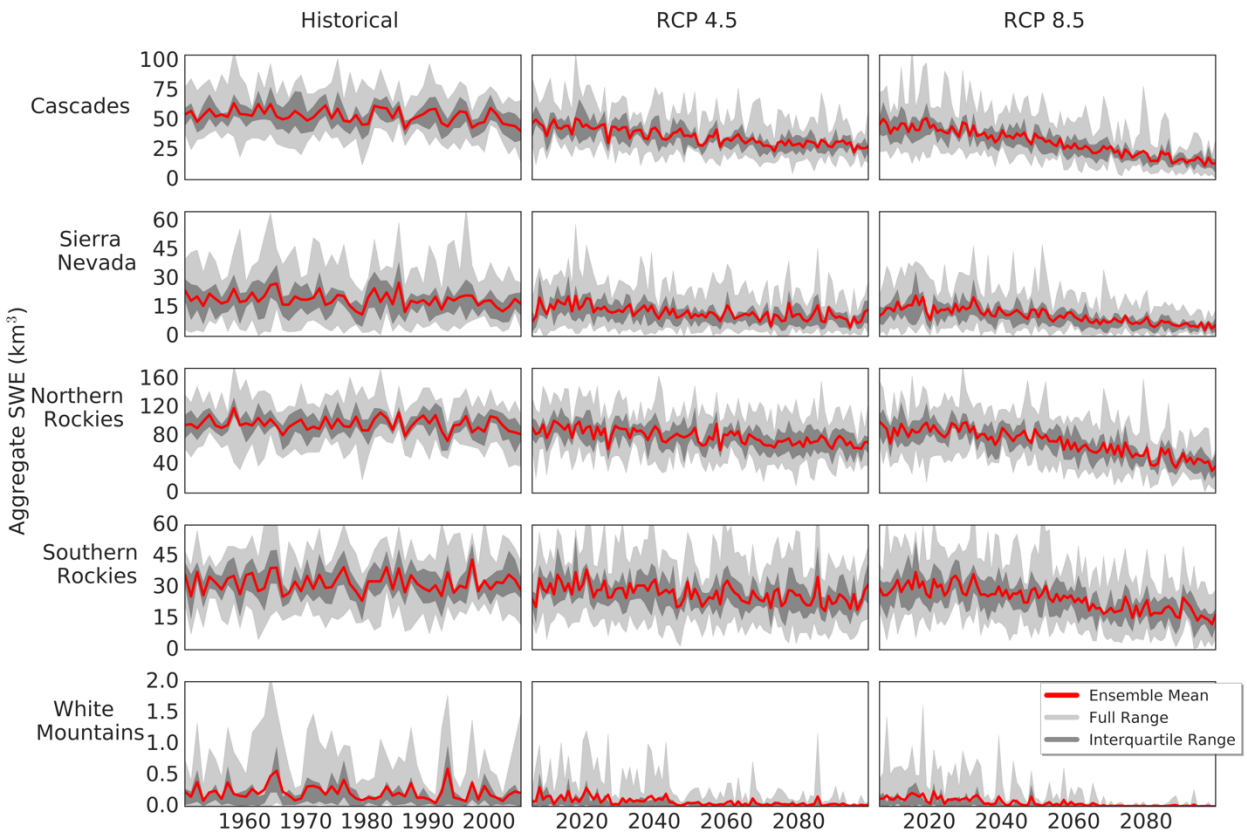

Figure 2.2. Simulated April 1 SWE aggregated by volume over each mountain range for the five mountain regions. *Light gray* shows the full range projected by the GCMs, *dark gray* shows the interquartile range, and *red* shows the ensemble mean of the GCMs.

Even though increases in temperature lead to a lower fraction of precipitation falling as snow and earlier melt, the spread in projected changes in precipitation contributes to uncertainty about the magnitude of spring snowpack change in some areas of the western USA. Figure 2.3 compares the spread in April 1 SWE projections (from all ten GCMs) for RCP 8.5 for the 2050s with the mean change in April 1 SWE (across all ten models) between the future and historic period (1970–1999). A higher value indicates that the range of SWE projections is larger than the mean projected change in SWE. For example, a value of 4 indicates that the range of SWE projections is 4 times greater than the mean projected change in SWE. High ratios occur in parts of the Cascades, Sierras, and much of the Northern and Southern Rockies, while low ratios occur

in mid to lower-elevation areas. Luce (2018) used the same metric based on snow simulations at selected SNOTEL sites and found similar results for locations in the Northern and Southern Rockies.

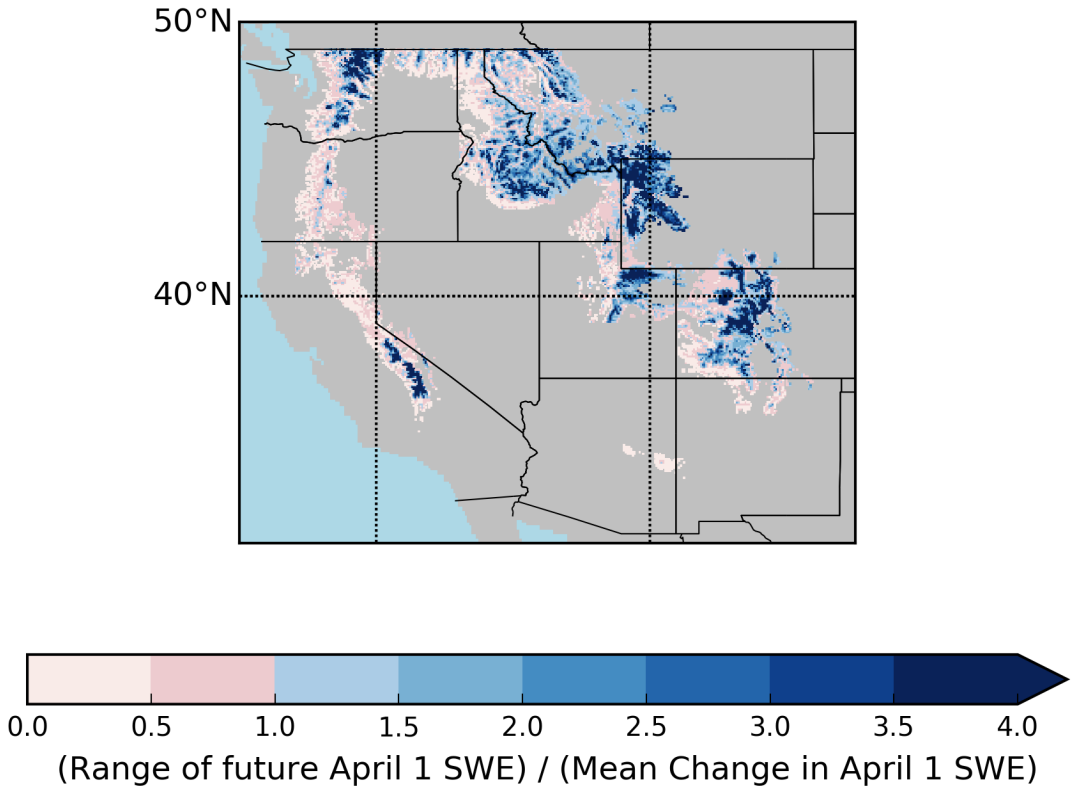

Figure 2.3. Uncertainty in projected losses of SWE (absolute value of the difference between maximum and minimum April 1 SWE projected by the GCMs for RCP 8.5 2040-2069 divided by the mean projected change). Red areas indicate that the mean projected change is greater than the spread between GCMs. Blue areas indicate that the spread is larger than the mean projected change.

2.3.3 Projected changes in soil moisture

Figure 2.4 shows the ensemble mean total column soil moisture storage for summer (June– August) for the historical period as well as projected changes for the 2050s for RCP 8.5. For each grid cell, the minimum annual average summer soil moisture from the control simulation has been subtracted from each year in the historical and future time periods. For most upland regions, large decreases in summer soil moisture result from earlier snowmelt, reducing

soil moisture recharge that historically occurs during late spring and early summer snowmelt. The largest decreases occur in the Sierra Nevada and Southern Cascades, as well as parts of the Northern and Southern Rockies. Absolute declines in soil moisture in these mountain systems are accentuated because they historically have higher summer soil moisture. By contrast, changes in soil moisture for lowland regions are smaller in magnitude and feature differing signals. The largest decrease occurs in the Coastal North, with smaller decreases in the Coastal South and parts of the Lower Colorado and Missouri basins. Soil moisture storage is projected to increase in the Northwest Interior, Great Basin, and the southern part of the Lower Colorado. However, individual GCMs show varied projections for the lowland regions (Figure A3.7). The spread between GCMs for soil moisture in the lowlands is due to the dependence of summer soil moisture on winter, spring, and summer precipitation (Figures A3.2 and A3.3).

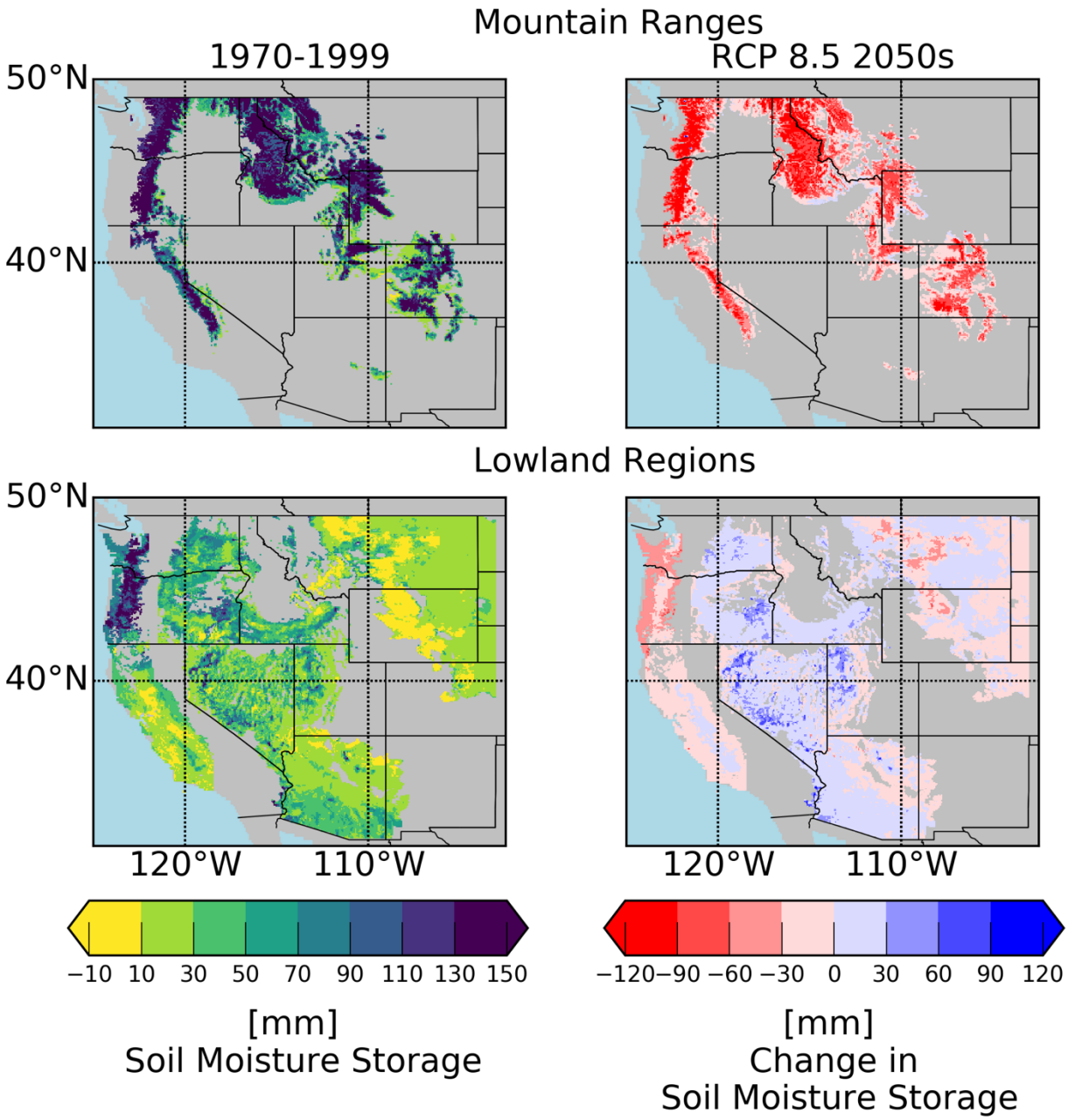

Figure 2.4. Ensemble-mean simulated summer (JJA) soil moisture in storage for control simulations (left column) and change in storage between RCP 8.5 2040–2069 and the control period (right column) for the mountain ranges and lowland regions. The minimum summer soil moisture from the control period has been subtracted from each grid cell for control and future periods.

2.3.4 Projected changes in fuel moisture

Figure 2.5 shows historical and projected changes in 100-h DFM averaged over June–September, which encompasses much of the primary fire season for the western USA. Historical DFM values are substantially lower at low-elevation sites relative to the uplands as higher elevation areas typically receive more precipitation and have lower temperature and vapor pressure deficits. In the mountain ranges, nearly all areas experience decreases in DFM, from a relatively minor decrease in the 2020s to a much larger relative decrease (greater than 25%) by the 2080s. This pattern is particularly strong in the Cascades and Northern Rockies, areas that were also projected to experience increased aridity during the fire season based on decreasing summer soil moisture. DFM projections for the lowlands are more varied. Most of the lower elevations are projected to see declines in DFM, although at substantially smaller magnitudes than for neighboring higher elevation regions. Portions of the Lower Colorado show increases in DFM by the 2080s, presumably due to increases in summer precipitation in downscaled climate projections. The increasing and decreasing signals observed for 100-h DFM are largely the same for 1000-h DFM (Figure A3.8), with larger decreases in 100-h DFM in the Northwest Interior and Missouri regions.

Projected changes in DFM are not robust across GCMs in all areas. Figure A3.9 shows the number of models with positive changes minus the number of models with negative changes in 100-h DFM for RCP 8.5 in the 2080s. A negative number indicates that a majority of models shows a decrease in DFM, while a positive number indicates an increase in DFM. There is less agreement among models in the Sierra Nevada and Coastal South, as well as the Southern Cascades and the Southern Rockies, with little to no agreement in the southern part of the

Coastal South and the Lower Colorado. Results for 1000-h DFM are similar, except with greater agreement for the Great Basin and Lower Colorado regions (Figure A3.10).

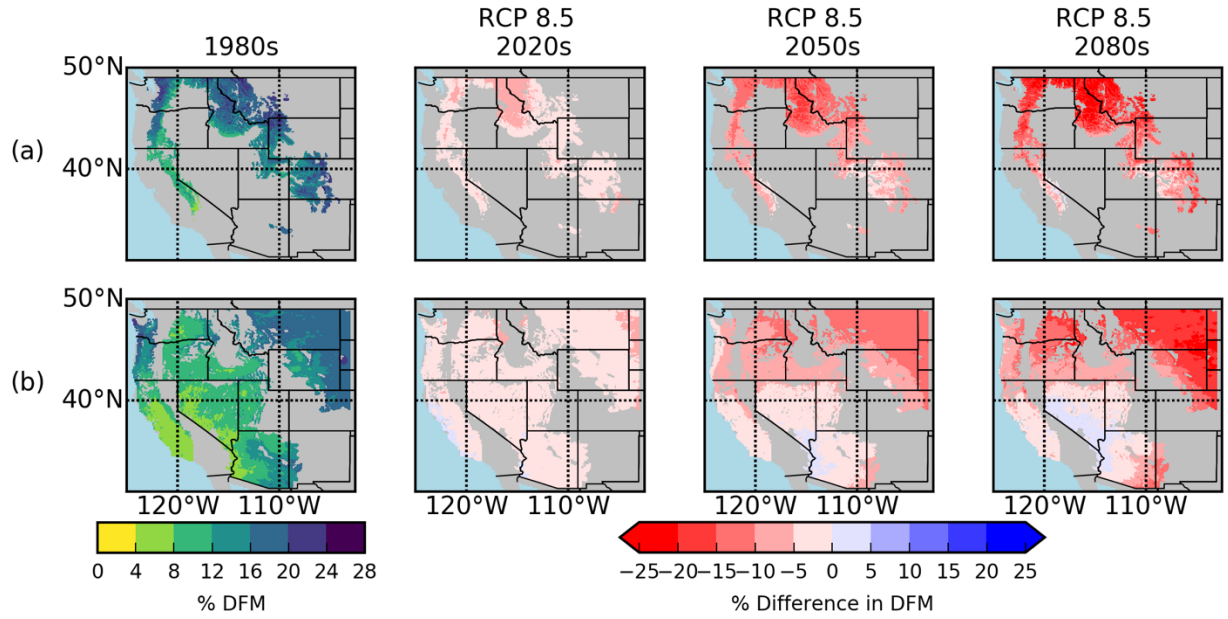

Figure 2.5. Ensemble-mean summer (JJAS) 100-h dead fuel moisture (DFM) shown over the five mountain ranges and b the six lowland regions, for the control period (1970–1999) and RCP 8.5 2010–2039, 2040–2069, and 2070–2099. For the control period, % DFM is shown, and for future periods, the% difference in DFM. DFM was calculated using the NFDRS algorithm for fuel moisture.

2.4 Discussion

Our projected snowpack changes are generally consistent with previous studies that have examined changing snowpack in the western USA (e.g. Maurer, 2007). Our results show relatively large declines in snowpack in all mountain ranges for all future scenarios and GCMs (Figure A3.4). Spring snowpack in mountains near the Pacific Coast is extremely sensitive to warming temperatures, while snowpack in more continental mountain ranges (Northern and Southern Rockies) is more sensitive to changes in precipitation (Figure A3.6), a result that is consistent with Adam et al., (2009) and other recent studies (e.g., Scalzitti et al., 2016; Luce et al., 2014). This sensitivity to warming temperatures explains the strong decline in snowpack in

the Cascades and Sierra Nevada that is robust to potential increases in precipitation. The Cascades are projected to lose up to 81% of April 1 SWE storage, or up to 47.3 km^3 of total SWE by the 2080s. The Sierra Nevada are projected to lose up to 76% of SWE storage, or up to 13.4 km^3 of total SWE.

These declines translate into dramatic losses of a key source of water storage for the surrounding regions, many of which primarily rely on snowmelt for water supply. For example, the San Joaquin Basin in California has over 80 dams, with a total storage capacity of about 9.5 km^3 (7.7 million acre-feet) on the San Joaquin, Merced, Tuolumne, and Stanislaus rivers (California Environmental Protection Agency 2011). The maximum projected loss of SWE storage in the Sierra Nevada exceeds the San Joaquin Basin total storage capacity by 40%. Even the average projected loss of SWE storage in the Sierra Nevada for RCP 8.5 in the 2080s (11.3 km^3) exceeds the San Joaquin total storage capacity.

Future projected declines in April 1 SWE translate to declining summer soil moisture for all mountain ranges. Low summer soil moisture, in turn, is closely linked to fire potential and burned area in forested systems like the Northern Rockies (e.g., Higuera et al. 2015). Thus, projected declines of summer soil moisture in the mountain ranges lead to increased drought and are likely to increase the potential for wildfire in systems where large fires have historically coincided with such conditions (e.g., Westerling et al., 2003), but significant uncertainty remains with regard to projected changes in snowpack, soil moisture, and fire potential. Our findings are mostly consistent with previous studies that have identified the Sierra Nevada, Cascades, and Northern Rockies as the most at-risk areas in the western USA for increasing fire activity in a changing climate (Westerling et al. 2011a, Westerling et al. 2011b; Barbero et al. 2015; Littell et

al. 2010; McKenzie and Littell 2016), with the exception of fire potential projections in the Yellowstone region in Westerling et al. (2011b), which our results contradict.

Summer soil moisture at lower elevations shows a mixed response to climate change. The Northwest Interior, Lower Colorado, and Great Basin are projected to experience increased summer soil moisture, while modest decreases are projected for the Missouri and Coastal North regions. The Coastal South region lacks a strong signal. Summer soil moisture increases in these basins are due to increased spring precipitation (Figure A3.3), which supersedes the effects of warming temperatures (Table A3.2). There is much larger uncertainty in precipitation than temperature projections (Kharin et al. 2013); hence, the lack of robust agreement for areas where spring snowpack does not strongly influence summer soil moisture. The weaker drought-fire relationships, particularly for rangeland-dominated regimes, and lack of robust changes in soil moisture are less informative for projecting future fire potential in the lowland regions.

Similar differences are apparent in DFM changes between mountains and lowland regions. Decreases in 100-h DFM across mountain ranges, in concert with declines in soil moisture, suggest the potential for increased fire activity. Decreases in DFM in the lowland regions may enhance fire potential in flammability-limited fire regimes, but may not substantially alter fire potential in arid systems. Moreover, the models show a lack of agreement in changes in DFM in areas where the projected change in summer soil moisture lacks a distinct signal, such as in the Coastal South region (Figure A3.7). The confounding signals of increased summer soil moisture and decreased DFM in regions such as the Northwest Interior may have interesting impacts on fire regimes that warrant additional analysis, but are beyond the scope of this study.

2.5 Conclusions

Projected effects of climate change across the western USA contrast strongly for mountains and lowlands. The water balance of the mountainous portions of the domain is strongly linked to snow accumulation and ablation, which is strongly temperature-sensitive but varies across the domain. Changes in April 1 SWE in the higher-elevation areas of the Northern and Southern Rockies, North Cascades, and Southern Sierra are more uncertain due to larger spread in precipitation projections, whereas in other parts of the mountainous west, temperature projections dominate. Warming temperatures will result in declining snow water storage, and consequently, moisture inputs to the soil column will increase in winter and decrease in spring and summer. The result will be substantial reductions in summer soil moisture storage and increases in water deficit. We project large decreases in DFM in mountain ranges, which would increase fire potential.

The main conclusions of our work are as follows:

- In the five mountain regions, we project large declines in spring snowpack and summer soil moisture, primarily due to warming temperatures. This will result in April 1 SWE losses by the 2080s of up to 81% for the Cascades and 76% for the Sierra Nevada mountains.
- Ensemble mean summer soil moisture is projected to decrease in the mountain ranges and to increase in lowland regions. In the lowland regions, trends are not robust across GCMs due to differences in precipitation projections.
- Dead fuel moisture content (as represented by 100-h and 1000-h DFM) is projected to decrease in the mountain ranges and mostly increase in the lowland regions (for the ensemble mean). Lowland increases are of much smaller magnitude than the mountain

decreases. Changes in fuel moisture content, however, are not robust across the western USA.

- Overall, we conclude that the mountain ranges are on average likely to experience higher fire potential under future climate projections. Other parts of our domain may also experience increased potential, but there is greater uncertainty in the lowland regions, where there is less agreement between GCMs, as well as in the Sierra Nevada, where there is disagreement between soil moisture and fuel moisture projections.

2.6 Acknowledgements

This work was made possible in part through grant GS277A-B from the Northwest Climate Science Center to the University of Washington. The authors would like to thank Charles Luce, Anne Nolin, and an anonymous reviewer for their helpful comments and insights.

2.7 References

Abatzoglou, J. T., & Kolden, C. A. (2013). Relationships between climate and macroscale area burned in the western United States. *International Journal of Wildland Fire*, *22*(7), 1003–1020. https://doi.org/10.1071/WF13019

Abatzoglou, J. T., & Williams, A. P. (2016). Impact of anthropogenic climate change on wildfire across western US forests. *Proceedings of the National Academy of Sciences*, *113*(42), 11770–11775. https://doi.org/10.1073/pnas.1607171113

Adam, J. C., Hamlet, A. F., & Lettenmaier, D. P. (2009). Implications of global climate change for snowmelt hydrology in the twenty-first century. *Hydrological Processes*, *23*(7), 962–972. https://doi.org/10.1002/hyp.7201

Barbero, R., Abatzoglou, J. T., Larkin, N. K., Kolden, C. A., & Stocks, B. (2015). Climate change presents increased potential for very large fires in the contiguous United States. *International Journal of Wildland Fire*, *24*(7), 892–899. https://doi.org/10.1071/WF15083

Barnett, T. P., Adam, J. C., & Lettenmaier, D. P. (2005). Potential impacts of a warming climate on water availability in snow-dominated regions. *Nature*, *438*(7066), 303–309. https://doi.org/10.1038/nature04141

Behnke, R., Vavrus, S., Allstadt, A., Albright, T., Thogmartin, W.E., Radeloff, V.C. (2016). Evaluation of downscaled, gridded climate data for the conterminous United States. *Ecol Appl* 26(5):1338–1351. doi:10.1002/15-1061

California Environmental Protection Agency, State Water Resources Control Board (2011) Lower San Joaquin River Committee Administrative Materials. Available at: http://www.waterboards.ca.gov/centralvalley/water_issues/salinity/lower_sanjoaquin_river_committee/administrative_materials/2011apr28/2011apr28_mtg_ag_item4_rsrc_dev.pdf

Cayan, D. R. (1996). Interannual Climate Variability and Snowpack in the Western United States. *Journal of Climate*, *9*(5), 928–948. https://doi.org/10.1175/1520-0442(1996)009<0928:ICVASI>2.0.CO;2

Cohen, J. D., & Deeming, J. E. (1985). The national fire-danger rating system: Basic equations. *Gen. Tech. Rep. PSW-82. Berkeley, CA: Pacific Southwest Forest and Range Experiment Station, Forest Service, U.S. Department of Agriculture; 16 p*, *082*. https://doi.org/10.2737/PSW-GTR-82

Dennison, P. E., Brewer, S. C., Arnold, J. D., & Moritz, M. A. (2014). Large wildfire trends in the western United States, 1984–2011. *Geophysical Research Letters*, *41*(8), 2928–2933. https://doi.org/10.1002/2014GL059576

Flannigan, M. D., Logan, K. A., Amiro, B. D., Skinner, W. R., & Stocks, B. J. (2005). Future Area Burned in Canada. *Climatic Change*, *72*(1), 1–16. https://doi.org/10.1007/s10584-005-5935-y

Gutmann, E., Pruitt, T., Clark, M.P., Brekke, L., Arnold, J.R., Raff, D.A., Rasmussen, R.M. (2014). An intercomparison of statistical downscaling methods used for water resource assessments in the United States. *Water Resour Res* 50:7167–7186. doi:10.1002/2014WR015559

Hamlet, A. F., Mote, P. W., Clark, M. P., & Lettenmaier, D. P. (2005). Effects of Temperature and Precipitation Variability on Snowpack Trends in the Western United States. *Journal of Climate*, *18*(21), 4545–4561. https://doi.org/10.1175/JCLI3538.1

Higuera, P. E., Abatzoglou, J. T., Littell, J. S., & Morgan, P. (2015). The Changing Strength and Nature of Fire-Climate Relationships in the Northern Rocky Mountains, U.S.A., 1902-2008. *PLOS ONE*, *10*(6), e0127563. https://doi.org/10.1371/journal.pone.0127563

Kharin, V. V., Zwiers, F. W., Zhang, X., & Wehner, M. (2013). Changes in temperature and precipitation extremes in the CMIP5 ensemble. *Climatic Change*, *119*(2), 345–357. https://doi.org/10.1007/s10584-013-0705-8

Kormos, P. R., Luce, C. H., Wenger, S. J., & Berghuijs, W. R. (2016). Trends and sensitivities of low streamflow extremes to discharge timing and magnitude in Pacific Northwest mountain streams. *Water Resources Research*, *52*(7), 4990–5007. https://doi.org/10.1002/2015WR018125

Liang, X., Lettenmaier, D. P., Wood, E. F., & Burges, S. J. (1994). A simple hydrologically based model of land surface water and energy fluxes for general circulation models. *Journal of Geophysical Research: Atmospheres*, *99*(D7), 14415–14428. https://doi.org/10.1029/94JD00483

Littell, J. S., & Gwozdz, R. B. (2011). Climatic Water Balance and Regional Fire Years in the Pacific Northwest, USA: Linking Regional Climate and Fire at Landscape Scales. In D. McKenzie, C. Miller, & D. A. Falk (Eds.), *The Landscape Ecology of Fire* (pp. 117–139). https://doi.org/10.1007/978-94-007-0301-8_5

Littell, J. S., McKenzie, D., Peterson, D. L., & Westerling, A. L. (2009). Climate and wildfire area burned in western U.S. ecoprovinces, 1916–2003. *Ecological Applications*, *19*(4), 1003–1021. https://doi.org/10.1890/07-1183.1

Littell, J. S., Oneil, E. E., McKenzie, D., Hicke, J. A., Lutz, J. A., Norheim, R. A., & Elsner, M. M. (2010). Forest ecosystems, disturbance, and climatic change in Washington State, USA. *Climatic Change*, *102*(1), 129–158. https://doi.org/10.1007/s10584-010-9858-x

Littell, J. S., Peterson, D. L., & Tjoelker, M. (2008). Douglas-Fir Growth in Mountain Ecosystems: Water Limits Tree Growth from Stand to Region. *Ecological Monographs*, *78*(3), 349–368. https://doi.org/10.1890/07-0712.1

Livneh, B., Rosenberg, E. A., Lin, C., Nijssen, B., Mishra, V., Andreadis, K. M., … Lettenmaier, D. P. (2013). A Long-Term Hydrologically Based Dataset of Land Surface Fluxes and States for the Conterminous United States: Update and Extensions. *Journal of Climate*, *26*(23), 9384–9392. https://doi.org/10.1175/JCLI-D-12-00508.1

Luce, C. H., Abatzoglou, J. T., & Holden, Z. A. (2013). The Missing Mountain Water: Slower Westerlies Decrease Orographic Enhancement in the Pacific Northwest USA. *Science*, *342*(6164), 1360–1364. https://doi.org/10.1126/science.1242335

Luce, Charles H. (2018). Effects of Climate Change on Snowpack, Glaciers, and Water Resources in the Northern Rockies. In J. E. Halofsky & D. L. Peterson (Eds.), *Climate Change and Rocky Mountain Ecosystems* (pp. 25–36). https://doi.org/10.1007/978-3-319-56928-4_3

Luce, Charles H., Lopez-Burgos, V., & Holden, Z. (2014). Sensitivity of snowpack storage to precipitation and temperature using spatial and temporal analog models. *Water Resources Research*, *50*(12), 9447–9462. https://doi.org/10.1002/2013WR014844

Lundquist, J. D., & Flint, A. L. (2006). Onset of Snowmelt and Streamflow in 2004 in the Western United States: How Shading May Affect Spring Streamflow Timing in a Warmer World. *Journal of Hydrometeorology*, *7*(6), 1199–1217. https://doi.org/10.1175/JHM539.1

Lute, A. C., Abatzoglou, J. T., & Hegewisch, K. C. (2015). Projected changes in snowfall extremes and interannual variability of snowfall in the western United States. *Water Resources Research*, *51*(2), 960–972. https://doi.org/10.1002/2014WR016267

Maurer, E. P. (2007). Uncertainty in hydrologic impacts of climate change in the Sierra Nevada, California, under two emissions scenarios. *Climatic Change*, *82*(3), 309–325. https://doi.org/10.1007/s10584-006-9180-9

McKenzie, D., & Littell, J. S. (2017). Climate change and the eco-hydrology of fire: Will area burned increase in a warming western USA? *Ecological Applications*, *27*(1), 26–36. https://doi.org/10.1002/eap.1420

Minder, J. R., Mote, P. W., & Lundquist, J. D. (2010). Surface temperature lapse rates over complex terrain: Lessons from the Cascade Mountains. *Journal of Geophysical Research: Atmospheres*, *115*(D14). https://doi.org/10.1029/2009JD013493

Mizukami, N., Clark, M. P., Gutmann, E. D., Mendoza, P. A., Newman, A. J., Nijssen, B., … Brekke, L. D. (2015). Implications of the Methodological Choices for Hydrologic Portrayals of Climate Change over the Contiguous United States: Statistically Downscaled Forcing Data and Hydrologic Models. *Journal of Hydrometeorology*, *17*(1), 73–98. https://doi.org/10.1175/JHM-D-14-0187.1

Mizukami, N., P. Clark, M., G. Slater, A., D. Brekke, L., M. Elsner, M., R. Arnold, J., & Gangopadhyay, S. (2013). Hydrologic Implications of Different Large-Scale Meteorological Model Forcing Datasets in Mountainous Regions. *Journal of Hydrometeorology*, *15*(1), 474–488. https://doi.org/10.1175/JHM-D-13-036.1

Mote, P. W. (2006). Climate-Driven Variability and Trends in Mountain Snowpack in Western North America. *Journal of Climate*, *19*(23), 6209–6220. https://doi.org/10.1175/JCLI3971.1

Mote, P. W., Hamlet, A. F., Clark, M. P., & Lettenmaier, D. P. (2005). Declining mountain snowpack in western north america*. *Bulletin of the American Meteorological Society*, *86*(1), 39–50. https://doi.org/10.1175/BAMS-86-1-39

Northwest Knowledge Network (NKN) University of Idaho applied climate science lab, http://climate.northwestknowledge.net/

Rupp, D. E., Abatzoglou, J. T., Hegewisch, K. C., & Mote, P. W. (2013). Evaluation of CMIP5 20th century climate simulations for the Pacific Northwest USA. *Journal of Geophysical Research: Atmospheres*, *118*(19), 10,884-10,906. https://doi.org/10.1002/jgrd.50843

Scalzitti, J., Strong, C., & Kochanski, A. (2016). Climate change impact on the roles of temperature and precipitation in western U.S. snowpack variability. *Geophysical Research Letters*, *43*(10), 5361–5369. https://doi.org/10.1002/2016GL068798

Sillmann, J., Kharin, V. V., Zwiers, F. W., Zhang, X., & Bronaugh, D. (2013). Climate extremes indices in the CMIP5 multimodel ensemble: Part 2. Future climate projections. *Journal of Geophysical Research: Atmospheres*, *118*(6), 2473–2493. https://doi.org/10.1002/jgrd.50188

Simard, A. J. (1968). *The moisture content of forest fuels - I: A review of the basic concepts*. *14*. Retrieved from https://www.cfs.nrcan.gc.ca/publications?id=24782

Stavros, E. N., Abatzoglou, J. T., McKenzie, D., & Larkin, N. K. (2014). Regional projections of the likelihood of very large wildland fires under a changing climate in the contiguous Western United States. *Climatic Change*, *126*(3), 455–468. https://doi.org/10.1007/s10584-014-1229-6

Stewart, I. T., Cayan, D. R., & Dettinger, M. D. (2004). Changes in Snowmelt Runoff Timing in Western North America under a `Business as Usual' Climate Change Scenario. *Climatic Change*, *62*(1), 217–232. https://doi.org/10.1023/B:CLIM.0000013702.22656.e8

Stewart, I. T., Cayan, D. R., & Dettinger, M. D. (2005). Changes toward Earlier Streamflow Timing across Western North America. *Journal of Climate*, *18*(8), 1136–1155. https://doi.org/10.1175/JCLI3321.1

Taylor, K. E., Stouffer, R. J., & Meehl, G. A. (2011). An Overview of CMIP5 and the Experiment Design. *Bulletin of the American Meteorological Society*, *93*(4), 485–498. https://doi.org/10.1175/BAMS-D-11-00094.1

Turner, D. P., Conklin, D. R., Vache, K. B., Schwartz, C., Nolin, A. W., Chang, H., … Bolte, J. P. (2017). Assessing mechanisms of climate change impact on the upland forest water balance of the Willamette River Basin, Oregon. *Ecohydrology*, *10*(1), e1776. https://doi.org/10.1002/eco.1776

Westerling, A. L., Gershunov, A., Brown, T. J., Cayan, D. R., & Dettinger, M. D. (2003). Climate and Wildfire in the Western United States. *Bulletin of the American Meteorological Society*, *84*(5), 595–604. https://doi.org/10.1175/BAMS-84-5-595

Westerling, A. L., Bryant, B. P., Preisler, H. K., Holmes, T. P., Hidalgo, H. G., Das, T., & Shrestha, S. R. (2011). Climate change and growth scenarios for California wildfire. *Climatic Change*, *109*(1), 445–463. https://doi.org/10.1007/s10584-011-0329-9

Westerling, A. L., Hidalgo, H. G., Cayan, D. R., & Swetnam, T. W. (2006). Warming and Earlier Spring Increase Western U.S. Forest Wildfire Activity. *Science*, *313*(5789), 940–943. https://doi.org/10.1126/science.1128834

Westerling, Anthony L., Turner, M. G., Smithwick, E. A. H., Romme, W. H., & Ryan, M. G. (2011). Continued warming could transform Greater Yellowstone fire regimes by mid-21st century. *Proceedings of the National Academy of Sciences*, *108*(32), 13165–13170. https://doi.org/10.1073/pnas.1110199108

Wood, A. W., Leung, L. R., Sridhar, V., & Lettenmaier, D. P. (2004). Hydrologic Implications of Dynamical and Statistical Approaches to Downscaling Climate Model Outputs. *Climatic Change*, *62*(1), 189–216. doi: 10.1023/B:CLIM.0000013685.99609.9e

Chapter 3

Interactions between permafrost and snow cover for limited warming versus RCP 8.5 and their implications for carbon release from permafrost

This chapter is in preparation, to be submitted to the *Journal of Geophysical Research – Atmospheres*.

Abstract

Snow cover is strongly affected by rising surface air temperatures (SATs) and increases in precipitation due to the effects of climate change. Changes in the timing and amount of snow, in turn, strongly affect the soil thermal regime. In this study, we examine how projected changes in SWE and snow season timing over the circumpolar Arctic interact with warming temperatures to impact permafrost extent and associated vulnerability of soil organic carbon (SOC) stock. We use three twenty-first century warming scenarios: 1.5°C and 2°C global-mean warming and Representative Concentration Pathway (RCP) 8.5. These warming scenarios are encapsulated in two climate model ensembles: the Community Earth System Large Ensemble (CESM-LE) and the Low Warming Ensemble (CESM-LWE). We find that even for the low emissions scenarios represented by the LWE, projected changes in the timing and amount of peak SWE are large, with the majority of the domain projected to experience significant decreases in SWE. These changes have a strong effect on soil thermal regimes, translating in dramatic losses in permafrost by the end of the twenty-first century. Overall, given the amount of permafrost projected to be lost, the vulnerability of SOC stocks is high, particularly for RCP 8.5, and could result in large increases of carbon released into the atmosphere.

3.1 Introduction

Seasonal snow cover, comprising an extent of about 45 x 10^6 km^2 in the northern hemisphere, is the largest component of the terrestrial cryosphere and has important effects on climate (Brutel-Vuilmet et al., 2013). Snow plays three major roles in modulating Arctic climate conditions: 1) increasing surface albedo and thus cooling the land surface, 2) acting as a barrier (and heat sink) between the atmosphere and the ground and thereby controlling energy and water exchange between the land and atmosphere, and 3) influencing large-scale atmospheric circulation, which in turn leads to altered rainfall patterns (Gastineau et al., 2017; Zhang, 2005; Wang et al., 2018). The first of those roles is the major driver of the snow-albedo feedback, which is one of the key causes of polar amplification of climate change, a widely-documented phenomenon called Arctic amplification (Serreze et al., 2009).

Terrestrial snow cover is also strongly affected by other components of the Arctic climate system. Sea ice is a key driver of Arctic climate, and observed changes in sea ice over the past several decades have already resulted in rising surface air temperatures (SATs) over the Arctic Ocean. Recent declines in sea ice extent (SIE) have also resulted in enhanced ocean surface evaporation, which has led to increases in precipitation both in observations and model simulations (Rawlins et al., 2010; Bintanja & Selten, 2014; Park et al., 2015). Climate models project that Arctic precipitation will increase by 50-60% over the course of the twenty-first century due to warming, with a large decrease in the fraction of precipitation falling as snow. Because of these combined changes, rainfall is projected to become the dominant form of precipitation by 2100 in the Arctic (Bintanja and Andry, 2017; Bintanja, 2018). The interplay between increases in SATs and precipitation have complicated and varying effects on snow cover in the Arctic and depend on whether or not SATs cross the freezing point. In areas where

SATs become warmer than the freezing point, snow cover decreases as rain becomes dominant. In areas where temperatures remain well below or near the freezing point, snow cover may increase (Ghatak et al., 2010; Deser et al., 2010). Snow cover extent in much of the Arctic has decreased over the past 40 years at an average rate of ~0.8 million km^2/decade (Brown and Robinson, 2011). However, in parts of Eurasia and the Canadian Arctic snowfall has increased (Ghatak et al. 2012). Ghatak et al. (2010) show that increasing snowfall over Siberia is strongly correlated with decreasing September sea ice over the Arctic, a pattern apparent from late-twentieth century observations and which emerges from model simulations by the mid-twenty-first century. Deser et al. (2010) describe a similar spatial pattern of increases in snowfall in Eurasia based on model simulations, and Liu et al. (2012) use reanalysis data in North America to document increases in snowfall which they also tie to decreases in SIE. An analysis of twenty climate models from the Coupled Model Intercomparison Project (CMIP3) also found increases in snow water equivalent (SWE) in the coldest parts of the Northern Hemisphere, such as northernmost North America and most of Siberia, and decreases in SWE in the rest of the circumpolar Arctic (Räisänen, 2008).

While the sign of future changes in the amount of snow varies spatially across the Arctic, projected changes in the timing of the snow season and in snow cover extent are in robust agreement across the circumpolar Arctic. Brutel-Vuilmet et al. (2013) found a decrease of -3.4 +/- 1.1% in observed snow cover extent, averaged over the months of March and April, from 1979-2005 (using the Rutgers University Global Snow product; Robinson & Frei, 2000). Wang et al. (2018) found that simulated ensemble-mean change in annual mean snow area extent (computed as the snow cover fraction multiplied by the land area for each grid cell) between 2071-2100 and 1971-2000 varied from -14.47% (Representative Concentration Pathway (RCP)

4.5) to -8.02% (1.5°C global-mean warming) averaged over Northern hemisphere land areas. In addition to decreases in snow cover extent, the length of the snow season is also projected to shorten. Historical reanalysis data and model experiments over the period 1979-2009 show that the snow onset date is occurring later in the year, the snow-free date earlier in the year, and the duration of the snow season has decreased (Liston and Hiemstra, 2011). Changes in the timing and duration of the snow season, as well as projected changes in the magnitude and areal extent of SWE, together have profound implications for ground thermal conditions (Zhang 2005; Stieglitz et al., 2003; Lawrence & Slater, 2010; Park et al., 2015; Park et al., 2012).

The mechanistic interactions between snow and the ground thermal regime depend on a variety of factors, including snow onset and disappearance timing, snow season duration, snow cover and snow density (Zhang 2005). Generally, the presence of snow acts as a barrier to heat exchange between the atmosphere and the underlying soil. Snow has an extremely low thermal conductivity and thereby acts as an insulator, shielding soil beneath it from fluctuations in air temperature. At the same time, the presence of snow also acts as a heat sink through its high latent heat capacity. Because of the role of snow cover as an insulator, the soil surface beneath snow can have a much lower or higher temperature than the snow surface and/or overlying air temperature.

Lawrence and Slater (2010) conducted a series of off-line experiments with the Community Land Model (CLM) to better understand the impacts of changes in snowfall, snow depth and snow season length on soil temperatures. The authors found that in areas where mean SWE was projected to increase, between 10-30% of total soil warming could be attributed to increases in SWE, which was also responsible for around 16% of the projected decline in permafrost extent in the 21st century. They also found that the shortening of the snow season

contributed to soil warming. By contrast, in areas where SWE was projected to decrease, this trend counteracted the effects of warming temperatures by providing less insulation to underlying ground conditions, resulting in decreasing the amount of soil warming that was projected to occur. Overall, the authors found that the opposing impacts of changes in snow amount and season length either exacerbate or offset the impact of warming air temperatures, and this balance depends on specific snow, climatic and vegetation conditions across the Arctic. Biskaborn et al. (2019) used a global data set of soil temperature observations to study these interactions and found that changes in air temperature and snow conditions had a greater effect on colder permafrost versus warmer permafrost (with soil temperatures closer to 0°C) because much of the heat influx into warmer permafrost was subsumed by the phase change.

However, the ways in which the impacts of warming temperatures and changing snow conditions reinforce or oppose each other to affect the ground thermal regime both for a) differing levels of warming and b) diverse hydroclimates across the Arctic remain largely unknown. Because changes in the ground thermal regime affect permafrost and, consequently, carbon release from permafrost, it is important to better understand how changes in the snow season and warming temperatures interact and will affect permafrost trajectories in the 21st century. This study seeks to fill this gap by asking the question of how projected changes in SWE and snow season timing interact with warming temperatures to affect permafrost extent and associated release of carbon from permafrost. To answer this question, we employ three different twenty-first century warming scenarios encompassed in two climate model ensembles: the Community Earth System Model (CESM) Large Ensemble (CESM-LE; Kay et al., 2014) and the Low Warming Ensemble (LWE; Sanderson et al., 2016; Sanderson et al., 2017). We use the eleven ensemble members available from the LWE and the thirty-five ensemble members

available from the CESM-LE. The three warming scenarios (two from the LWE, one from the CESM-LE) include 1.5°C and 2°C global-mean warming and Representative Concentration Pathway (RCP) 8.5. Because of the complex dependence of permafrost changes on the balance between warming temperatures and increases in precipitation, including the role of natural variability by drawing upon multiple climate model ensembles allows us to understand a range of possible precipitation futures and how these translate to permafrost trajectories.

3.2 Data and methods

3.2.1 An overview of CESM

The Community Earth System Model version 1 (CESM1) is a fully-coupled global climate model (GCM) and is comprised of the following component models: the Community Atmosphere Model (CAM5) with 30 vertical levels, Parallel Ocean Program (POP2) ocean model with 60 vertical levels, the Community Land Model (CLM4) land model, and the Los Alamos sea ice model (CICE) (Hurrell et al., 2013). It also participated in the CMIP5 experiment (Taylor et al., 2011). CLM4 has been widely used to better understand changes in the snow season and permafrost in the twenty-first century, both in stand-alone modeling studies and as part of the CESM (Wang et al., 2018). The full life cycle of snow as well as thermal processes of the soil (including an explicit representation of organic matter and a deep soil column) are included in the model (Oleson et al., 2010).

3.2.1.1 CESM and Snow Water Equivalent (SWE)

The snow model in CLM4 consists of up to five layers and includes explicit representations of snow processes such as accumulation, melt, compaction, aging and transfer of

water mass between layers. The thermal conductivity of snow (λ_{sno}), which is critical for representing the extent to which snow buffers heat exchange between the atmosphere and underlying soil, is parameterized based on the method of Jordan (1991); also see Lawrence et al. (2010). λ_{sno} depends on the density of air and ice as well as the density of snow, which uses the Anderson 1976 formulation (Oleson et al., 2010). Increases in λ_{sno} due to processes such as metamorphism, melting and refreezing, reduce the insulative capacity of snow over soil. The snow model in CLM4 has been evaluated against both satellite and in situ products and has been generally found to capture temporal variation in both SWE and snow cover fraction, but with a too-fast and too-early snow ablation process (Wang et al., 2016), likely due to the tendency of CLM4 to underestimate SWE and snow depth (Toure et al., 2015).

3.2.1.2 CESM and soil thermal regimes

The soil temperature formulation in CLM4 solves the heat conduction equation numerically for a fifteen-layer soil column, with a lower boundary condition defined as a zero-heat flux at the bottom of the soil column. Soil temperatures are first calculated without a phase change and then readjusted if a phase change occurs. The depths of the fifteen soil layers are discretized exponentially so as to define a larger number of soil layers near the surface where the soil water gradient is larger (Oleson et al., 2010). Thermal and hydraulic properties of a given soil layer are calculated as a weighted combination of the mineral and organic properties of the layer (Lawrence et al., 2008).

3.2.2 Climate model ensembles

3.2.2.1 The CESM-LE project

The CESM-LE project was designed to address the need for separating the effects of natural variability from future climate change. The thirty-five ensemble members differ only in their atmospheric initial conditions and only by small round-off level differences; all ensemble members use the same model (CESM1) and the same external forcing (RCP 8.5 well-mixed greenhouse gases) and are run at a 1° horizontal resolution for all model components from 1920-2100, excluding ensemble member 1, which was run from 1850-2100 (Kay et al., 2014). As a result, the spread in the CESM-LE is solely generated from internal climate variability.

3.2.2.2 The LWE project

The LWE is an ensemble of CESM simulations (also using CESM1) that were designed to provide impact-relevant long-term climate data for stabilization pathways at 1.5°C and 2°C levels of global-mean warming by the end of the twenty-first century, as well as a 1.5°C overshoot case, to enable the assessment of climate impacts at the levels of warming dictated by the Paris Agreement of December 2015. The 1.5°C and 2°C cases are designed such that global-mean temperatures do not exceed 1.5°C and 2°C increases as compared to preindustrial levels (taken as the 1850-1920 mean), whereas the 1.5°C overshoot case briefly exceeds 1.5°C, peaks in 2060 and then decreases to 1.5°C by 2100. The ensemble includes ten realizations for each warming scenario, with a study design consistent with previous large ensemble studies such as the CESM-LE. Each LWE ensemble member branches from the corresponding CESM-LE member starting in 2005 (Sanderson et al. 2016; 2017). We use the 1.5°C and 2°C warming scenarios in this study.

3.2.3 Data

3.2.3.1 Climate model output

We accessed CESM-LE and LWE output data through the Earth System Grid (https://www.earthsystemgrid.org/) available via the National Center for Atmospheric Research (NCAR) Climate Data Gateway. We obtained daily SWE data (H2OSNO) and monthly soil temperatures (TSOI) and surface air temperatures (TBOT) from both ensembles for our analysis.

3.2.3.2 Carbon data

To represent the horizontal and vertical distribution of organic matter in the soil, we used version 2 of the Northern Circumpolar Soil Carbon Database dataset (NCSCDv2; Hugelius et al., 2013a and 2013b; accessed from https://bolin.su.se/data/ncscd/netcdf.php). We used a gridded version of the dataset at a 0.25°-resolution available in Network Common Data Format (NetCDF). The NCSCDv2 dataset includes estimates of soil organic carbon (SOC) stocks for the 0-3 m depth range in soils as well as estimates of carbon in deeper deltaic and Yedoma region deposits. It was created by using geographic data on soil coverage and pedon data with SOC storage, and upscaled to create estimates of total SOC stocks (Hugelius et al., 2013a; Hugelius et al., 2013b).

3.2.4 Methods

3.2.4.1 Study domain

Our study domain is pan-Arctic and includes all drainages to the Arctic ocean (Figure 3.1). We have confined the study to the circumpolar Arctic, rather than the entire Northern Hemisphere, since the mechanistic processes that we explore in this paper under future climate

conditions are most significant at higher latitudes. For this study, we use a 50-km near-equal-area North Pole stereographic grid that has been typically used for the study domain over which the Regional Arctic System Model (RASM) has been run (Hamman et al., 2016). This grid is used for our study to be able to draw upon the hydroclimate classes developed for RASM analysis. Consequently, we have regridded all data from the 1° global grid of CESM-LE and LWE output to the 50-km near-equal-area North Pole stereographic grid using nearest-neighbor remapping for soil and air temperatures and first-order conservative area remapping for SWE model output. We describe the hydroclimate classes in further detail in Section 2.4.3.

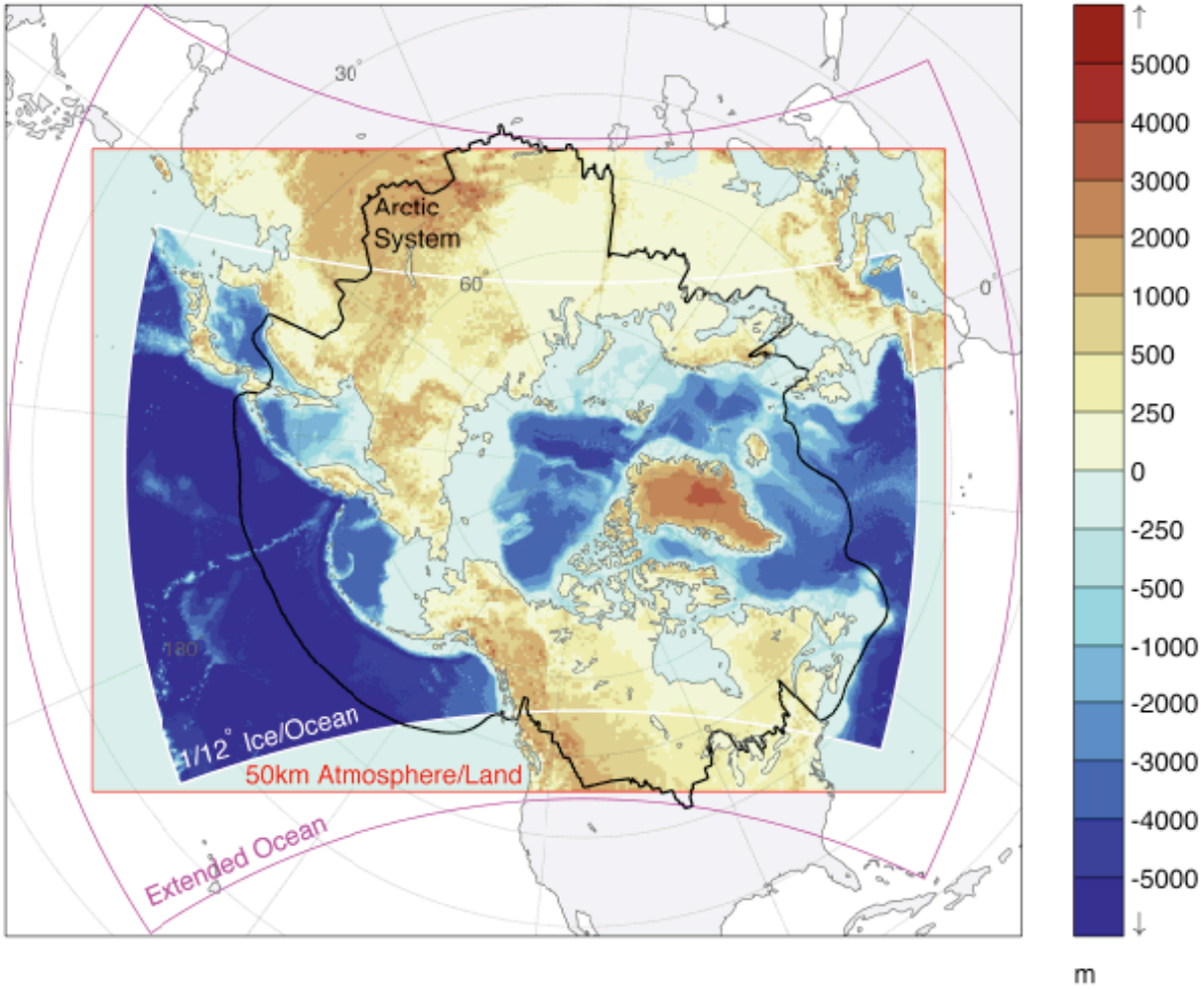

Figure 3.1. Circumpolar Arctic study domain, including all drainage basins into the Arctic Ocean.

3.2.4.2 Time periods

The climatological time periods used for analysis (unless otherwise stated) are 1975-2005 for the historical period and 2070-2099 for the future period. The motivation for these choices is twofold: 1) to be consistent with the impact-relevant analysis conducted by Sanderson et al. (2017) of the low-warming ensemble, and 2) to use the last climatological period of the twenty-first century so as to avoid analyzing a transient climate period of the LWE.

3.2.4.3 Hydroclimate classes

We derived nine hydroclimate classifications by overlaying the Brown et al (1997) permafrost map with the Köppen-Geiger climate classes present in our pan-Arctic domain. Köppen-Geiger classes are taken from a global map at a 5-arc-minute resolution representative of the period 1986-2010 (Rubel et al., 2017). The Brown et al. (1997) permafrost map was derived from a global map made available by the International Permafrost Association (IPA) available at a 0.05° resolution. Figure 3.2 shows the nine hydroclimate classes used in this analysis. The hydroclimate classifications are based on hydroclimatology and the presence or absence of permafrost, thus there are multiple instances of the same Köppen-Geiger class with and without permafrost represented in the nine classes.

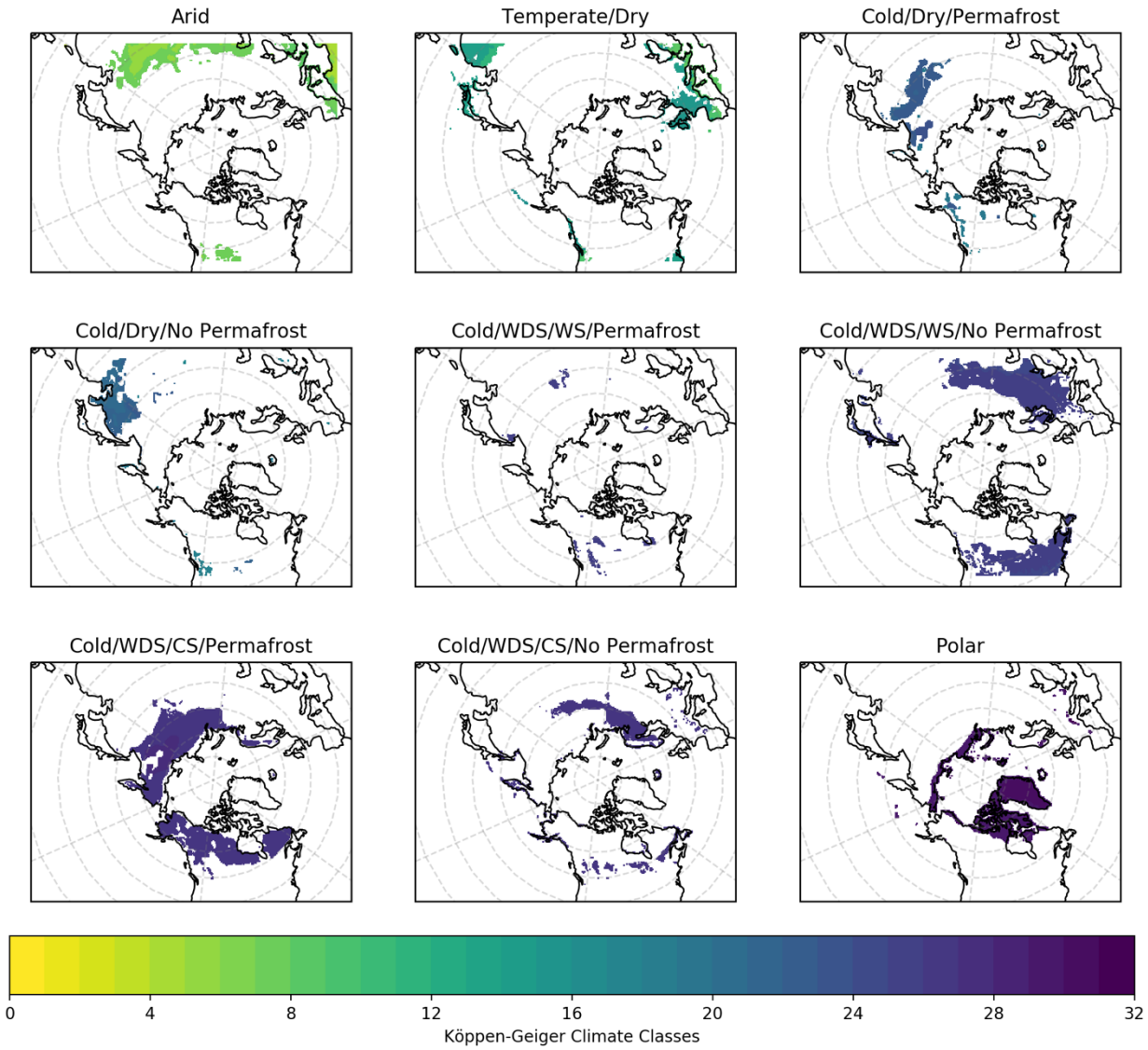

Figure 3.2. Nine hydroclimate classes used in our snow analysis, based on Köppen-Geiger climate class and the presence or absence of permafrost. Colors represent different Köppen-Geiger climate classes in a given hydroclimate class. WDS: without dry season, WS: warm summer, CS: cold summer.

3.2.4.4 Snow analysis

We conducted all snow analysis on daily snow data with the snow year defined as starting on September 1. The first day of SWE presence (after September 1) was labeled the day of snow onset and the snow disappearance date defined as the date at which snow was no longer present for the remainder of the year, thus we do not account for isolated early or late season

short duration snow events. Snow duration was calculated as the difference between the snow onset and disappearance dates. Peak SWE was defined as the day over the course of the snow year with the largest amount of SWE. We performed this analysis on each gridcell for each ensemble member for the three warming scenarios for the historical (1975-2005) and end-of-century (2070-2099) time periods.

3.2.4.5 Permafrost analysis

To calculate the presence of permafrost, we used the mean soil temperature (MST) method of Slater and Lawrence (2013). This method uses the annual mean soil temperature (MST) at some depth (the authors use 3.5m below the surface) as a proxy for permafrost, with annual MST below 0°C indicating the presence of permafrost. Permafrost presence is often calculated by considering soil at a depth within 3.5 m of the surface maintaining a temperature at or below 0°C for the current and previous year to contain permafrost, typically called the TSL method. However, the TSL and MST methods produce extremely similar permafrost area extents for most GCMs, including CESM, thus we use the MST method. For calculating MST using soil temperatures from CLM's 15-layer soil model, we use the soil layer with a depth closest to that of 3.5m, which extends from 2.9 to 4.7m below the surface.

3.2.4.6 Carbon release analysis

We regridded the NCSCDv2 dataset to the 50-km near-equal-area pan-Arctic stereographic grid using first-order conservative area remapping, including the NetCDF files corresponding to SOC stocks for each vertical level (0-30cm, 0-100cm, 100-200cm, 200-300cm). We then combined this gridded data with our analysis of permafrost trajectories and

expected permafrost loss under the most extreme climate warming scenario (RCP 8.5) from the CESM-LE to create a projection of possible carbon release from 2070-2099.

3.3 Results

3.3.1 Future changes in SWE over the twenty-first century

3.3.1.1 Projected changes in the timing and amount of peak SWE

The timing and amount of peak SWE is projected to shift dramatically in the twenty-first century, but trends are spatially heterogeneous across the circumpolar Arctic and differ substantially between the 1.5°C, 2°C and RCP 8.5 scenarios. Figure 3.3a shows the ensemble-mean change in peak SWE over the pan-Arctic domain for 1.5°C, 2°C and RCP 8.5 (top row) and the standard deviation across the ensemble for each warming scenario (bottom row), averaged over the historical period (1975-2005) and future period (2070-2099) for each snow year, which we define as starting on September 1 of each year. Slight increases in peak SWE occur in interior Alaska and Canada of less than 50 mm, while Siberia is projected to experience significantly larger increases in SWE of up to 206 mm in the northernmost tundra areas for RCP 8.5. The rest of the domain is projected to experience decreases in peak SWE, with the largest decreases occurring in coastal Alaska and British Columbia, northern Europe and coastal Greenland. Although the ensembles show variation in the amount of peak SWE projected to increase or decrease, the signal (positive or negative trend) is robust across ensemble members for a given region.

The timing of peak SWE also shows varied spatial patterns across the circumpolar Arctic. Figure 3.3b shows the shift in timing of peak SWE for the ensemble mean (top row) and the standard deviation across the ensemble (bottom row) for the three warming scenarios. Blue

(positive) indicates that peak SWE has shifted to later in the year, while red (negative) indicates that peak SWE has shifted to earlier in the year. Parts of Eurasia for the 1.5°C and 2°C warming scenarios show shifts in peak SWE to 12-24 days later in the year, and coastal Greenland shows much larger shifts of one or more months. But most of the domain shows shifts to earlier in the year of 1-2 weeks. In RCP 8.5, peak SWE shifts to earlier in the year by 2-3 weeks over most of the domain, including in the parts of Eurasia that showed shifts to earlier in the year for the 1.5°C and 2°C warming scenarios. The largest temporal shifts in peak SWE by 2-3 weeks to earlier in the year occur for RPC 8.5 in the North American boreal forest and Eurasia, while the largest shifts to later in the year of 1-2 months occur in coastal Greenland. As in Figure 3.3a, the signal in shifting peak SWE is largely robust across the ensemble members.

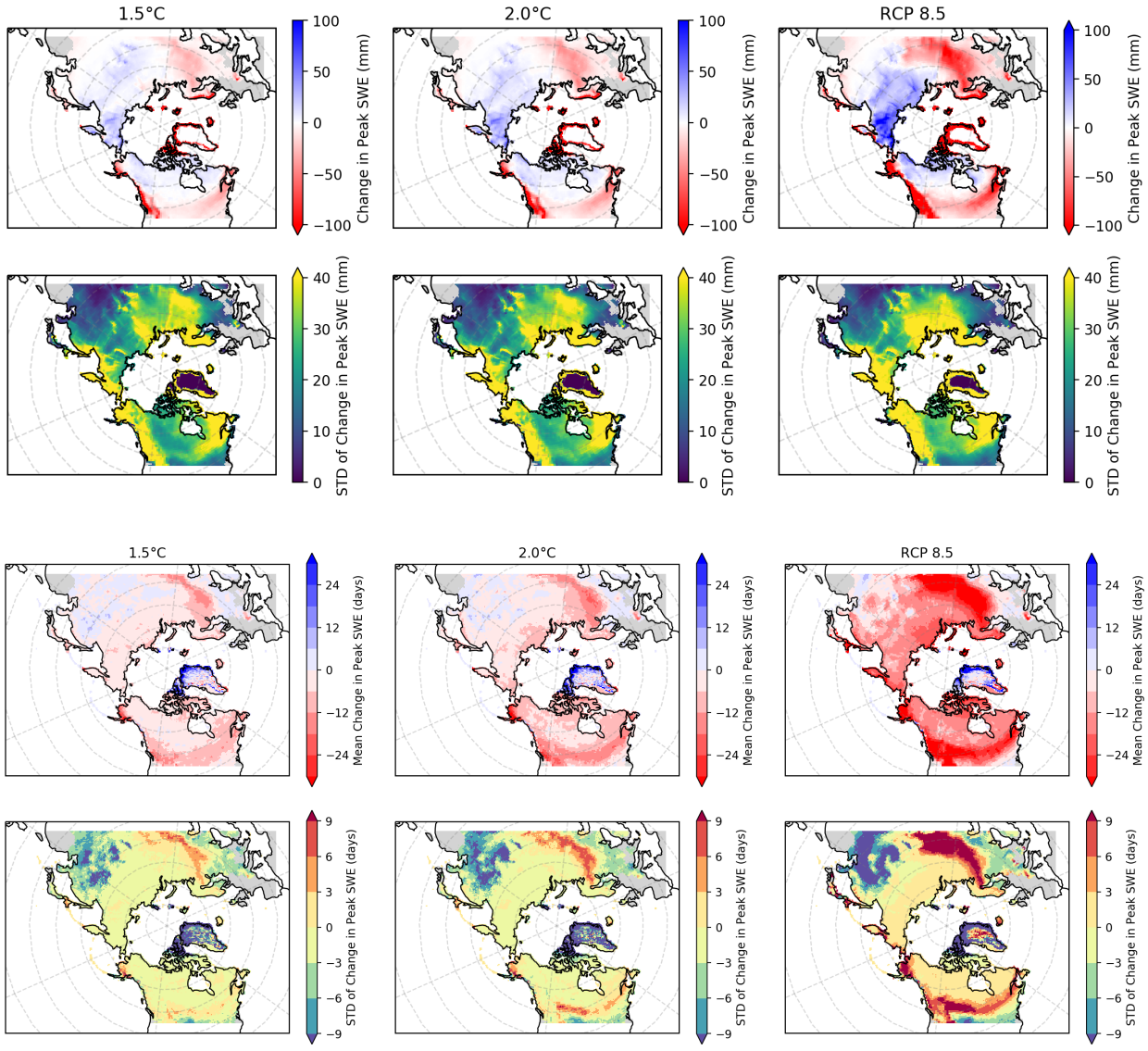

Figure 3.3. Projected changes in the amount and timing of peak SWE for the three warming scenarios. Figure 3.3a shows projected changes in the amount of SWE as a difference between future (2070-2099) and historical (1975-2005) as the ensemble-mean (top row) and standard deviation (bottom row). Figure 3.3b shows projected changes in the timing of peak SWE for the same warming scenarios and time periods, with the ensemble-mean change in peak SWE (top row) and standard deviation (bottom row).

3.3.1.2 Projected changes in the timing of the snow season: snow onset, snow disappearance and snow duration

The length of the snow season is projected to change robustly across the Arctic, with a later date of first snowfall, an earlier date of snow disappearance and a shorter snow season

duration. Figure 3.4 shows the ensemble-mean shift in snow onset (4a), snow disappearance (4b) and snow season duration (4c) between the future (2070-2099) and historical (1975-2005) periods for each warming scenario. For this analysis, we mask gridcells with a historical mean snow duration of less than two months. The date of snow onset shifts on average across the domain by 0.85, 1.2 and 3 weeks for the three warming scenarios, respectively, with a maximum for RCP 8.5 of a 10-week shift over parts of northern Europe. While much of the tundra parts of the domain shift by only a few days for 1.5°C, under RCP 8.5 those same areas shift by at least a week, and most parts of the tundra shift by more than two weeks. The snow disappearance date shifts to earlier in the year by about one week for all parts of the domain except for the North American boreal forest and part of Northern Europe, which shifts by 1-2 weeks. For RCP 8.5, the snow disappearance date for the North American boreal forest, Northern Europe and part of Central Asia shifts by up to two months. The snow season duration shrinks across the entire pan-Arctic domain for all warming scenarios, but the number of days by which the snow season is shortened changes significantly between 1.5°C warming and RCP 8.5, with most of the domain shifting by less than 20 days for 1.5°C but for RCP 8.5 the snow season is shortened by 2-3 months. Overall, the greatest shortening of the snow season duration occurs in the North American boreal forest, the northernmost part of Canada, and Europe. These parts of the domain are projected to experience the greatest amount of warming (relative to other parts of the pan-Arctic domain) by the end of the twenty-first century, thus in these areas increases in SATs are overwhelming coincident increases in precipitation.

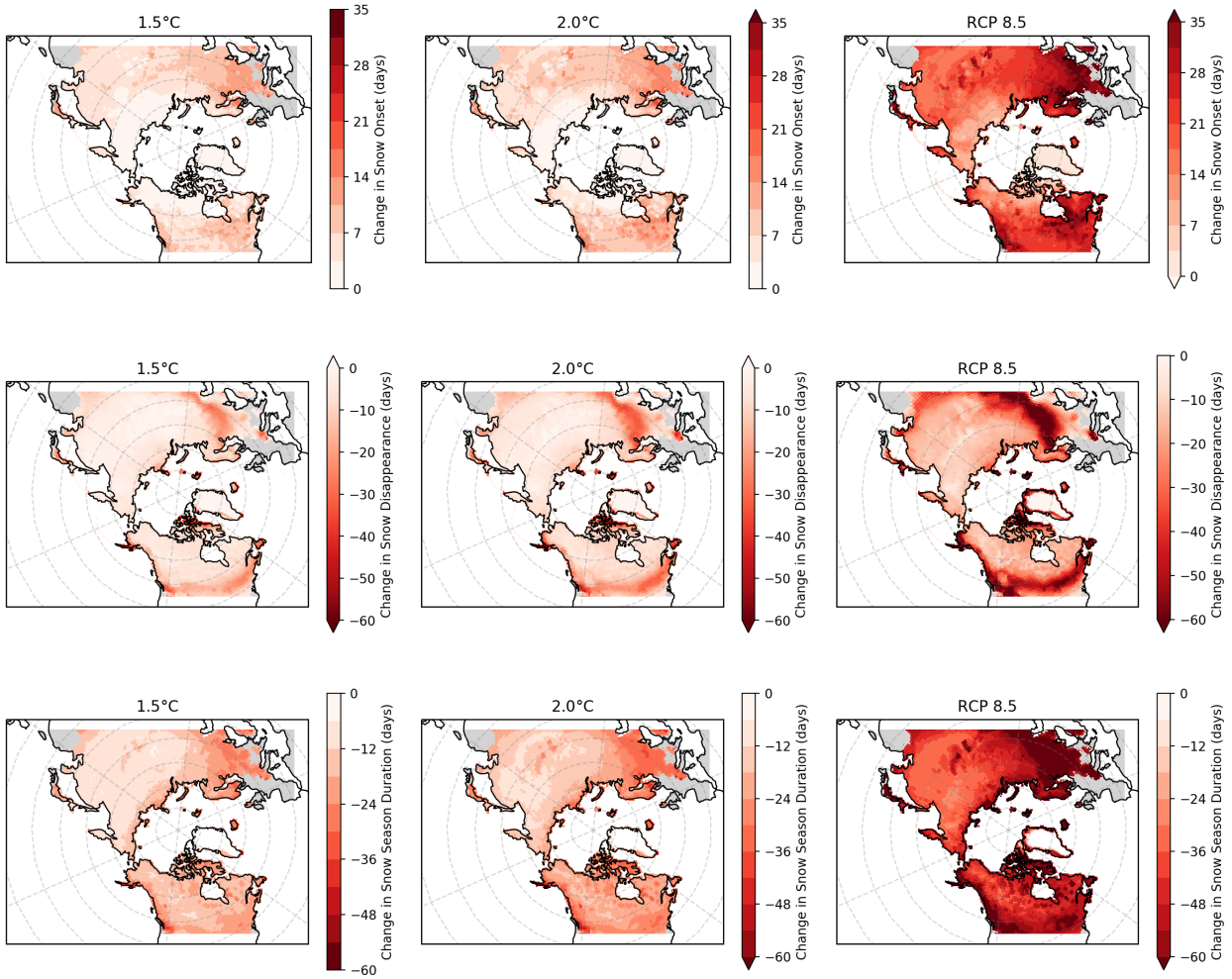

Figure 3.4. Projected changes in the timing of the snow season for the three warming scenarios, with differences between the future (2070-2099) and historical (1975-2005) periods. Figure 3.4a (top row) shows the change in snow onset, Figure 3.4b (middle row) shows snow disappearance date, and Figure 3.4c shows the change in snow season duration.

3.3.2 Future changes in soil temperatures over the twenty-first century

3.3.2.1 Changes in soil temperatures per °C warming

Projected increases in SAT and precipitation have strong effects on the ground thermal regime, but these effects vary across the Arctic. There is also significant vertical heterogeneity because of the damping effect of diurnal variation in the soil. Changes in air temperature have varying effects on soil temperature depending on local snow conditions and the opposing effects

of increasing precipitation, the decreasing length of the snow season and increased SATs, as well as whether or not increased SATs have resulted in shifts in precipitation from snow to rain. Figure 3.5a shows projected changes in soil temperatures for the first, seventh and tenth soil layers, corresponding to depths of 0 m, 0.62 m, and 4.7 m, respectively, for each warming scenario. These soil layers are representative of three distinct patterns with respect to variation in SAT: the surface layer is highly dependent on diurnal variation, the seventh soil layer roughly corresponds to the depth at which the soil is no longer dependent on diurnal variation and only varies seasonally, and the tenth soil layer responsive only to changes in the annual mean air temperature. Figure 3.5b shows projected changes in soil temperatures per °C annual-mean SAT warming in the twenty-first century (2005-2100) for the same soil layers as in Figure 3.5a. The change in soil temperature shows a damping signal between warming scenarios for each soil layer as the amount of annual-mean warming increases from 1.5°C to RCP 8.5. Changes in soil temperatures of ~2°C/°C annual-mean warming are evident in some parts of the Arctic, such as the boreal forest in the seventh layer, and ~1°C/°C in parts of the tundra for the tenth soil layer. For RCP 8.5., few parts of the domain exhibit greater than 1°C/°C warming except for small areas along the coast of Greenland. For all three soil layers shown, coastal Greenland lacks the damping signal characteristic of the rest of the domain, which suggests that soil temperature warming throughout the soil column is keeping pace with increases in SATs, likely due to the large volume of SWE lost in that area (see Figure 3.3a).

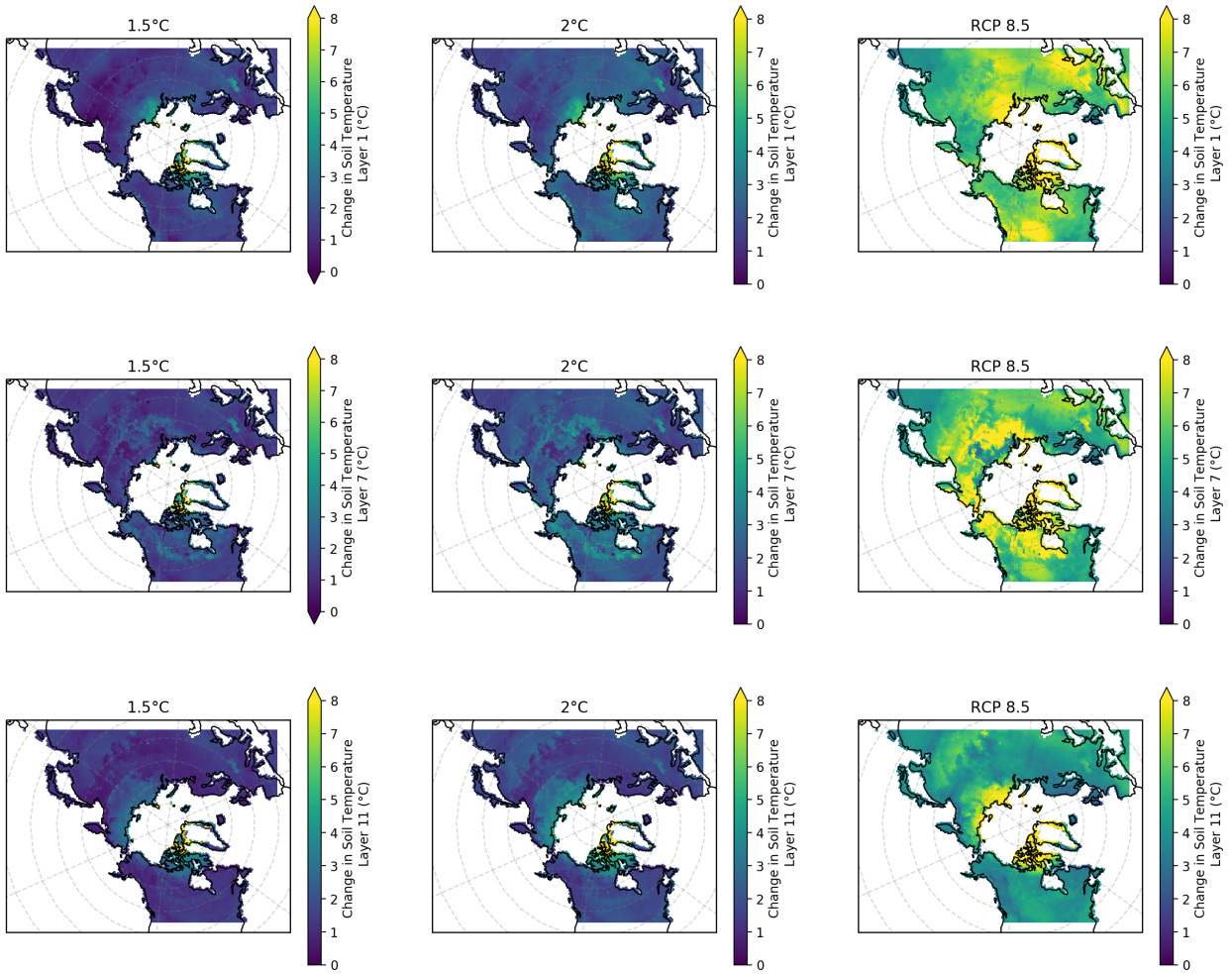

Figure 3.5a. Projected change in soil temperatures for the three warming scenarios between future (2070-2099) and historical (1975-2005) periods. Rows represent soil layer temperatures at depths of 0m (top row), 0.62m (middle row), and 4.7m (bottom row).

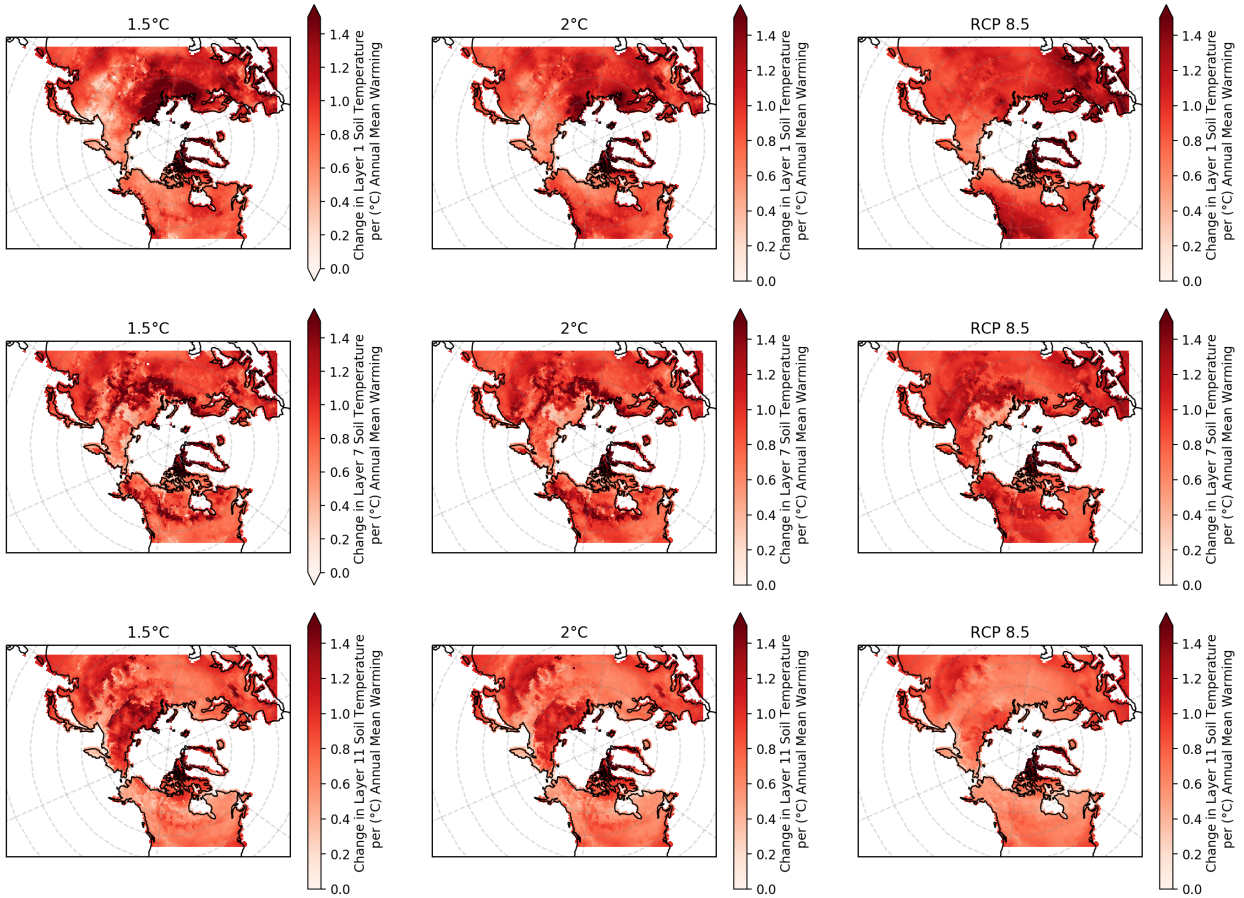

Figure 3.5b. Projected change in soil temperatures per °C warming for the three warming scenarios, time periods and soil layer depths as in Figure 3.5a.

3.3.3 Future trajectories of permafrost

Changes in the ground thermal regime affect the distribution and areal coverage of circumpolar permafrost, resulting in loss of permafrost area as well as shifts from continuous to discontinuous permafrost and a deepening of the active layer, the layer of soil that seasonally freezes and thaws, in areas characterized by discontinuous and sporadic permafrost. Figure 3.6 shows projected changes in the amount of permafrost area (in million km^2) over the circumpolar Arctic, with the ensemble-mean for each warming scenario shown in solid, darker lines and the full range of each ensemble shown shaded. The projected loss of permafrost area remains roughly the same for the 1.5°C and 2°C scenarios until around 2040, after which it diverges. By

the end of the twenty-first century the ensemble-mean projected loss in permafrost area is about 1.5 million km^2 larger for 2°C than 1.5°C warming; ensemble-mean permafrost area is 10.9 million km^2 for 1.5°C and 9.2 million km^2 for 2°C . Loss of permafrost area is significantly larger for RCP 8.5, with the ensemble-mean permafrost area 2.0 million km^2 by 2100, a loss of 13.5 million km^2 since the end of the twentieth century (averaged over the historical period, shown in black).

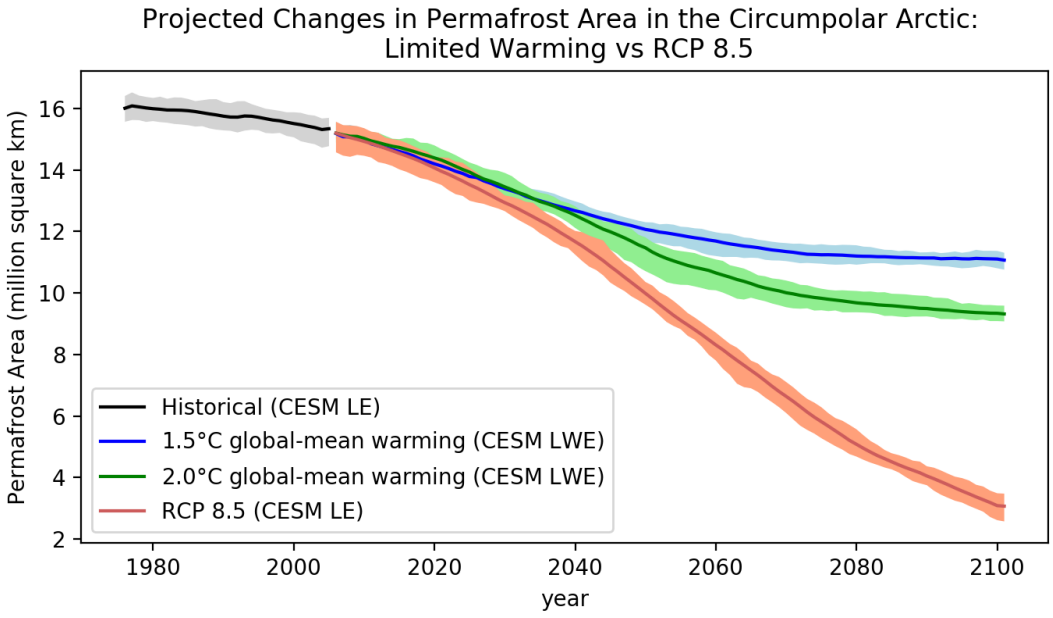

Figure 3.6. Projected changes in permafrost area for the three warming scenarios from 1975-2100. Shaded areas for each ensemble represent the full ensemble range for the 11 members of the LWE and the 35 members of the CESM-LE.

Another way of understanding permafrost trajectories in the Arctic is to examine the amount of permafrost lost in conjunction with the amount of cumulative warming anomalies for each warming scenario. Cumulative freezing degree days (FDD; days with temperatures below 0°C) and their inverse, thawing degree days (TDD; days with temperatures greater than 0°C), have been closely linked to Arctic SIE anomalies; Ricker et al. (2017) found that a record low in Arctic SIE coincided with a negative peak anomaly of 1000 cumulative FDDs over the Barents

Sea. We define a similar metric to TDDs, which we call thawing degree months (TDMs). TDMs are defined as months where monthly mean temperature is greater than 0°C. Daily surface air temperature was not archived as part of the LWE and CESM-LE, only monthly surface temperature is available for the full ensembles, which is why we use a metric based on monthly rather than daily data. We calculate cumulative TDM anomalies for each grid cell, meaning the cumulative departure from the climatological mean number of TDMs for 1975-2005. Figure 3.7 shows cumulative yearly TDM anomalies from 2021-2100 across the circumpolar Arctic and total circumpolar permafrost area for each warming scenario. We exclude the period from 2006-2020 since the number of cumulative TDM anomalies was too noisy relative to the historical TDM values. For the two LWE warming scenarios, the climatological average of yearly cumulative TDM anomalies stabilizes at 5.31×10^3 and 9.07×10^3 for the end of the twenty-first century (2070-2099), respectively, and permafrost area continues to decrease after this stabilization, with an additional loss of ~2 million km^2 of permafrost area by 2100. For RCP 8.5, the number of cumulative TDM anomalies does not stabilize and increases steadily to a maximum of 3.45×10^4 by 2100. In part, this is due to how the LWE warming scenarios were constructed, whereby warming stabilizes by the 2080s (see Sanderson et al. 2016 for more details on this), which does not occur for RCP 8.5. However, this figure also shows that permafrost area loss continues beyond the point at which warming anomalies plateau, which could indicate continued permafrost loss past the point where changes in surface temperature plateau.

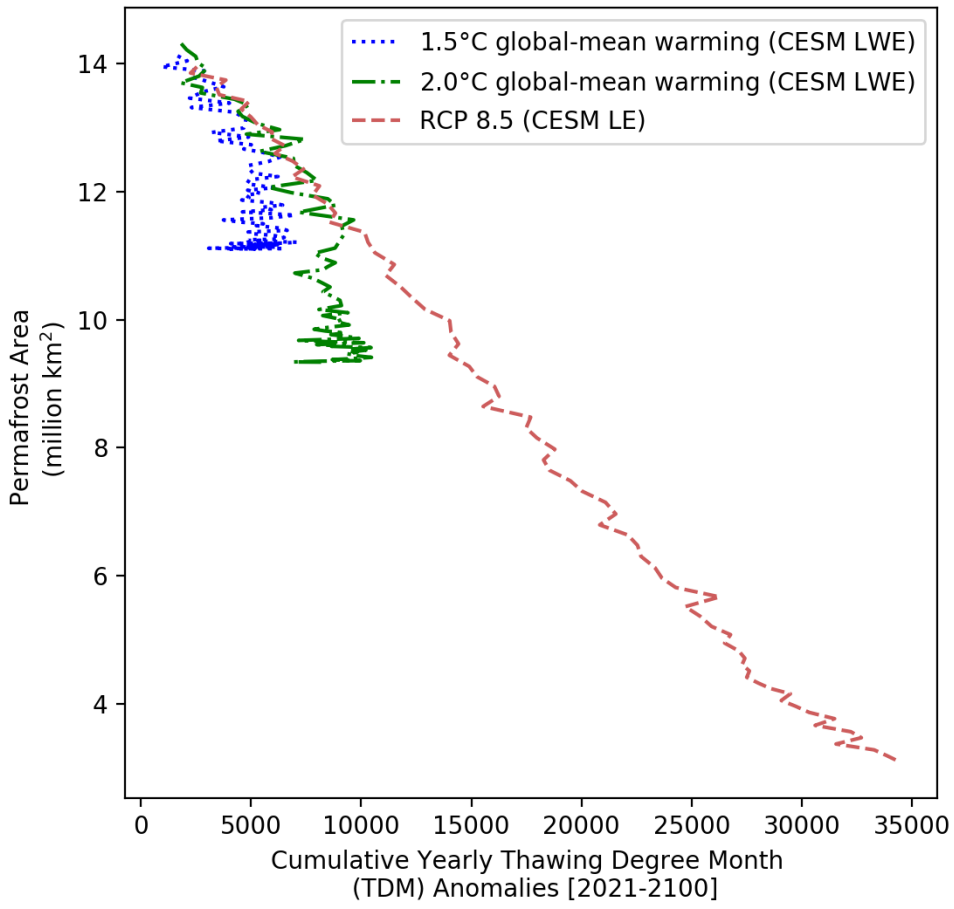

Figure 3.7. Projected permafrost area changes and cumulative Thawing Degree Month (TDM) anomalies. TDMs are defined as months in which monthly mean temperature is above 0°C.

3.3.4 Combined impacts of changes in SWE and surface air temperatures on the ground thermal regime

Although changes in SATs and SWE both impact the ground thermal regime, they have differential effects depending on the extent to which future changes in temperature and precipitation occur and which effect dominates. Figure 3.8 shows a scatterplot for each of the nine hydroclimate classes, with each point representing a single gridcell in that hydroclimate class. Different point markers represent different warming scenarios. Change in SAT is

calculated over the winter (NDJFM) months, change in soil temperature is the mean August climatological temperature of the seventh soil layer (corresponding to a depth of 0.62m) over each ensemble, and mean SWE is averaged over winter (NDJFM) as well. Each point is shaded by its percent change in ensemble-mean winter SWE, with a 1:1 line shown in black. We chose the seventh soil layer for analysis because it is sufficiently deep so as not to be affected by the diurnal cycle of surface temperature but rather by seasonal fluctuations in surface temperature. The nine hydroclimate classes show a range of behaviors between effects from increases in SATs and precipitation. Nearly all of the gridcells in the three warmest classes, arid, temperate_dry and cold_wds_ws no permafrost, lose their snow under projected warming conditions. In the colder permafrost classes (namely cold_dry_perma and cold_wds_cs_perma), many gridcells experience increases in mean SWE, with the largest increases in SWE also occurring for gridcells experiencing the greatest amount of SAT increase.

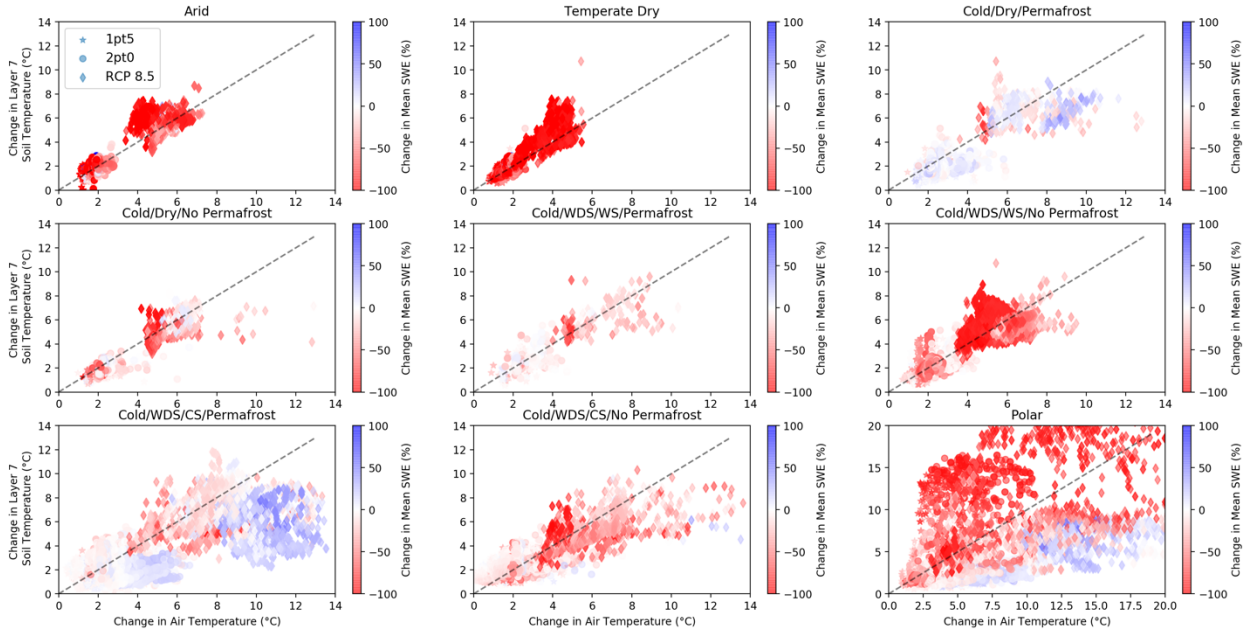

Figure 3.8. Projected changes in mean SWE and soil temperature (represented by the seventh layer, corresponding to a depth of 0.62 m), for each of the nine hydroclimate classes defined in Figure 3.2.

It is notable that for those gridcells projected to experience increases in mean SWE, their soil temperatures do not warm as much as other gridcells in those classes, suggesting that increases in SWE are insulating the soil from experiencing additional warming from increasing SATs. This behavior is particularly apparent in the cold_wds_cs_perma class, where SATs increase up to 14°C for some gridcells. However, increases in soil temperatures for those same gridcells do not exceed a delta value of just over 4°C, while other gridcells in the same class that experience decreases in mean SWE have soil temperatures increasing by the same magnitude as that of SAT. The same behavior is apparent in the polar class as well, where gridcells with increases in mean SWE experience much smaller increases in soil temperatures relative to increases in SATs, with all gridcells experiencing increases in mean SWE falling below the 1:1 line. By contrast, gridcells projected to experience decreases in mean SWE experience much more comparable increases in soil temperatures to increases in SATs. The majority of gridcells in the cold_wds_cs no perma class experience analogous increases in soil temperature as in SATs. The same behavior is evident in the warmer permafrost class, cold_wds_ws_perma, with the exception of a small number of gridcells with relatively minor increases in soil and air temperature. Gridcells with decreases in SWE are losing insulation that previously buffered soil temperatures from being affected by SATs and are thus vulnerable to soil temperatures increasing in tandem with SATs and associated increases in active layer thickness and carbon release.

3.3.5 Implications of permafrost trajectories on carbon release

Projected changes in the ground thermal regime have strong effects on the potential for soil carbon to be released from previously frozen soil. The pan-Arctic domain holds significant

amounts of soil organic carbon (SOC), which becomes increasingly vulnerable as permafrost thaws and the soil active layer deepens. Figure 3.9 shows the amount of SOC stocks (in kg/m^2), over the pan-Arctic domain, for soil depths of 0-100cm, 100-200cm, and 200-300cm (9a) and total SOC stocks overlain by the amount of permafrost remaining for RCP 8.5 and the amount of permafrost lost for RCP 8.5 relative to the historical period (9b). As is evident from the figure, the largest amount of SOC is concentrated in the permafrost region of the Arctic and is generally in the first 100cm of soil, where some gridcells in Central Asia and Canada have total SOC stocks exceeding 500 kg/m^2. The amount of SOC decreases deeper in the soil column, with the exception of some small areas in Canada which contain more than 500 kg/m^2 at a depth of 300cm below the surface. But the majority of SOC stocks are concentrated in the parts of the Arctic where continuous permafrost is projected to be lost, which is stippled in Figure 3.9b.

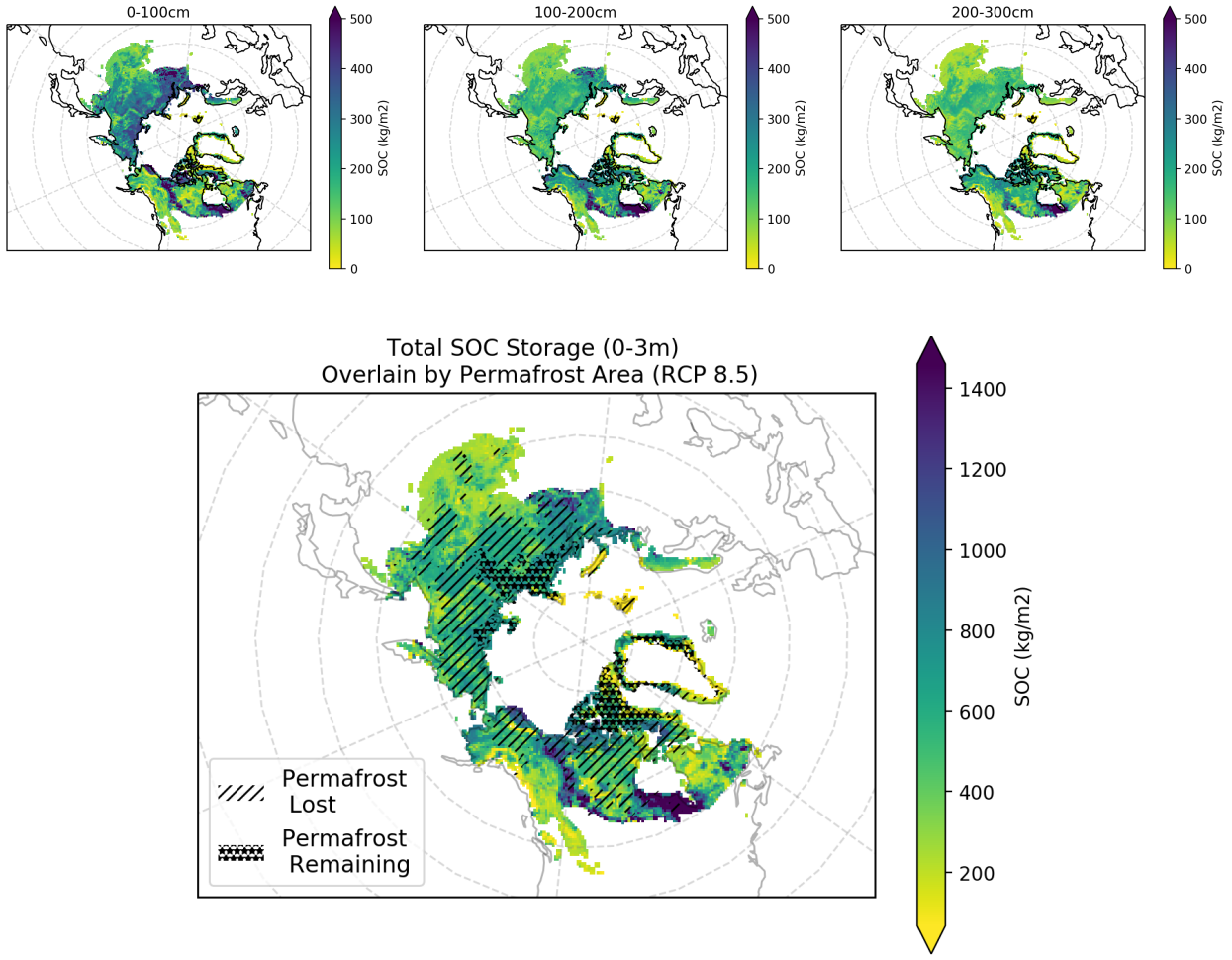

Figure 3.9. Implications for soil organic carbon (SOC) stocks from permafrost losses. Figure 3.9a (top) shows the amount of SOC stocks in three soil layers: 0-30cm (left), 100-200cm (middle), and 200-300cm (right), as estimated by the Northern Circumpolar Carbon Database version 2 (NCSCD v2) dataset. Figure 3.9b shows the total SOC stock (sum of all layers) overlain by the amount of permafrost area lost between the historical period (1975-2005) and future (2070-2099) periods.

Most of the historically permafrost-covered area contains an average of 600 kg/m^2 of SOC stocks, and in much of this area SOC is concentrated in the first 30cm of soil (see Figure 3.9a), which under RCP 8.5. will no longer be permanently frozen, meaning that the soil will seasonally thaw and the SOC in this layer could be released into the atmosphere. Table 3.1 shows the amount of vulnerable SOC stock (in Gigatons) due to permafrost loss by the 2080s for the three warming scenarios for each soil layer. The amount of vulnerable SOC for the 2°C

warming scenario is about twice that of 1.5°C , and then for RCP 8.5 the amount of SOC that could be released is significantly larger. Most concerning is that the largest amount of SOC is contained in the 0-100 cm (near-surface) layer, which is the layer most vulnerable to warming SATs in the Arctic as active layer thicknesses deepen. Considered in conjunction with the permafrost trajectories discussed earlier, the potential for large amounts of carbon to be released into the atmosphere as permafrost shifts occur is large.

	1.5°C	2°C	RCP 8.5
0-30cm	0.95	1.78	6.22
0-100cm	2.08	3.88	13.53
100-200cm	1.88	3.37	10.47
200-300cm	1.45	2.64	8.63

Table 3.1. Vulnerable soil organic carbon (SOC) stock (in GtC) due to permafrost loss by the 2080s for the soil layers defined in the NCSCDv2.

3.4 Discussion

We have used the low warming ensemble and the CESM-LE, representing three distinct future warming scenarios, including 1.5°C and 2°C global-mean warming pathways from the low warming ensemble and RCP 8.5 for the CESM-LE, to examine how changes in snow cover, induced by projected increases in precipitation and SATs, affect soil temperatures and hence permafrost across the circumpolar Arctic and how changes in permafrost and active layer depth impact the climate system. Although we did not directly examine sea ice metrics, we used a proxy for SIE anomalies, cumulative yearly TDM anomalies. Past terrestrial studies of

interactions between SWE and soil thermal regimes had not compared these interactions for different levels of warming. Our results for changes in SWE are largely consistent with previous studies (e.g. Deser et al., 2010; Liu et al., 2012) in that we found substantial increases in SWE projected over Eurasia for the higher-warming scenarios (2°C and RCP 8.5), smaller yet insignificant increases over the Canadian Arctic, and decreases in most other parts of the domain. Ghatak et al. (2012) found that projected increases in Eurasian snow cover would not occur without sea ice loss in the Arctic Ocean, and Liu et al. (2012) had the same conclusion and extended it to encompass the Canadian Arctic as well. We found significant differences in the number of cumulative yearly TDM anomalies between the different low warming scenarios, with nearly twice as many TDM anomalies occurring by 2100 for the 2°C versus the 1.5°C warming scenario. Sigmond et al. (2018) found a corresponding difference between these scenarios for sea ice loss as well, with the probability of ice-free conditions occurring increasing from every forty to every five years between the two scenarios. Together, these indicate that changes in sea ice could be correlated with terrestrial changes in SWE, and changes in sea ice are a strong driver of Arctic amplification and associated changes in precipitation driven by increased surface evaporation. The recent work on Arctic amplification by Dai et al. (2019) analyzing sea ice cover in historical reanalysis data and output from 38 CMIP5 models reinforces this argument.

Permafrost is strongly affected by these differential changes in snow cover. Our results for permafrost trajectories under limited warming and RCP 8.5 are also consistent with existing studies with which to compare. No studies thus far have calculated permafrost trajectories for the low warming ensemble or analyzed soil warming in the low warming ensemble relative to RCP 8.5. But for RCP 8.5, Slater and Lawrence (2013) found that permafrost area would decrease to just over 2 million km^2 by 2100, averaged over 17 CMIP5 models (including CESM), which is

very close to our estimate. Wang et al. (2019) found that 12.65 million km^2 of permafrost remained by 2100, also by averaging over CMIP5 models, but their estimate likely departs significantly from ours and that of Slater and Lawrence (2013) because the authors used the Kudryavtsev method (see Kudryavtsev et al., 1977), rather than the mean soil temperature (MST) method of Slater and Lawrence (2013), which we use. Why their method results in such a drastically larger estimate is beyond the scope of this study, but it is likely because it may not correctly account for future climate change.

Regardless, with such a large loss of permafrost projected, and given the large amount of SOC stocks in the circumpolar Arctic (see Figure 3.9a), there is a high likelihood that the amount of carbon released from melting permafrost will accelerate through the end of the twenty-first century. The amount of vulnerable SOC stocks in the Arctic due to projected permafrost losses is extremely large (see Table 3.1), and our study departs from past studies of permafrost trajectories under climate warming by quantifying soil carbon stocks that are potentially at risk due to permafrost loss under different warming scenarios. Since we used continuous permafrost loss rather than active layer thickness to calculate these values, we cannot infer the depth of SOC stock that would be affected by loss of permafrost, e.g. the soil column depth affected could be shallow in some vulnerable areas and much deeper in others. But even if we only consider that the top 30cm of SOC is particularly vulnerable to permafrost melt, that would still amount to 6.2 Gt of SOC for RCP 8.5. For reference, total CO_2 emissions in 2017 from fossil fuels and industry were 36.2 Gt (Global Carbon Project), thus a conservative projection of the amount of SOC that would be released into the atmosphere is about one-sixth of that total.

3.5 Conclusion

In conclusion, our results illustrate the profound changes that will occur in the Arctic terrestrial system, even under conditions of low emissions scenarios represented by the 1.5°C and 2°C global-mean warming pathways. In particular, our key findings are:

1) Projected changes in the timing and amount of peak SWE are large, with the majority of the domain projected to experience significant decreases in SWE, particularly coastal Greenland. Siberia, by contrast, is projected to experience substantial increases in SWE, and these patterns intensify from the lower to higher warming scenarios. The timing of peak SWE shifts to earlier in the year by 2-3 weeks for most of the domain for RCP 8.5, with the exception of Greenland, which shifts to later in the year due to the changing seasonality of snow cover in coastal Greenland.
2) Changes in SWE have a strong effect on soil thermal regimes, with the entire soil column showing significant warming by the end of the twenty-first century. This is projected to result in a loss of permafrost of up to 11.5 million km^2 for RCP 8.5, averaged over the CESM-LE.
3) The vulnerability of SOC stocks in the Arctic is high, particularly for RCP 8.5. A conservative estimate of the amount of vulnerable SOC for RCP 8.5, only in the top layer of soil, could potentially result in a loss of 6.2 Gt of carbon to the atmosphere, though the actual number is likely to be significantly higher.

Since current emissions are not being constrained by the 2015 Paris Agreement, encapsulated in the low emissions scenarios, it is highly likely that we will see even larger changes than those we see for those scenarios by the end of the twenty-first century. Current emission reduction policies limit global-mean warming to about 3°C by 2100 (Sigmond et al. 2018), putting the Arctic on a

warming pathway that looks much like the most extreme warming that we discuss in this study if nations around the world do not commit to supporting the Paris Agreement.

3.6 References

Bintanja, R. (2018). The impact of Arctic warming on increased rainfall. *Scientific Reports*, *8*(1), 1–6. https://doi.org/10.1038/s41598-018-34450-3

Bintanja, R., & Andry, O. (2017). Towards a rain-dominated Arctic. *Nature Climate Change*, *7*(4), 263–267. https://doi.org/10.1038/nclimate3240

Bintanja, R., & Selten, F. M. (2014). Future increases in Arctic precipitation linked to local evaporation and sea-ice retreat. *Nature*, *509*(7501), 479–482. https://doi.org/10.1038/nature13259

Biskaborn, B. K., Smith, S. L., Noetzli, J., Matthes, H., Vieira, G., Streletskiy, D. A., … Lantuit, H. (2019). Permafrost is warming at a global scale. *Nature Communications*, *10*(1), 1–11. https://doi.org/10.1038/s41467-018-08240-4

Brown, J., Sidlauskas, F. J., & Delinski, G. (1997). *Circum-Arctic map of permafrost and ground ice conditions*. Reston, Va. : Denver, Colo: The Survey ; For sale by Information Services.

Brown, R. D., & Robinson, D. A. (2011). Northern Hemisphere spring snow cover variability and change over 1922–2010 including an assessment of uncertainty. *The Cryosphere*, *5*(1), 219–229. https://doi.org/10.5194/tc-5-219-2011

Brutel-Vuilmet, C., Ménégoz, M., & Krinner, G. (2013). An analysis of present and future seasonal Northern Hemisphere land snow cover simulated by CMIP5 coupled climate models. *The Cryosphere*, *7*(1), 67–80. https://doi.org/10.5194/tc-7-67-2013

Dai, A., Luo, D., Song, M., & Liu, J. (2019). Arctic amplification is caused by sea-ice loss under increasing CO 2. *Nature Communications*, *10*(1), 1–13. https://doi.org/10.1038/s41467-018-07954-9

Deser, C., Tomas, R., Alexander, M., & Lawrence, D. (2010). The Seasonal Atmospheric Response to Projected Arctic Sea Ice Loss in the Late Twenty-First Century. *Journal of Climate*, *23*(2), 333–351. https://doi.org/10.1175/2009JCLI3053.1

Gastineau, G., García-Serrano, J., & Frankignoul, C. (2017). The Influence of Autumnal Eurasian Snow Cover on Climate and Its Link with Arctic Sea Ice Cover. *Journal of Climate*, *30*(19), 7599–7619. https://doi.org/10.1175/JCLI-D-16-0623.1

Ghatak, D., Frei, A., Gong, G., Stroeve, J., & Robinson, D. (2010). On the emergence of an Arctic amplification signal in terrestrial Arctic snow extent. *Journal of Geophysical Research: Atmospheres*, *115*(D24). https://doi.org/10.1029/2010JD014007

Ghatak, D., Deser, C., Frei, A., Gong, G., Phillips, A., Robinson, D. A., & Stroeve, J. (2012). Simulated Siberian snow cover response to observed Arctic sea ice loss, 1979–2008. *Journal of Geophysical Research: Atmospheres*, *117*(D23). https://doi.org/10.1029/2012JD018047

Global Carbon Project. Accessed July 15, 2019. https://www.globalcarbonproject.org/.

Hamman, J., Nijssen, B., Brunke, M., Cassano, J., Craig, A., DuVivier, A., … Zeng, X. (2016). Land Surface Climate in the Regional Arctic System Model. *Journal of Climate*, *29*(18), 6543–6562. https://doi.org/10.1175/JCLI-D-15-0415.1

Hugelius, G., Tarnocai, C., Broll, G., Canadell, J. G., Kuhry, P., & Swanson, D. K. (2013a). The Northern Circumpolar Soil Carbon Database: Spatially distributed datasets of soil

coverage and soil carbon storage in the northern permafrost regions. *Earth System Science Data*, *5*(1), 3–13, doi: 10.5194/essd-5-3-2013

Hugelius, G., Bockheim, J.G., Camill, P., Elberling, B., Grosse, G., Harden, J.W., Johnson, K., Jorgenson, T., Koven, C.D., Kuhry, P., Michaelson, G., Mishra, U., Palmtag, J., Ping, C-L., O'Donnell, J., Schirrmeister, L., Schuur, E.A.G., Smith, L.C., Strauss, J., Yu., Z. (2013b). A new data set for estimating organic carbon storage to 3 m depth in soils of the northern circumpolar permafrost region. *Earth System Science Data*, *5*(1), 393-402, https://doi.org/10.5194/essd-5-393-2013

Hurrell, J. W., Holland, M. M., Gent, P. R., Ghan, S., Kay, J. E., Kushner, P. J., … Marshall, S. (2013). The Community Earth System Model: A Framework for Collaborative Research. *Bulletin of the American Meteorological Society*, *94*(9), 1339–1360. https://doi.org/10.1175/BAMS-D-12-00121.1

Jordan, R. (1991). *A One-Dimensional Temperature Model for a Snow Cover: Technical Documentation for SNTHERM.89.* (No. CRREL-SR-91-16). Retrieved from Cold Regions Research and Engineering Lab Hanover, NH: https://apps.dtic.mil/docs/citations/ADA245493

Kay, J. E., Deser, C., Phillips, A., Mai, A., Hannay, C., Strand, G., … Vertenstein, M. (2014). The Community Earth System Model (CESM) Large Ensemble Project: A Community Resource for Studying Climate Change in the Presence of Internal Climate Variability. *Bulletin of the American Meteorological Society*, *96*(8), 1333–1349. https://doi.org/10.1175/BAMS-D-13-00255.1

Kudryavtsev, V. A., Garagulya, L. S., Kondrat yeva, K. A., & Melamed, V. G. (1977). *Fundamentals of Frost Forecasting in Geological Engineering Investigations (Osnovy*

Merzlotnogo Prognoza pri Inzhenerno-Geologicheskikh Issledovaniyakh), (No. CRREL-TL-606). Retrieved from COLD REGIONS RESEARCH AND ENGINEERING LAB HANOVER N H website: https://apps.dtic.mil/docs/citations/ADA039677

Lawrence, D. M., & Slater, A. G. (2010). The contribution of snow condition trends to future ground climate. *Climate Dynamics*, *34*(7), 969–981. https://doi.org/10.1007/s00382-009-0537-4

Lawrence, D. M., Slater, A. G., Romanovsky, V. E., & Nicolsky, D. J. (2008). Sensitivity of a model projection of near-surface permafrost degradation to soil column depth and representation of soil organic matter. *Journal of Geophysical Research: Earth Surface*, *113*(F2). https://doi.org/10.1029/2007JF000883

Liston, G. E., & Hiemstra, C. A. (2011). The Changing Cryosphere: Pan-Arctic Snow Trends (1979–2009). *Journal of Climate*, *24*(21), 5691–5712. https://doi.org/10.1175/JCLI-D-11-00081.1

Liu, J., Curry, J. A., Wang, H., Song, M., & Horton, R. M. (2012). Impact of declining Arctic sea ice on winter snowfall. *Proceedings of the National Academy of Sciences*, *109*(11), 4074–4079. https://doi.org/10.1073/pnas.1114910109

Oleson, K. W., Lawrence, D. M., B, G., Flanner, M. G., Kluzek, E., J, P., … Decker, M. (2010). *Technical Description of version 4.0 of the Community Land Model (CLM)*.

Park, H., Fedorov, A. N., Zheleznyak, M. N., Konstantinov, P. Y., & Walsh, J. E. (2015). Effect of snow cover on pan-Arctic permafrost thermal regimes. *Climate Dynamics*, *44*(9), 2873–2895. https://doi.org/10.1007/s00382-014-2356-5

Park, H., Yabuki, H., & Ohata, T. (2012). Analysis of satellite and model datasets for variability and trends in Arctic snow extent and depth, 1948–2006. *Polar Science*, *6*(1), 23–37. https://doi.org/10.1016/j.polar.2011.11.002

Räisänen, J. (2008). Warmer climate: Less or more snow? *Climate Dynamics*, *30*(2), 307–319. https://doi.org/10.1007/s00382-007-0289-y

Rawlins, M. A., Steele, M., Holland, M. M., Adam, J. C., Cherry, J. E., Francis, J. A., … Zhang, T. (2010). Analysis of the Arctic System for Freshwater Cycle Intensification: Observations and Expectations. *Journal of Climate*, *23*(21), 5715–5737. https://doi.org/10.1175/2010JCLI3421.1

Ricker, R., Hendricks, S., Girard-Ardhuin, F., Kaleschke, L., Lique, C., Tian-Kunze, X., … Krumpen, T. (2017). Satellite-observed drop of Arctic sea ice growth in winter 2015–2016. *Geophysical Research Letters*, *44*(7), 3236–3245. https://doi.org/10.1002/2016GL072244

Robinson, D. A., & Frei, A. (2000). Seasonal Variability of Northern Hemisphere Snow Extent Using Visible Satellite Data. *The Professional Geographer*, *52*(2), 307–315. https://doi.org/10.1111/0033-0124.00226

Rubel, F., Brugger, K., Haslinger, K., & Auer, I. (2017). The climate of the European Alps: Shift of very high resolution Köppen-Geiger climate zones 1800–2100. *Meteorologische Zeitschrift*, *26*(2), 115–125. https://doi.org/10.1127/metz/2016/0816

Sanderson, B. M., O'Neill, B. C., & Tebaldi, C. (2016). What would it take to achieve the Paris temperature targets? *Geophysical Research Letters*, *43*(13), 7133–7142. https://doi.org/10.1002/2016GL069563

Sanderson, B. M., Xu, Y., Tebaldi, C., Wehner, M., O'Neill, B. C., Jahn, A., … Lamarque, J. F. (2017). Community climate simulations to assess avoided impacts in 1.5 and 2°C futures. *Earth System Dynamics*, *8*(3), 827–847. https://doi.org/10.3929/ethz-b-000191578

Serreze, M. C., Barrett, A. P., Stroeve, J. C., Kindig, D. N., & Holland, M. M. (2009). The emergence of surface-based Arctic amplification. *The Cryosphere*, 9.

Sigmond, M., Fyfe, J. C., & Swart, N. C. (2018). Ice-free Arctic projections under the Paris Agreement. *Nature Climate Change*, *8*(5), 404–408. https://doi.org/10.1038/s41558-018-0124-y

Slater, A. G., & Lawrence, D. M. (2013). Diagnosing Present and Future Permafrost from Climate Models. *Journal of Climate*, *26*(15), 5608–5623. https://doi.org/10.1175/JCLI-D-12-00341.1

Stieglitz, M., Déry, S. J., Romanovsky, V. E., & Osterkamp, T. E. (2003). The role of snow cover in the warming of arctic permafrost. *Geophysical Research Letters*, *30*(13). https://doi.org/10.1029/2003GL017337

Taylor, K. E., Stouffer, R. J., & Meehl, G. A. (2011). An Overview of CMIP5 and the Experiment Design. *Bulletin of the American Meteorological Society*, *93*(4), 485–498. https://doi.org/10.1175/BAMS-D-11-00094.1

Toure, A. M., Rodell, M., Yang, Z.-L., Beaudoing, H., Kim, E., Zhang, Y., & Kwon, Y. (2015). Evaluation of the Snow Simulations from the Community Land Model, Version 4 (CLM4). *Journal of Hydrometeorology*, *17*(1), 153–170. https://doi.org/10.1175/JHM-D-14-0165.1

Wang, A., Xu, L., & Kong, X. (2018). Assessments of the Northern Hemisphere snow cover response to 1.5 and 2.0 °C warming. *Earth System Dynamics*, *9*(2), 865–877. https://doi.org/10.5194/esd-9-865-2018

Wang, A., Zeng, X., & Guo, D. (2016). Estimates of Global Surface Hydrology and Heat Fluxes from the Community Land Model (CLM4.5) with Four Atmospheric Forcing Datasets. *Journal of Hydrometeorology*, *17*(9), 2493–2510. https://doi.org/10.1175/JHM-D-16-0041.1

Wang, C., Wang, Z., Kong, Y., Zhang, F., Yang, K., & Zhang, T. (2019). Most of the Northern Hemisphere Permafrost Remains under Climate Change. *Scientific Reports*, *9*(1), 1–10. https://doi.org/10.1038/s41598-019-39942-4

Zhang, T. (2005). Influence of the seasonal snow cover on the ground thermal regime: An overview. *Reviews of Geophysics*, *43*(4). https://doi.org/10.1029/2004RG000157

Chapter 4

New Land Surface Parameters for the Variable Infiltration Capacity Model Version 5 for Regional Earth System Modeling in the Circumpolar Arctic

This chapter is in preparation, to be submitted to *Geoscientific Model Development*.

Abstract

The Variable Infiltration Capacity version 5 (VIC-5) hydrology model is a macroscale model that has been used extensively in standalone hydrologic modeling and has also been coupled to the Regional Arctic System Model (RASM), a fully-coupled regional climate model that is run over a pan-Arctic domain. In this study, we describe the design of a new parameter set for application in VIC-5 in both standalone and fully-coupled earth system simulations. We discuss the challenges involved in designing a high-resolution parameter set in the Arctic and show how simulated streamflow differs significantly between coupled and uncoupled simulations, with fully-coupled RASM simulated streamflow performing better in comparison to observations. This somewhat surprising difference is due to a large difference in the magnitude of precipitation between coupled and uncoupled runs. Permafrost, by contrast, shows little difference between runs, despite a large difference in surface temperature when the land surface is coupled to the climate system. We conclude that attention needs to be paid to how parameters should be designed for standalone versus fully-coupled land surface modeling. Additionally, our method for parameter derivation is applicable to any geographical domain and resolution globally, and our scripts for deriving parameter sets are implemented in Python and publicly available via GitHub.

4.1 Introduction

The land surface is responsible for partitioning available energy and water as well as controlling photosynthesis and the land-atmosphere exchange of carbon dioxide (Sellers et al., 1997). Consequently, robust modeling of the climate system as a whole requires representation of these critical processes, which has been the rationale for the development of land surface models (LSMs) and their application both as standalone models and in earth system models (ESMs). LSMs – in both contexts – have two significant characteristics: 1) they represent physical processes that relate to energy, water and carbon exchange as well as interactions between those, and 2) they are designed for application in large spatial domains (e.g. regional or global) with short temporal scales (Prentice et al., 2015). To model these processes, they require gridded land surface properties as input data, such as land cover type, leaf area index (LAI), albedo, soil texture, among others (Bohn and Vivoni, 2019). However, producing gridded spatial fields of these land surface properties over large spatial domains is a major challenge in macroscale hydrologic modeling (Mizukami et al., 2017). For land surface properties that can be measured, in-situ observations and remote sensing products have been useful for deriving gridded values at high-resolution. However, in-situ observations are often not available at high-resolution, and satellite imagery may only be representative of a single snapshot in time (Bohn and Vivoni, 2019) or may only be available at a coarser resolution than the desired model resolution. Moreover, some required model parameters, such as those that are model-specific and do not have a physical corollary, cannot be directly related to measured quantities and must be either calibrated or assigned values empirically and/or based on a priori assumptions.

Because of these challenges, large domain studies, such as over the contiguous United States (CONUS), have sometimes used uncoordinated sub-regional calibrations performed by

multiple institutions at different times, termed "patchwork parameters." However, since there is no consensus on how to upscale these parameters to larger domains, studies have oftentimes instead used a priori parameterizations based on some combination of expert opinion, case studies conducted in regions other than the one being studied, field data, hydrologic theory, and, at times, datasets of questionable quality and provenance (Beck et al., 2016). Relying on a priori parameterizations, rather than calibration, also has the advantage of avoiding oft-used computationally intensive calibration methods, such as the shuffled complex evolution (SCE) method (Duan et al., 1993).

A more recent method to address these parameter regionalization and calibration challenges has been the development of the Multiscale Parameter Regionalization (MPR) approach, which uses transfer functions to convert geophysical properties such as soil texture information, organic matter content, and land cover to model parameters at the resolution of the geophysical data and then upscales them to the desired model resolution (Mizukami et al., 2017). The MPR approach was first developed by Samaniego et al. (2010) and implemented in the mesoscale Hydrologic Model (mHM) and was then adapted by Mizukami et al. (2017) and implemented over the CONUS using the Variable Infiltration Capacity (VIC) model (Liang et al., 1994). The MPR method used what has been termed the "large-sample" hydrologic modeling approach (Gupta et al., 2014), meaning that the authors (e.g. Mizukami et al., 2017) used 531 gauged basins across the CONUS, representing a wide variety of climate regimes, to calibrate the parameters in the transfer functions. They used the CONUS domain basin-scale hydrometeorology dataset developed by Newman et al. (2015), which included observed daily streamflow data for 671 basins from the Hydro-Climate Data Network, for both basin-specific and joint multibasin calibrations. For basin-specific calibrations, the global transfer functions

were calibrated independently for each basin, whereas for the joint multibasin calibration, a single set of global transfer function parameters were calibrated for the entire US. VIC simulations using VIC parameters estimated with the global transfer function parameters were compared to benchmark simulations where VIC was calibrated independently for each of the 531 basins (Newman et al., 2017). However, Mizukami et al. (2017) found that the benchmark individual basin-calibrated simulations far outperformed both of the MPR-implementation calibrations.

Past applications of the Variable Infiltration Capacity (VIC) model, excluding the work of Mizukami et al. (2017) with their application of the MPR approach, have typically relied on a combination of satellite imagery, Food and Agricultural Organization (FAO) soil maps and extensive basin calibrations for deriving input parameter sets (Bohn and Vivoni 2019). Vegetation parameters that were initially used in the VIC model over the CONUS (e.g. Hansen et al., 2000) were developed by using a coarse-resolution land cover map based on Advanced Very High-Resolution Radiometer (AVHRR) imagery from the early 1990s, and despite significant land cover change globally that occurred in the interim, hydrological studies over the western US (e.g. Gergel et al., 2017) and the CONUS (e.g. Livneh et al., 2013; Livneh et al., 2015) have nonetheless used these parameters. The VIC model itself has also undergone significant infrastructural changes (e.g. Hamman et al, 2018) as well as physics changes. Advances in VIC parameter development, such as the work of Bohn and Vivoni (2019) in developing new vegetation parameters, as well as the MPR approach, have been less relevant to the Arctic, which is unique in that there is a dearth of observations – both in-situ streamflow data as well as satellite data – that may be used for deriving model input parameters.

However, these parameters are significant for modeling Arctic streamflow, which is a key part of the Arctic freshwater cycle. The largest source of freshwater to the Arctic Ocean comes from streamflow, consisting of around 38% of the total freshwater flux into the Arctic Ocean, with other significant inputs from precipitation (24%), inflow from the Pacific Ocean (30%), and inflow from the Atlantic Ocean (8%) (Serreze et al., 2006). Consequently, streamflow fluxes play a key role in the Arctic climate system. Standalone pan-Arctic studies (Su et al., 2006; Adam et al., 2006; Slater et al., 2007) have faced the challenge of how to calibrate the VIC parameters that govern water fluxes (hereafter referred to as CW parameters), including the infiltration parameter b_i, which controls the amount of water that can infiltrate into the soil, the first two soil layer thicknesses D_1 and D_2, and the four baseflow parameters: d_1, the linear reservoir coefficient; d_2, the nonlinear reservoir coefficient, d_3, the depth at which baseflow transitions from linear to nonlinear; and d_4, the exponent used in the Nijssen et al., (2001) baseflow formulation (Su et al., 2006). While CONUS-wide studies have used long-term streamflow data for oft-extensive basin calibration, there are few long-term streamflow records for drainage basins in the Arctic, save for the R-ArcticNet streamflow records, which include sparse data records and typically ended in the 1990s. Su et al. (2006) and Adam et al. (2006) used recommended values from the literature (Liang et al., 1996; Nijssen et al., 2001) for the CW parameters except for b_i and D_2, which they calibrated.

Fully-coupled modeling studies using VIC, such as the work of Hamman et al. (2016) and Hamman et al. (2017) with the Regional Arctic System Model (RASM), have not calibrated model parameters due to these particular challenges faced with deriving parameters in the Arctic. RASM is a fully-coupled regional climate model that is comprised of the Weather Research and Forecasting (WRF) model, the Parallel Ocean Program (POP) model, the Los Alamos Sea Ice

(CICE) model, the RVIC streamflow routing model, and the VIC land surface model (Hamman et al., 2016). Rather than calibrating parameters, past RASM studies used CW and soil class-related parameters originally derived at a 1° resolution from Sheffield et al. (2006) and the previously-mentioned land cover types (Hansen et al., 2000). They also imposed homogeneous soil depths across the pan-Arctic domain and used an a priori approximation for d_4 inside the permafrost domain, $d_4 \approx 0$, so that runoff would not be generated via baseflow from frozen soils. Since the version of the VIC model used in RASM1 (4.0.6 with modifications) did not have an explicit representation of frozen soils, this a priori parameterization was intended to mimic the presence of frozen soils (Hamman et al., 2016). Although RASM-simulated streamflow with this parameter set performed well in comparison to the limited in-situ streamflow observations available as well as reanalysis data, the parameter methodology is clearly an example of the parameter regionalization challenge discussed by Beck et al. (2016). Moreover, the authors did not compare the performance of RASM-simulated streamflow in fully-coupled simulations to uncoupled simulations (Hamman et al., 2017). Fully-coupled RASM simulations involve active component models with exchange of energy and water fluxes between the atmosphere, ocean, land, sea ice and routing components, whereas uncoupled VIC simulations are run with prescribed meteorological forcing data and streamflow routing through a routing model (RVIC; Hamman et al., 2016).

To address these historical parameter challenges with VIC implementations in both standalone and fully-coupled studies, we developed a new, high-resolution parameter set for application in the VIC version 5 model (hereafter referred to as VIC-5 to distinguish it from the version of VIC previously implemented in RASM) over a pan-Arctic domain. The parameters are designed for application in VIC-5 both as a standalone model coupled to RVIC as well as for

fully-coupled RASM simulations (which also use RVIC to route flow from the land surface to coastal grid cells). Given the limited in-situ streamflow records available in the Arctic, we developed a system of hydroclimate classes by overlaying the Brown et al. (1997) permafrost map with the Köppen-Geiger climate classes present in our pan-Arctic study domain and use these hydroclimate classes to assign values for the CW parameters. We use available high-resolution global datasets derived from remote sensing and machine learning as well as the plant functional types (PFTs; Bonan et al., 2002) implemented in the Community Land Model (CLM). We apply our parameter set in both standalone VIC-5 simulations and fully-coupled RASM simulations and examine simulated streamflow and permafrost in our standalone versus fully-coupled runs. We use this comparison to illustrate differences in performance of a parameter set in standalone versus fully-coupled simulations and the resultant challenges inherent to designing a parameter set that can be applied in both contexts.

4.2 Data and Methods

We used a selection of high-resolution global datasets derived from remote sensing and machine learning to create the VIC-5 parameter sets. Table 4.1 lists the source datasets, the provenance of the datasets, their native resolution, and relevant citations. In the following sections we describe our rationale for how we designed the parameter methodology, our selection of the source datasets and development of the hydroclimate classifications for the CW parameters.

Type of Dataset	Source of Dataset	Native Resolution	Relevant Citations
Soil Texture and Organic Matter	ISRIC SoilGrids	1-km; 7 vertical layers to depth of 3m	Hengl et al. 2014; Hengl et al. 2017
Vegetation Classes	CLM 4.5 Input Dataset	0.05°	N/A
LAI and Vegetation Height	CLM 4.5 Input Dataset	25-km	N/A
Elevation (DEM)	GTOPO DEM; Oak Ridge National Laboratory	0.05°	N/A
Climatological Temperature and Precipitation	WORLDCLIM	1-km; monthly	Hijmans et al., 2005
Permafrost Presence/Absence	Northern Circumpolar Carbon Database (NCSCD)	0.05°	Brown et al., 1997
Köppen-Geiger Climate Classes	Oak Ridge National Laboratory	0.05°	Rubel et al., 2017
Baseflow Parameters	Nijssen et al., 2001	1°	Nijssen et al., 2001
GMT Time Zone	VIC-4 RASM Parameters	50-km	Hamman et al., 2016; Hamman et al., 2017
Maximum Snow Albedo	Barlage et al., 2005	Vegetation-Type Specific	Barlage et al., 2005

Table 4.1. Source datasets that are used for the parameter derivation process, along with their native resolution, the type of dataset, and relevant citations for each.

4.2.1 Study Domain

We use our parameter sets for VIC-5 simulations over a pan-Arctic domain, which includes all drainage basins into the Arctic Ocean. Figure 1 shows the geographic extent of our domain. We use the Regional Arctic System Model (RASM) grid, a 50-km near-equal-area North Pole stereographic grid (Hamman et al., 2016).

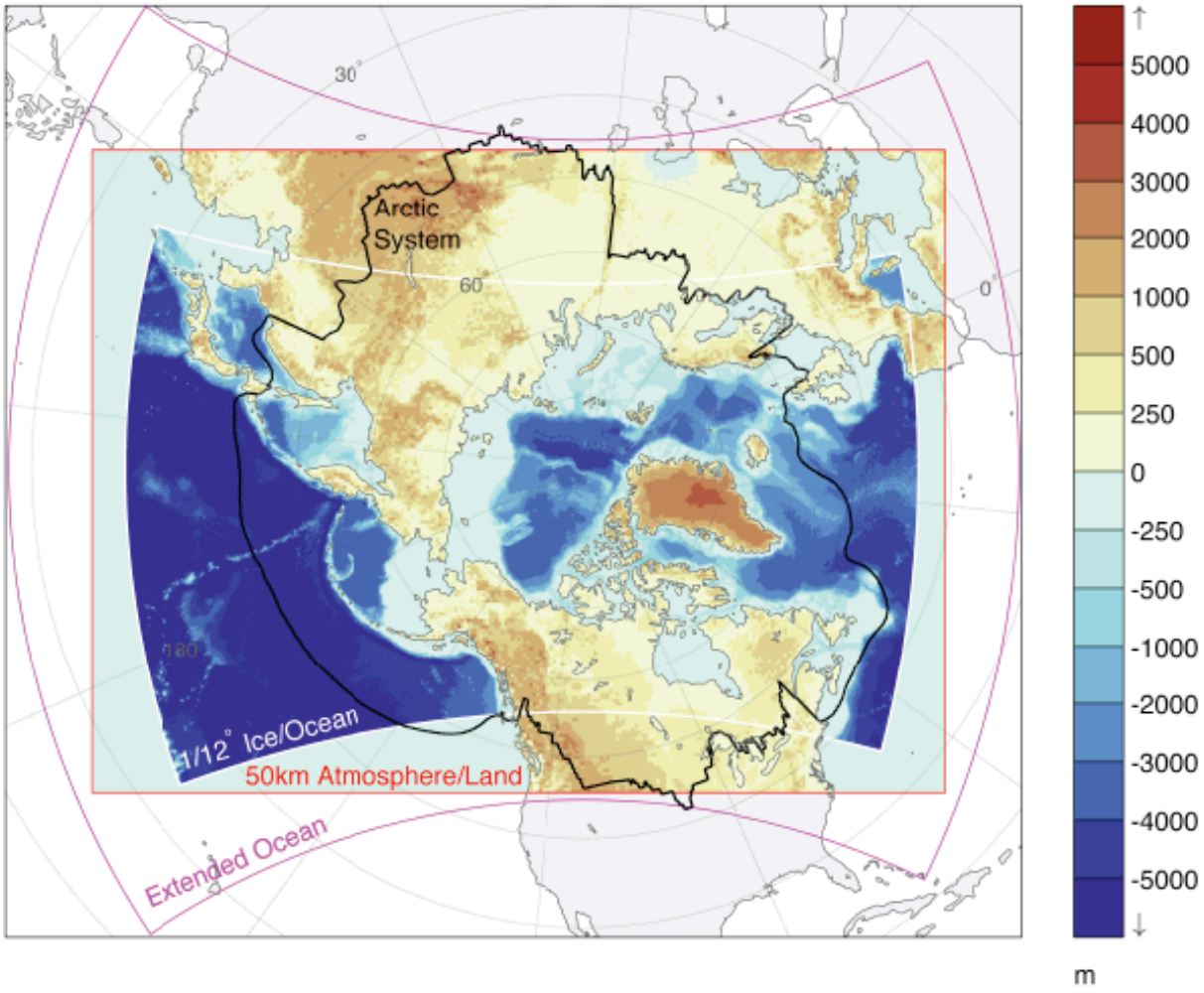

Figure 4.1. Circumpolar Arctic study domain, including all drainage basins into the Arctic Ocean.

4.2.2 Methodology

In developing the parameter sets, one of our biggest methodological challenges was the question whether or not we were willing to accept spatially discontinuous parameter fields. This question arose in two specific ways: 1) whether or not to use available higher-resolution datasets with spatial domains limited to the Arctic, and 2) how to account for parameter regionalization challenges for the CW parameters. We initially considered using higher-resolution Arctic-specific data, such as the circumpolar Arctic vegetation map (Walker et al., 2005; Raynolds et

al., 2019), but ultimately decided against using it, as we would have had to merge it with a global dataset and our circumpolar study domain would have had discontinuous vegetation fields, which could have resulted in corresponding discontinuities in our hydrologic simulations. Thus, we limited our source datasets to those with global coverage, and we used the latest available global datasets derived from machine learning and remote sensing.

Although we strongly considered using the MPR approach for the CW parameters , we ultimately decided not to use the MPR approach due to specific problems with applying the MPR framework to a data-sparse region. First and foremost is the problem of having insufficient calibration data. There is limited streamflow data available in the Arctic: the majority of data is available only through the R-ArcticNet database and only at a monthly timestep, and the majority of data records ended just after the fall of the Soviet Union in the 1990s (Hamman et al., 2016). The data records present both spatial and temporal challenges: they are available for a limited number of basins in the Arctic, and what data exists is often missing monthly values, making it significantly harder to use for calibration. The second problem is that the data available does *not* lend itself to the large-sample hydrologic modeling approach of Gupta et al. (2014) in that it is not sufficiently representative of a wide variety of climate regimes, nor is the time series for some of the stations of sufficient duration. Additionally, some of the basins are extremely large and hence encompass multiple hydroclimatic regimes. Because of these reasons, we decided not to adapt the MPR approach for the CW parameters; instead we designed a hydroclimate classification for deriving b_i and the soil layers, which we describe in Section 2.3.6. For the baseflow parameters, we used the 1° global values from Nijssen et al. (2001). Although we initially tried using our hydroclimate class approach for the baseflow parameters as well, we found that using the 1° global values resulted in simulated streamflow that performed better in

comparison to observations. However, this result depended on whether parameters were applied in standalone VIC-5 simulations or in fully-coupled RASM simulations, the technical differences of which we explain further in Section 3. Overall, this points to a particular challenge of hydrologic modeling, analogous to the results of Mizukami et al. (2017) with calibrating individual basins versus joint calibrations: at times the more methodologically sound choice does not result in better model performance, and it is necessary to revert to coarse-resolution datasets and/or a priori assumptions that lead to better model performance.

4.2.3 Source Datasets

4.2.3.1 Vegetation classes

Previous land cover types implemented in the VIC model had typically been the previously mentioned AVHRR-based data from 1992-1993 based on the National Land Data Assimilation System (NLDAS) vegetation types (Bohn and Vivoni, 2019). These included twelve vegetation classes that were upscaled from the 1-km dataset that was developed using a classification tree approach (Hansen et al., 2000). Rather than continuing to use the NLDAS vegetation classes, we selected the land cover classification system used in the CESM to be in line with coupled modeling efforts and to use ecosystem-level classifications that would be more meaningful in analyzing land-atmosphere interactions in the context of the Arctic climate system. The CESM uses a system of PFTs, which is a system of plant classification intended to represent biogeophysical and biogeochemical differences between different categories of plants in terms of their functional characteristics. The system also includes a class for bare ground, which includes bodies of water (Oleson et al., 2010). There are 17 possible PFTs (including bare

ground), not all of which are present in our study domain. Table 4.2 shows a comparison of the formerly-used NLDAS classes versus the PFTs used in our parameter set. We use a 0.05° resolution global dataset for PFT distribution that has been used as a data input to CLM 4.5 for CESM2 simulations.

NLDAS Vegetation Classes (Hansen et al., 2000)	Plant Functional Types (PFTs) (Bonan et al., 2002b)
Evergreen Needleleaf Forest	Needleleaf Evergreen Tree - Temperate
Deciduous Needleleaf Forest	Needleleaf Evergreen Tree – Boreal
Evergreen Broadleaf Forest	Needleleaf Deciduous Tree – Boreal
Deciduous Broadleaf Forest	Broadleaf Evergreen Tree – Tropical
Mixed Forest	Broadleaf Evergreen Tree – Temperate
Woodland	Broadleaf Deciduous Tree – Tropical
Savanna	Broadleaf Deciduous Tree – Temperate
Closed Shrubland	Broadleaf Deciduous Tree - Boreal
Open Shrubland	Broadleaf Evergreen Shrub – Temperate
Grassland	Broadleaf Deciduous Shrub – Temperate
Cropland	Broadleaf Deciduous Shrub – Boreal
Bare Soil/Water Bodies	C3 Arctic Grass
	C3 Grass
	C4 Grass
	C3 Unmanaged Rainfed Crops
	Bare Soil/Water Bodies

Table 4.2. Vegetation classes from the National Land Data Assimilation System (NLDAS) and the Plant Functional Types (PFTs) used in the Community Land Model. NLDAS classes were formerly used for VIC-4 parameters; we use the PFTs for our VIC-5 parameters.

4.2.3.2 Soil Texture and Organic Matter Data

The VIC model requires specification of a number of soil texture characteristics, all of which depend on the relative content of clay, sand, and silt as well as the bulk density of the soil. Organic matter is an optional specification and including parameter data on organic content of the soil allows for including it in calculating heat conduction through the soil column. For both soil texture and organic matter, we use the International Soil Reference and Information Centre

(ISRIC) World Soil Information database, called SoilGrids (https://www.isric.org). Global SoilGrids data is available at multiple high resolutions (up to 250m) and we use the 1-km global data product available as GeoTiff files (Hengl et al., 2014; Hengl et al., 2017) which includes one file each for the clay, sand, silt and bulk density contents of soil globally. Each file includes seven soil layers to a depth of 3m. SoilGrids data was created by applying multiple linear regression (for sand, silt, clay and bulk density percentages) and General Linear Models (for organic carbon content) to available pedon data as well as other environmental predictor data (Hengl et al., 2014).

4.2.3.3 LAI and Vegetation Height

The VIC model requires specification of monthly LAI, vegetation height and vegetation displacement, which is typically calculated as 2/3 of the vegetation height, for each vegetation type. For monthly LAI and vegetation height, we use LAI and vegetation canopy height that is specific to each PFT and was available at a 25-km resolution. Although we attempted to use a higher-resolution LAI and vegetation height source dataset to enable moving to higher resolutions in later work, a higher-resolution data product was not available when we first began this study.

4.2.3.4 Climatological Temperature and Precipitation

The VIC model requires specification of annual average precipitation as well as annual average temperature as input values. For these variables, we used monthly precipitation and temperature data from the WorldClim – Global Climate Data website (https://www.worldclim.org), available as global GeoTiffs of ~1-km, which covers the time

period 1960-1990. The dataset was created by interpolating average monthly climate data from weather stations on a 30 arc-second grid, using a number of major climate databases compiled by the Global Historical Climatology Network (Hijmans et al., 2005). Because both climatological temperature and precipitation do not include years after 1990, the time series likely does not include a strong climate change signal, but we chose to use this dataset due to its high resolution in comparison to available reanalysis datasets which are available at a coarser resolution.

4.2.3.5 Hydroclimate Classes and the CW Parameters

Devising a system of hydroclimate classifications was our solution to the parameter regionalization problem discussed in the introduction. We designed our hydroclimate classes by overlaying Köppen-Geiger climate classes, a system of hydroclimate classification based on temperature and precipitation, with a permafrost map that showed either the presence or absence of permafrost. For the Köppen-Geiger classes, we used a global map at a 5-arc-minute resolution representative of the period 1986-2010 (Rubel et al., 2017). The presence or absence of permafrost is taken from the Brown et al. (1997) permafrost map, available as a gridded global NetCDF product at a 0.05° resolution. By overlaying these two data products, we derived a system of nine hydroclimate classes present in our pan-Arctic domain.

We then used the hydroclimate classes to assign values for the CW parameters, including the infiltration parameter b_i and all three soil layers, D_1, D_2 and D_3. Initial values for the hydroclimate classes for these parameters were taken from Su et al. (2006). Figure 4.2 shows the nine hydroclimate classes present in the Arctic domain, and the color shading in the figure represents different Köppen-Geiger climate classes. If the parameter derivation process were applied globally, the same methodology would apply except that additional hydroclimate classes

would be present, and the CW parameter a priori values would need to be assigned from the outset.

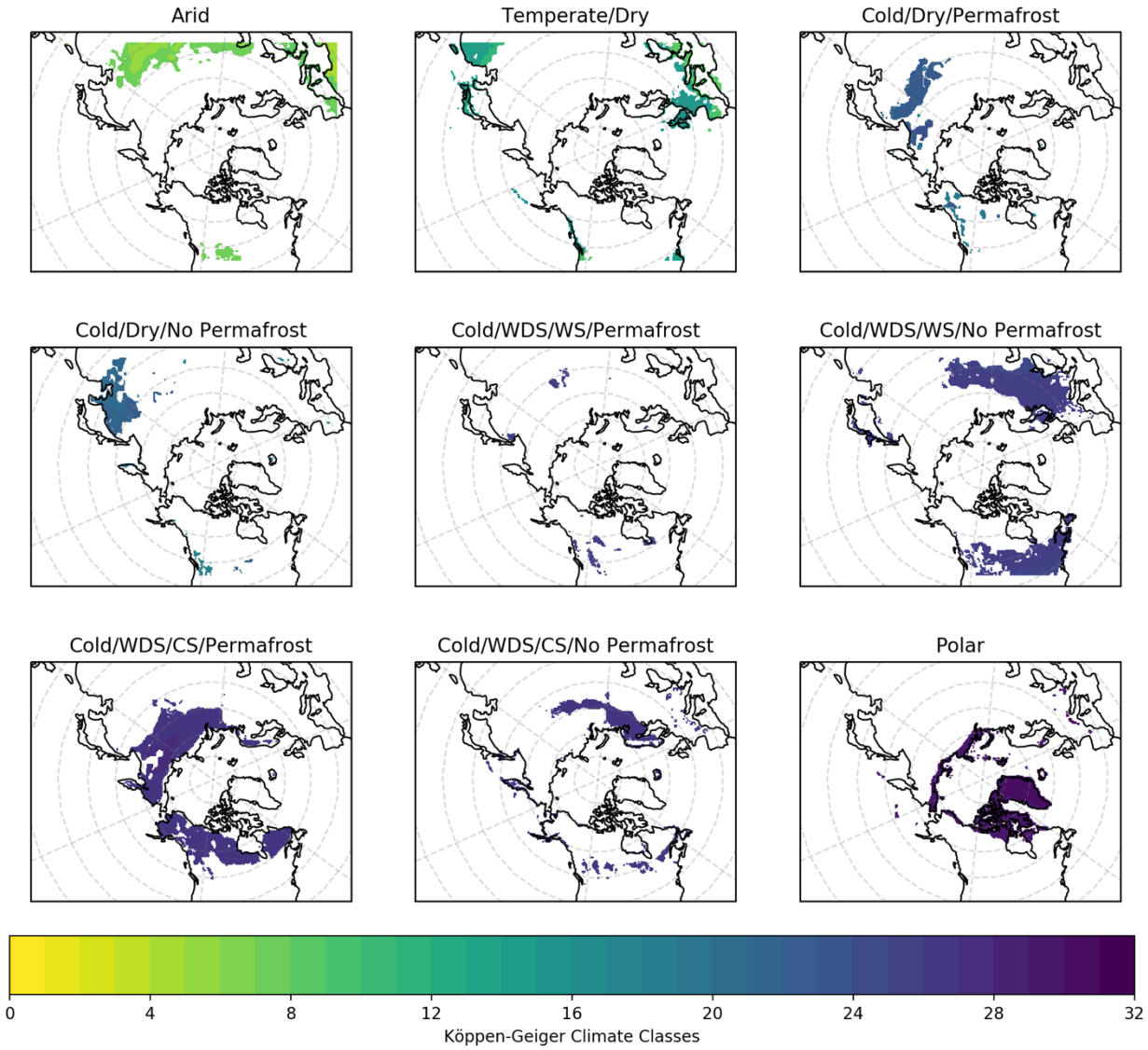

Figure 4.2. Nine hydroclimate classes used in our snow analysis, based on Köppen-Geiger climate class and the presence or absence of permafrost. Colors represent different Köppen-Geiger climate classes in a given hydroclimate class. WDS: without dry season, WS: warm summer, CS: cold summer.

4.2.3.6 Parameter Derivation Using Source Datasets

4.2.3.6.1 Derived Soil Parameters

Using the percent content of soil, silt and clay from the ISRIC SoilsGrid data, we then assigned each layer for each gridcell to a soil class using the United States Department of Agriculture (USDA) Agricultural Research Service (ARS) system of classification. To do this, we utilized a function that classifies soil texture, produced by the USDA Natural Resources Conservation Service. We then used these soil classes to assign the following parameter values based on Carsel and Parrish (1988): saturated hydraulic conductivity, the wilting and critical points, residual moisture, quartz content, and *expt* (or *b*), the exponent in Campbell's equation for saturated hydraulic conductivity. After assigning these values to each soil layer for each gridcell, we then aggregate over the seven ISRIC soil layers to the three VIC soil layers by either taking an arithmetic or harmonic mean. We use a harmonic mean for aggregating over soil layers for saturated hydraulic conductivity, since it represents a rate of change, and apply an arithmetic mean for all other derived soil quantities. The bubble pressure, or air-entry tension head, is derived from *b*, the exponent in Campbell's equation for saturated hydraulic conductivity, using the methods of Cosby et al. (1984). VIC requires specification of mineral bulk density as well as organic matter bulk density if organic matter content is provided. For the former, we used a constant value of 1300 kg/m^3 and took the SoilsGrid bulk density to be the bulk density of the organic matter.

4.2.3.6.2 Derived Vegetation/Land Cover Parameters

For all land cover parameters excluding LAI, vegetation height and displacement, we use the values from Hamman et al. (2016). We map the NLDAS classes to PFTs using a function we designed that numerically maps NLDAS classes to their corresponding PFTs.

4.2.3.8 Elevation

The VIC model also requires elevation information. For this, we use the GTOPO global digital elevation model available at a 0.0083° resolution from the Oak Ridge National Lab (https://webmap.ornl.gov). The dataset includes one elevation band representing elevation in meters above sea level with ocean areas masked out (GTOPO 30, USGS).

4.2.4 Parameter Derivation Process

Our parameter derivation process is self-contained in a publicly available GitHub repository and is implemented entirely in Python using packages designed for large geospatial datasets, including dask and xarray (Hoyer and Hamman, 2017), and the Climate Data Operators package using python bindings for regridding. An overview of the required source datasets with information on how to obtain them is included in the `inputdata_readme.md` file in the main directory. Both the SoilsGrid files and the WorldClim files are available as GeoTiffs, thus the main directory includes scripts to regrid them to NetCDFs. The regridding subdirectory contains all scripts needed to regrid all of the source datasets from their native resolution to the desired resolution, which is specified in the configuration file in the regridding subdirectory, titled `regridding.cfg`. A required data input file is a CF-compliant NetCDF domain file (formatted identically to the CESM land domain file) that specifies the domain gridcell centers, vertices, and

which gridcells are land if there is a land/ocean mask included in the study domain, and an example domain file is included in the main directory for reference. Figure 4.3 shows a diagram of the parameter derivation workflow, along with required inputs. After all source datasets have been regridded to the desired resolution and the script to make hydroclimate classes for the study domain has been run, the Jupyter notebook in the main directory, titled `initial_parameters.ipynb`, produces a NetCDF file with all land surface parameters for VIC-5 simulations. Optional data inputs to be used in the derivation process, including organic matter, combined bulk density, and maximum snow albedo, can be specified in the configuration file. Maximum snow albedo is based on the values from Barlage et al. (2005). When these optional data inputs are specified in the configuration file, those parameters will also be in the output parameter NetCDF file.

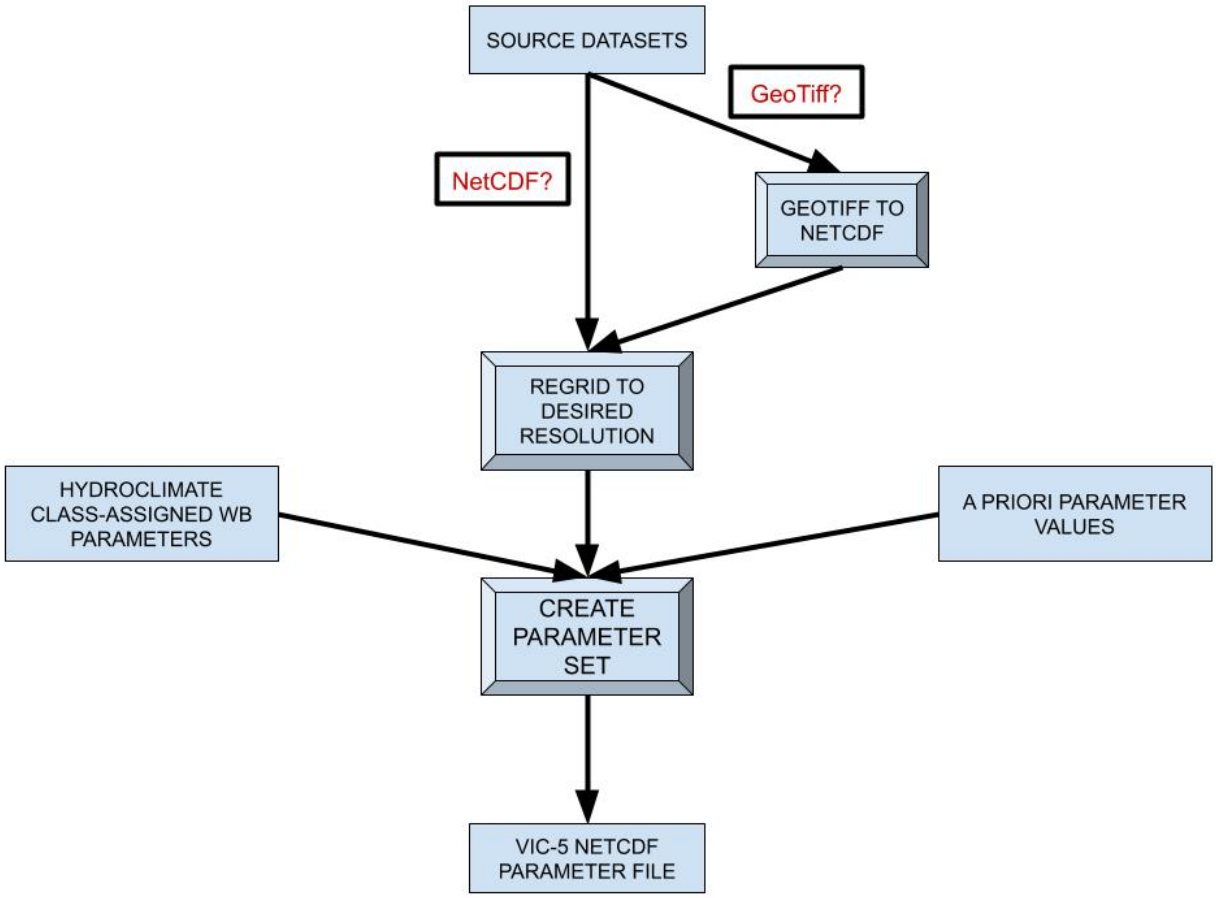

Figure 4.3. Workflow describing the parameter derivation process from start to finish. Required inputs include the source datasets, which are regridded to the desired model resolution from their native resolution, for all of the data sources listed in Table 4.1. These are combined with hydroclimate class-assigned infiltration and soil depth parameters and a priori parameter values to create a new parameter set for the desired domain and resolution.

Although we have applied our results herein at a 50-km resolution over a pan-Arctic domain, the process may be adapted for any resolution coarser than 6-km (the resolution of the coarsest base dataset) and for any domain globally. Thus far, we have used the method to develop 25-km VIC-5 parameters which are consistent with the 50-km parameters.

4.2.5 Streamflow simulations

Hamman et al. (2017) showed that RASM-simulated streamflow performed well in comparison to reanalysis data and better represented the annual cycle of streamflow than some existing datasets, particularly in ungauged areas. Thus, one of the primary goals in deriving a new parameter set for VIC-5 was to be able to simulate Arctic streamflow that would perform at least as well as in Hamman et al. (2017). To assess this, we compared coastal streamflow from: a) uncoupled VIC-4 and VIC-5 runs and b) fully-coupled RASM2 (with VIC-4) and RASM 2.1 (with VIC-5) with several different gridded observation datasets and reanalysis datasets. The uncoupled VIC runs use prescribed meteorological forcings: VIC-4 is run with Sheffield et al. (2006) and VIC-5 with CRU-NCEP v7 (Viovy 2018), and both were coupled to RVIC for streamflow routing. Both VIC runs span the time period 1979-2012, and we analyzed the period 1990-2010 to account for spinup. The fully-coupled RASM2 and RASM2.1 runs cover the same time period, with an identical period of analysis as well. RASM2 is configured as RASM1 in Hamman et al. (2016 and 2017), with the Parallel Ocean Program (POP) ocean model, Weather Research and Forecasting (WRF) model, Los Alamos CICE sea ice model, RVIC, and VIC-4 (4.0.4, with modifications), but with WRF 3.7 rather than 3.1. RASM2.1 is wired identically but uses VIC-5 versus VIC-4. It is important to note that in the RASM2.1 simulation results we show, there are two key differences from RASM2: 1) VIC version (VIC-5 versus VIC 4.0.4 with modifications) and 2) VIC parameter set.

4.3 Results

4.3.1 Streamflow simulations

To compare our uncoupled and fully-coupled streamflow simulations to observed streamflow as well as other model-based streamflow estimates, we use the following datasets: gridded observations that interpolate coastal streamflow from the R-ArcticNet database (Dai et al., 2009), COREv2 runoff data, which builds off of streamflow from Dai et al. (2009) but includes model estimates for ungauged areas as well as an adjustment to close the global water budget, and high-resolution regional atmospheric climate model output over Greenland, which is considered to be the best-performing dataset for freshwater discharge over Greenland (Bamber et al., 2012). Figure 4.4 shows simulated streamflow from uncoupled (VIC-4 and VIC-5) and fully-coupled (RASM2 and RASM2.1) runs as well as observed streamflow from our three comparison datasets for the NW Canada and Alaska coast, the Siberian Shelf Coast, the Kara and Barrents Sea Coast and coastal Greenland. In comparing RASM2 and RASM2.1, the magnitudes of streamflow are similar for all four figures except for coastal Greenland, where peak monthly streamflow is about 50-100 km^3/month higher for RASM2 than in RASM2.1. The seasonal cycle of streamflow is very similar in the two versions as well, though peak streamflow occurs over June – July in RASM2.1 over the NW Canada and Alaska Coasts and only in June for RASM 2. The opposite pattern is present near the Kara and Barrents Sea. As Hamman et al. (2017) showed, RASM1-simulated streamflow performed well in comparison to observations, and this is apparent in Figure 4.4 as well with both RASM2 and RASM2.1. However, RASM 2.1 performs similarly in comparison to observations and model estimates for all of the coastal areas except for Greenland, where RASM2.1-simulated streamflow is closer to the Bamber et al. (2012) model-estimated coastal freshwater flux. Overall, it appears that RASM2.1-simulated

streamflow more closely matches observations than RASM2, indicating that VIC-5 and the updated parameter set have improved RASM-simulated streamflow.

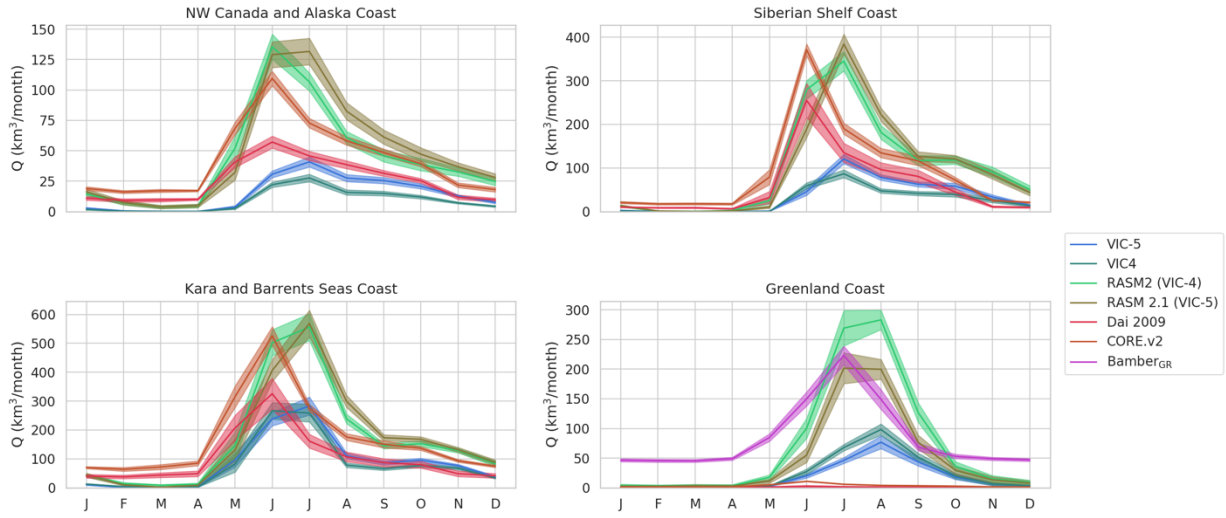

Figure 4.4. Coastal streamflow in fully-coupled RASM runs (RASM 2 and RASM 2.1) and uncoupled VIC runs (VIC-5 and VIC-4) compared to observed streamflow.

A somewhat surprising result in our streamflow comparison, however, was the stark difference between the magnitude and seasonal cycle of uncoupled and fully-coupled simulated streamflow. In comparing both uncoupled VIC-4 and VIC-5 to RASM2 and RASM2.1, respectively, RASM2.1-simulated streamflow is over four times that of VIC-5. For example, over the Siberian shelf coast, VIC-5-simulated streamflow peaks around 100 km^3, whereas for RASM2.1 streamflow, the peak occurs at 400 km^3. A similar disparity can be found over the NW Canada and Alaska Coast, and for the Kara and Barrents Seas coast, coupled streamflow exceeds uncoupled by a factor of two. Coastal Greenland is similar with the difference approximating a factor of three. Previous studies analyzing the land surface in RASM (e.g. Hamman et al. 2016 and Hamman et al., 2017) had not elucidated this behavior, hence the disparity between uncoupled VIC-5-simulated and RASM2.1-simulated streamflow was a surprising result from this work and one that did not have much, if any, precedent in the literature on parameterizing

LSMs. It led us to ask the question: what is different about the climate system in fully-coupled RASM2.1 runs versus standalone VIC-5 runs that led to such a dramatically different magnitude in the coastal freshwater flux?

4.3.2 Differences in surface climate between coupled and uncoupled simulations

Examining differences in the Arctic climate system between the two runs helped to explain why streamflow showed significantly different behavior. Figure 4.5 shows a comparison of mean daily climatological precipitation (shown monthly) in the two runs with VIC-5: standalone VIC-5 with streamflow routed by RVIC and RASM2.1. Precipitation from RASM 2.1 was archived through 2005 rather than 2010 as for VIC-5, thus we limit our precipitation analysis to 1990-2005. In the standalone VIC-5 run, precipitation is from CRU-NCEP v7, whereas in the fully-coupled run, precipitation is simulated by WRF. Initial conditions for the atmosphere are different due to the fact that the standalone VIC-5 run involves prescribed meteorological forcings while the RASM2.1 run is fully-coupled. But in spite of these differences, the difference in magnitude, as well as seasonality, is striking. RASM2.1 precipitation is significantly higher than precipitation in the VIC-5 run, and this difference is sufficiently large to explain the difference in magnitude of streamflow between the two runs. Of note is that the seasonal cycle of precipitation in the standalone run has a much more typical pattern than the fully-coupled run; the low inflection point in April-May is an odd characteristic and one that does not seem physical in nature.

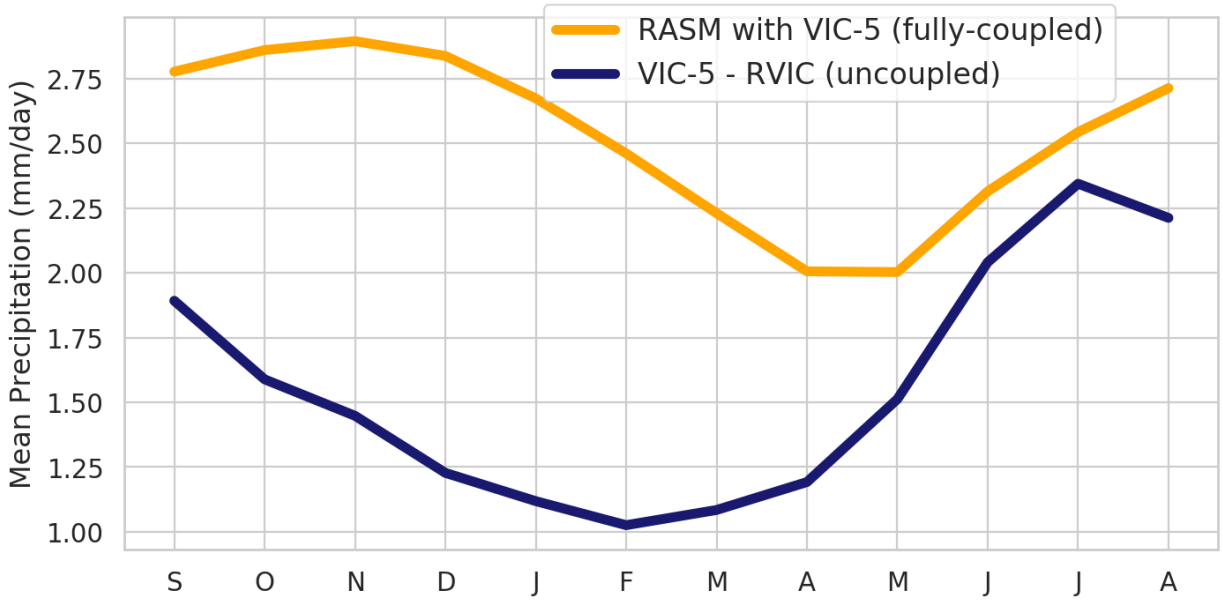

Figure 4.5. Comparison of mean daily precipitation, shown for each month, over the period 1990-2005, for RASM 2.1 (fully-coupled) and VIC-5 (uncoupled).

Figure 4.6a shows a mean annual precipitation over the RASM domain in uncoupled and fully-coupled simulations as well as the difference between the two runs. For the most part, spatial patterns are similar, and the largest differences in precipitation occur in the coastal areas, particularly on the North American coast as well as the Greenland coast. There is also some spatial difference over the Tibetan plateau, which is likely due to land-atmosphere exchange (increased surface evaporation) which is not occurring in the uncoupled run. For the coastal areas, the difference in magnitude of precipitation – given how large it is – is also likely due to coupled land-ocean exchanges of energy and water fluxes not present in the standalone run. However, Hamman et al. (2016) compared precipitation in fully-coupled runs with RASM 1 (using WRF 3.2 and VIC-4) to uncoupled VIC-4 runs over a similar time period (1989-2014) and found that generally precipitation was higher in the fully-coupled runs, often by up to 1.8 mm/day or more in the coastal areas. But precipitation in their uncoupled run was also smaller

than in the fully-coupled RASM 1 run in northern Europe in the summer as well as in the fall. It is important to note that the uncoupled VIC-4 run in Hamman et al. (2016) has different meteorological forcings; that run used the Sheffield et al. (2006) dataset rather than the CRU-NCEP meteorological data that we use for our VIC-5 uncoupled run. In comparing our results to those of Hamman et al. (2016), ours differ by both a) VIC version (VIC-4 versus VIC-5) and b) VIC parameter set. Notwithstanding, from their results as well as those of Cassano et al. (2017), RASM 1 was found to be drier in comparison to ERA-Interim reanalysis data, which was also evident from our streamflow comparison with RASM 2.1.

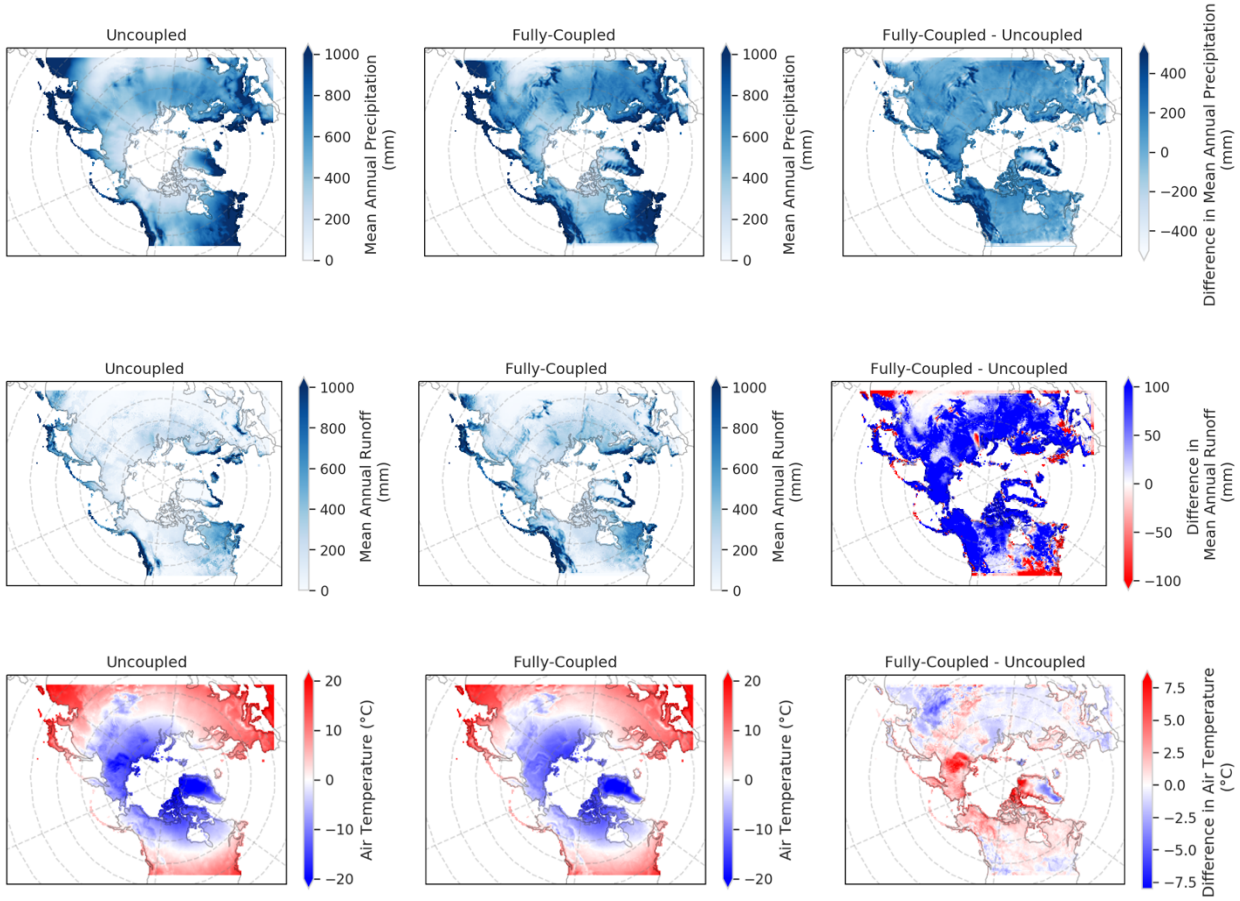

Figure 4.6. Surface climate differences in RASM 2.1 (fully-coupled) and VIC-5 (uncoupled), averaged over 1990-2005. 4.6a (top) shows mean annual precipitation, 4.6b (middle) shows mean annual runoff, and 4.6c (bottom) shows surface temperature.

Differences in total runoff over the domain follow a similar spatial pattern as for precipitation. Figure 4.6b shows mean annual runoff (as a sum of surface runoff and baseflow) in coupled versus uncoupled runs, including the difference between the two simulations. Differences between the two runs are most pronounced over coastal areas, as in precipitation, but Siberia also is more apparent in the runoff figures as an area with significant differences between the two runs in terms of runoff, suggesting that significantly different water flux exchanges are occurring in this area in the coupled run. Eurasia also shows non-negligible differences in runoff, and the Tibetan plateau is also striking as in the precipitation results.

In addition to differences in precipitation and total runoff, surface temperature also differs markedly between the two runs. Figure 4.6c shows annual mean climatological air temperature over the pan-Arctic domain in the two runs, with the rightmost figure showing differences in air temperature between the RASM2.1 and VIC-5 runs. Differences between the two runs do not follow a homogeneous pattern across the domain; colder parts of the Arctic are warmer in the fully-coupled simulation, whereas warmer parts of the Arctic are colder. Overall, the largest differences between the two runs occur in the tundra in Siberia and northern Alaska as well as in coastal Greenland, with differences in surface temperature of up to 8°C. At least in part, much of the differences in surface temperature between the two runs may be a result of surface temperatures being more constrained in the coupled run vis-à-vis the uncoupled run, since land-atmosphere and land-ocean exchanges of energy fluxes preclude the diurnal temperature range from more extreme fluctuations that occur in standalone hydrologic model runs. In comparing surface temperature in fully-coupled RASM 1 runs to uncoupled VIC-4 runs, Hamman et al. (2016) also found significantly different surface climates between the two runs, with surface temperature in the VIC-4 run generally warmer in the winter and cooler in the

summer. Notwithstanding, one of the important takeaways from this figure is that the effect of land-atmosphere coupling in the Arctic is creating a dramatically different surface climate when the land surface and atmosphere are able to exchange energy and moisture fluxes (in the fully-coupled run) than in the standalone VIC-5 run.

4.3.3 Permafrost in the RASM Domain

An important difference between VIC-5 and VIC-4 as implemented in RASM is the ability to simulate frozen soils, and permafrost comprises a key part of terrestrial climate in the Arctic and is closely tied to the Arctic hydrologic cycle. Permafrost covered around 24% of the northern hemisphere land surface as of 1999 (Zhang et al., 1999). It is also an important part of the carbon cycle, both regionally and globally, since soils at high latitudes store large amounts of soil organic carbon (Schuur et al., 2008). As a result, it is crucial for LSMs in ESMs to model permafrost extent that closely matches observed permafrost extent. Moreover, we wanted to understand whether differences in surface climate apparent in the two runs would also result in similarly dramatic differences in permafrost extent. Figure 4.7 shows simulated permafrost extent with VIC-5 (left panel) and simulated permafrost extent with RASM2.1 (right panel), both overlain with the Brown et al. (1997) permafrost map (the same map used for deriving the hydroclimate classes). As is evident from the figures, permafrost extent is very similar in the two runs, with both runs underestimating the amount of permafrost extent relative to observed permafrost extent, particularly in North America. In the VIC-5 run, total permafrost area is 20.9 million km^2, whereas it is 19.8 million km^2 in the RASM2.1 run and 22.7 million km^2 in the Brown et al. (1997) dataset. Thus VIC-5 permafrost extent exceeds that of RASM 2.1 by 1.1 million km^2 and is closer to the observed permafrost extent than RASM2.1. The minor difference

in permafrost extent between RASM2.1 and VIC-5 can be explained by the difference in surface climates between the two runs; Figure 6 showed that the colder parts of the domain, such as Siberia and Alaska, were warmer in RASM 2.1 than in VIC-5.

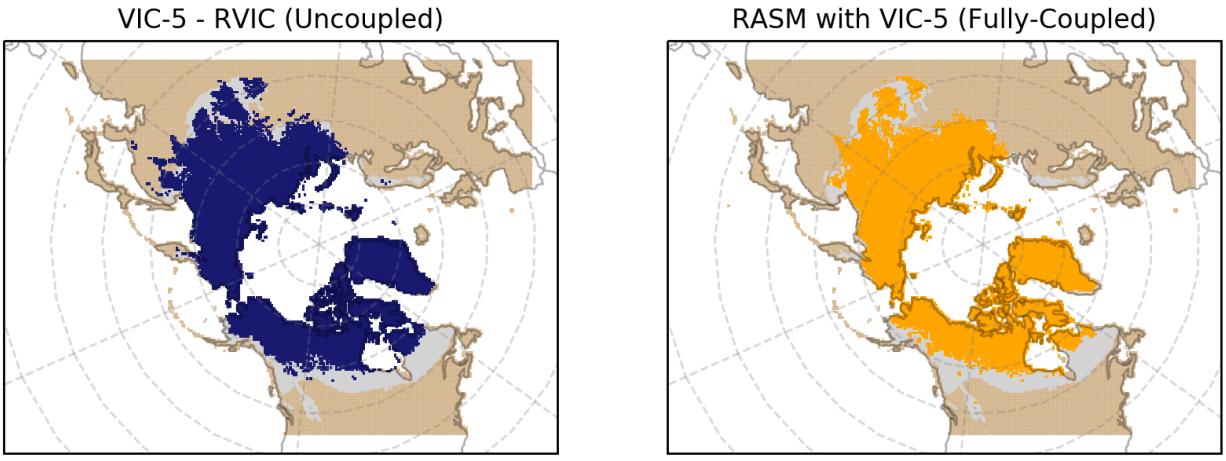

Figure 4.7. Simulated and observed permafrost for VIC-5 uncoupled (left) and VIC-5 fully-coupled with RASM 2.1 (right), both averaged over the period 1990-2010. Simulated permafrost is shown for the uncoupled (blue) and fully-coupled (orange) runs overlain on the observed permafrost extent from Brown et al. (1997) (grey).

4.4. Discussion

Together, our contrasting results for streamflow performance and permafrost extent, in comparison to observations, leads to important questions about the nature of land surface modeling in conjunction with fully-coupled climate modeling. How to optimize a parameter set in uncoupled and fully-coupled land surface modeling when coupled land-atmosphere, land-ocean and ocean-atmosphere exchanges of energy and water fluxes in a coupled modeling environment lead to dramatically different surface climates? Is it even possible to create a parameter set that performs well in coupled modeling as well as standalone modeling, and is this even a reasonable goal? There is a dearth of relevant literature in this regard, as most parameter development for LSMs has occurred in standalone LSMs rather than LSMs that are part of

climate models, and typically significantly less attention is paid to parameter inputs to LSMs in the context of climate modeling, as oftentimes LSM parameters are thought to have minimal effects on the climate system due to the land surface having a lesser impact on the climate system as a whole than other climate system components. Moreover, historically LSMs that are coupled to climate models have been LSMs of lower complexity than standalone LSMs, with development on the Community Land Model (CLM) over the past few decades a notable exception to this (see Oleson et al., 2010). Since climate modeling and land surface modeling have largely evolved as two distinctly separate modeling communities, model intercomparison projects have not explored this concept, except in a more limited sense, with analysis of coupled land-atmosphere models occurring in the Project for Intercomparison of Land Surface Parameterization Schemes (PILPS) phase 2c (Liang et al., 1998). Ning et al. (2019) provide a review article of the current state of fully-coupled atmosphere-hydrology simulations and how they have evolved over time, and one of their key recommendations is improving the ways in which hydrologic model parameters in fully-coupled climate models are designed, particularly in light of the move to hyper-resolution in regional climate modeling and the typical disparity between climate model simulations and their applicability on a regional or local scale.

We cannot conclude from our results that the parameter set alone led to the significant differences in our model results, as we also updated our model version from VIC-4 to VIC-5, but we can conclude that the representation of land surface model in a fully-coupled climate model has a strong effect on surface climate, as well as on the Arctic climate system. Thus, closer attention to the type of LSM and physical processes it represents, as well as its parameterizations, is an important area of research going forward for coupled climate modeling. Further research in this regard could include sensitivity studies in coupled and uncoupled

modeling environments to determine how parameter sensitivity varies in coupled modeling environments.

Another land surface modeling challenge that our results speak to is that of model tradeoffs. The surface climate from the fully-coupled run led to much better-performing streamflow fluxes in comparison to observations, but was also slightly warmer and thus had a simulated permafrost extent that was further from observed than in the standalone run (though not by a significant amount) . This result highlights a challenge that has already been identified in land surface modeling whereby optimizing for one modeling goal (for example, streamflow) leads to degraded performance in another goal (permafrost extent in this case). It is also particularly interesting in this study that the disparity was between a standalone modeling run and a fully-coupled run: in our study, permafrost extent was more realistic (e.g. closer to observed) in the standalone run than in the fully-coupled run, which leads to questions about the representation of frozen soils in the VIC model, and the extent to which surface climate feedbacks are affecting the soil thermal regime. One would expect that better exchange of land-atmosphere fluxes would lead to an improved representation of permafrost extent, thus this result warrants further study of why a seemingly improved surface climate would lead to a degraded simulation of permafrost.

4.5. Conclusion

In this study, we have designed a new method of deriving hydrologic model parameters. Although we have applied this method in the circumpolar Arctic, it is applicable to any geographic resolution and domain globally, and we have made all scripts publicly available on GitHub. Source datasets and their provenance are carefully documented so that the entire

parameter derivation process is reproducible and transparent. We applied the newly derived parameter set in both standalone VIC-5 and fully-coupled RASM simulations and explored the differences in performance between the two, which is a novel contribution to the modeling literature on hydrologic model parameter development. Overall, we conclude the following:

1) The performance of a given hydrologic modeling parameter set may differ markedly between coupled and uncoupled modeling runs
2) There are key tradeoffs that must be made in terms of optimizing parameter sets for certain modeling goals, e.g. streamflow simulations versus permafrost modeling
3) Further research should be done to explore how to parameterize hydrologic models coupled to regional and global climate models

4.6 References

Adam, J. C., Clark, E. A., Lettenmaier, D. P., & Wood, E. F. (2006). Correction of Global Precipitation Products for Orographic Effects. *Journal of Climate*, *19*(1), 15–38. https://doi.org/10.1175/JCLI3604.1

Bamber, J., Broeke, M. van den, Ettema, J., Lenaerts, J., & Rignot, E. (2012). Recent large increases in freshwater fluxes from Greenland into the North Atlantic. *Geophysical Research Letters*, *39*(19). https://doi.org/10.1029/2012GL052552

Barlage, M., Zeng, X., Wei, H., & Mitchell, K. E. (2005). A global 0.05° maximum albedo dataset of snow-covered land based on MODIS observations. *Geophysical Research Letters*, *32*(17). https://doi.org/10.1029/2005GL022881

Beck, H. E., Dijk, A. I. J. M. van, Roo, A. de, Miralles, D. G., McVicar, T. R., Schellekens, J., & Bruijnzeel, L. A. (2016). Global-scale regionalization of hydrologic model parameters. *Water Resources Research*, *52*(5), 3599–3622. https://doi.org/10.1002/2015WR018247

Bohn, T. J., & Vivoni, E. R. (2019). MOD-LSP, MODIS-based parameters for hydrologic modeling of North American land cover change. *Scientific Data*, *6*(1), 1–13. https://doi.org/10.1038/s41597-019-0150-2

Bonan, G. B., Levis, S., Kergoat, L., & Oleson, K. W. (2002). Landscapes as patches of plant functional types: An integrating concept for climate and ecosystem models. *Global Biogeochemical Cycles*, *16*(2), 5-1-5–23. https://doi.org/10.1029/2000GB001360

Brown, J., Sidlauskas, F. J., & Delinski, G. (1997). *Circum-Arctic map of permafrost and ground ice conditions*. Reston, Va. : Denver, Colo: The Survey ; For sale by Information Services.

Carsel, R. F., & Parrish, R. S. (1988). Developing joint probability distributions of soil water retention characteristics. *Water Resources Research*, *24*(5), 755–769. https://doi.org/10.1029/WR024i005p00755

Cassano, J. J., DuVivier, A., Roberts, A., Hughes, M., Seefeldt, M., Brunke, M., … Zeng, X. (2017). Development of the Regional Arctic System Model (RASM): Near-Surface Atmospheric Climate Sensitivity. *Journal of Climate*, *30*(15), 5729–5753. https://doi.org/10.1175/JCLI-D-15-0775.1

Cosby, B. J., Hornberger, G. M., Clapp, R. B., & Ginn, T. R. (1984). A Statistical Exploration of the Relationships of Soil Moisture Characteristics to the Physical Properties of Soils. *Water Resources Research*, *20*(6), 682–690. https://doi.org/10.1029/WR020i006p00682

Dai, A., Qian, T., Trenberth, K. E., & Milliman, J. D. (2009). Changes in Continental Freshwater Discharge from 1948 to 2004. *Journal of Climate*, *22*(10), 2773–2792. https://doi.org/10.1175/2008JCLI2592.1

Duan, Q. Y., Gupta, V. K., & Sorooshian, S. (1993). Shuffled complex evolution approach for effective and efficient global minimization. *Journal of Optimization Theory and Applications*, *76*(3), 501–521. https://doi.org/10.1007/BF00939380

Eaton, B., Gregory, J., Drach, B., Taylor, K., Hankin, S., Caron, J., … Juckes, M. (n.d.). *NetCDF Climate and Forecast (CF) Metadata Conventions*. 151.

Gergel, D. R., Nijssen, B., Abatzoglou, J. T., Lettenmaier, D. P., & Stumbaugh, M. R. (2017). Effects of climate change on snowpack and fire potential in the western USA. *Climatic Change*, *141*(2), 287–299. https://doi.org/10.1007/s10584-017-1899-y

Gupta, H. V., Perrin, C., Blöschl, G., Montanari, A., Kumar, R., Clark, M., & Andréassian, V. (2014). Large-sample hydrology: A need to balance depth with breadth. *Hydrology and Earth System Sciences*, *18*(2), 463–477. https://doi.org/10.5194/hess-18-463-2014

Hamman, J. J., Nijssen, B., Bohn, T. J., Gergel, D. R., & Mao, Y. (2018). The Variable Infiltration Capacity model version 5 (VIC-5): Infrastructure improvements for new applications and reproducibility. *Geoscientific Model Development (Online)*, *11*(8). https://doi.org/10.5194/gmd-11-3481-2018

Hamman, J., Nijssen, B., Brunke, M., Cassano, J., Craig, A., DuVivier, A., … Zeng, X. (2016). Land Surface Climate in the Regional Arctic System Model. *Journal of Climate*, *29*(18), 6543–6562. https://doi.org/10.1175/JCLI-D-15-0415.1

Hamman, J., Nijssen, B., Roberts, A., Craig, A., Maslowski, W., & Osinski, R. (2017). The coastal streamflow flux in the Regional Arctic System Model. *Journal of Geophysical Research: Oceans*, *122*(3), 1683–1701. https://doi.org/10.1002/2016JC012323

Hansen, M. C., Defries, R. S., Townshend, J. R. G., & Sohlberg, R. (2000). Global land cover classification at 1 km spatial resolution using a classification tree approach. *International Journal of Remote Sensing*, *21*(6–7), 1331–1364. https://doi.org/10.1080/014311600210209

Hengl, T., Jesus, J. M. de, MacMillan, R. A., Batjes, N. H., Heuvelink, G. B. M., Ribeiro, E., … Gonzalez, M. R. (2014). SoilGrids1km—Global Soil Information Based on Automated Mapping. *PLOS ONE*, *9*(8), e105992. https://doi.org/10.1371/journal.pone.0105992

Hengl, T., Jesus, J. M. de, Heuvelink, G. B. M., Gonzalez, M. R., Kilibarda, M., Blagotić, A., … Kempen, B. (2017). SoilGrids250m: Global gridded soil information based on machine learning. *PLOS ONE*, *12*(2), e0169748. https://doi.org/10.1371/journal.pone.0169748

Hijmans, R. J., Cameron, S. E., Parra, J. L., Jones, P. G., & Jarvis, A. (2005). Very high resolution interpolated climate surfaces for global land areas. *International Journal of Climatology*, *25*(15), 1965–1978. https://doi.org/10.1002/joc.1276

Hoyer, S., & Hamman, J. (2017). xarray: N-D labeled Arrays and Datasets in Python. *Journal of Open Research Software*, *5*(1), 10. https://doi.org/10.5334/jors.148

Liang, X., Lettenmaier, D. P., Wood, E. F., & Burges, S. J. (1994). A simple hydrologically based model of land surface water and energy fluxes for general circulation models. *Journal of Geophysical Research: Atmospheres*, *99*(D7), 14415–14428. https://doi.org/10.1029/94JD00483

Liang, X., Wood, E. F., & Lettenmaier, D. P. (1996). Surface soil moisture parameterization of the VIC-2L model: Evaluation and modification. *Global and Planetary Change*, *13*(1), 195–206. https://doi.org/10.1016/0921-8181(95)00046-1

Liang, X., Wood, E. F., Lettenmaier, D. P., Lohmann, D., Boone, A., Chang, S., … Zeng, Q. (1998). The Project for Intercomparison of Land-surface Parameterization Schemes (PILPS) phase 2(c) Red-Arkansas River basin experiment: 2. Spatial and temporal analysis of energy fluxes. *Global and Planetary Change*, *19*(1), 137–159. https://doi.org/10.1016/S0921-8181(98)00045-9

Livneh, B., Rosenberg, E. A., Lin, C., Nijssen, B., Mishra, V., Andreadis, K. M., … Lettenmaier, D. P. (2013). A Long-Term Hydrologically Based Dataset of Land Surface Fluxes and States for the Conterminous United States: Update and Extensions. *Journal of Climate*, *26*(23), 9384–9392. https://doi.org/10.1175/JCLI-D-12-00508.1

Livneh, B., Bohn, T. J., Pierce, D. W., Munoz-Arriola, F., Nijssen, B., Vose, R., … Brekke, L. (2015). A spatially comprehensive, hydrometeorological data set for Mexico, the U.S., and Southern Canada 1950–2013. *Scientific Data*, *2*(1), 1–12. https://doi.org/10.1038/sdata.2015.42

Mizukami, N., Clark, M. P., Newman, A. J., Wood, A. W., Gutmann, E. D., Nijssen, B., … Samaniego, L. (2017). Towards seamless large-domain parameter estimation for hydrologic models. *Water Resources Research*, *53*(9), 8020–8040. https://doi.org/10.1002/2017WR020401

Newman, A. J., Clark, M. P., Sampson, K., Wood, A., Hay, L. E., Bock, A., … Duan, Q. (2015). Development of a large-sample watershed-scale hydrometeorological data set for the contiguous USA: Data set characteristics and assessment of regional variability in

hydrologic model performance. *Hydrology and Earth System Sciences*, *19*(1), 209–223. https://doi.org/10.5194/hess-19-209-2015

Newman, Andrew J., Mizukami, N., Clark, M. P., Wood, A. W., Nijssen, B., & Nearing, G. (2017). Benchmarking of a Physically Based Hydrologic Model. *Journal of Hydrometeorology*, *18*(8), 2215–2225. https://doi.org/10.1175/JHM-D-16-0284.1

Nijssen, B., Schnur, R., & Lettenmaier, D. P. (2001). Global Retrospective Estimation of Soil Moisture Using the Variable Infiltration Capacity Land Surface Model, 1980–93. *Journal of Climate*, *14*(8), 1790–1808. https://doi.org/10.1175/1520-0442(2001)014<1790:GREOSM>2.0.CO;2

Ning, L., Zhan, C., Luo, Y., Wang, Y., & Liu, L. (2019). A review of fully coupled atmosphere-hydrology simulations. *Journal of Geographical Sciences*, *29*(3), 465–479. https://doi.org/10.1007/s11442-019-1610-5

Oleson, K. W., Lawrence, D. M., B, G., Flanner, M. G., Kluzek, E., J, P., … Decker, M. (2010). *Technical Description of version 4.0 of the Community Land Model (CLM)*.

Prentice, I. C., Liang, X., Medlyn, B. E., & Wang, Y.-P. (2015). Reliable, robust and realistic: The three R's of next-generation land-surface modelling. *Atmospheric Chemistry and Physics*, *15*(10), 5987–6005. https://doi.org/10.5194/acp-15-5987-2015

Raynolds, M. K., Walker, D. A., Balser, A., Bay, C., Campbell, M., Cherosov, M. M., … Troeva, E. (2019). A raster version of the Circumpolar Arctic Vegetation Map (CAVM). *Remote Sensing of Environment*, *232*, 111297. https://doi.org/10.1016/j.rse.2019.111297

Rubel, F., Brugger, K., Haslinger, K., & Auer, I. (2017). The climate of the European Alps: Shift of very high resolution Köppen-Geiger climate zones 1800–2100. *Meteorologische Zeitschrift*, *26*(2), 115–125. https://doi.org/10.1127/metz/2016/0816

Samaniego, L., Kumar, R., & Attinger, S. (2010). Multiscale parameter regionalization of a grid-based hydrologic model at the mesoscale. *Water Resources Research*, *46*(5). https://doi.org/10.1029/2008WR007327

Schuur, E. A. G., Bockheim, J., Canadell, J. G., Euskirchen, E., Field, C. B., Goryachkin, S. V., … Zimov, S. A. (2008). Vulnerability of Permafrost Carbon to Climate Change: Implications for the Global Carbon Cycle. *BioScience*, *58*(8), 701–714. https://doi.org/10.1641/B580807

Sellers, P.J., Dickinson, R.E., Randall, D.A., Betts, A.K., Hall, F.G., Berry, J.A., Collatz, G.J., Denning, A.S., Mooney, H.A., Nobre, C.A., Field, C.B., Henderson-Sellers A. (1997). Modeling the Exchanges of Energy, Water, and Carbon Between Continents and the Atmosphere. *Science 275*(5299), 502-509. doi: 10.1126/science.275.5299.502

Serreze, M.C., Barrett, A.P., Slater, A.G., Woodgate, R.A., Aagaard, K., Lammers, R.B., Steele, M. Moritz, R., Meredith, M., Lee, C.M. (2006). The large-scale freshwater cycle of the Arctic. *Journal of Geophysical Research, 111*(C11010). doi: 10.1029/2005JC003424.

Sheffield, J., Goteti, G., & Wood, E. F. (2006). Development of a 50-Year High-Resolution Global Dataset of Meteorological Forcings for Land Surface Modeling. *Journal of Climate*, *19*(13), 3088–3111. https://doi.org/10.1175/JCLI3790.1

Slater, A. G., Bohn, T. J., McCreight, J. L., Serreze, M. C., & Lettenmaier, D. P. (2007). A multimodel simulation of pan-Arctic hydrology. *Journal of Geophysical Research: Biogeosciences*, *112*(G4). https://doi.org/10.1029/2006JG000303

Su, F., Adam, J. C., Trenberth, K. E., & Lettenmaier, D. P. (2006). Evaluation of surface water fluxes of the pan-Arctic land region with a land surface model and ERA-40 reanalysis.

Journal of Geophysical Research: Atmospheres, *111*(D5). https://doi.org/10.1029/2005JD006387

Viovy, N. (2018). CRUNCEP Version 7 – Atmospheric Forcing Data for the Community Land Model. Research Data Archive at the National Center for Atmospheric Research, Computational and Information Systems Laboratory. http://rda.ucar.edu/datasets/ds314.3. Accessed 15 January 2018.

Walker, D. A., Raynolds, M. K., Daniëls, F. J. A., Einarsson, E., Elvebakk, A., Gould, W. A., … Team, T. other members of the C. (2005). The Circumpolar Arctic vegetation map. *Journal of Vegetation Science*, *16*(3), 267–282. https://doi.org/10.1111/j.1654-1103.2005.tb02365.x

Zhang, T., Barry, R. G., Knowles, K., Heginbottom, J. A., & Brown, J. (1999). Statistics and characteristics of permafrost and ground-ice distribution in the Northern Hemisphere. *Polar Geography*, *23*(2), 132–154. https://doi.org/10.1080/10889379909377670

Chapter 5

Conclusions and Future Work Recommendations

5.1 Conclusions

In this dissertation, I have examined changes in the cryosphere at mid- and high latitudes due to the effects of climate change by utilizing a hierarchy of models. I have explored differences between performance of a newly derived parameter set in standalone simulations with the Variable Infiltration Capacity version 5 (VIC-5) hydrology model versus in fully-coupled simulations with the Regional Arctic System Model (RASM) with VIC-5 as the land surface model component. This work was motivated by the four main research questions which I posed in Chapter 1: 1) How will climate change impact the cryosphere in the middle and high latitudes over the course of the twenty-first century? In particular, how will projected changes in temperature and precipitation reinforce or counter each other? 2) What is the role of the land surface in the coupled climate system? 3) How can we use a hierarchy of models – land surface models, regional climate models and global climate models – to advance our understanding of the coupled interactions between components in the Arctic climate system? 4) How should land surface model parameters be designed – specifically VIC-5 parameters – for application in both standalone modeling as well as fully-coupled modeling with RASM and what are the modeling tradeoffs involved? Chapters 2-4 attempt to answer these questions.

In Chapter 2, I conclude that large declines in spring snowpack and summer soil moisture are projected to occur across the mountainous western US, with April 1 Snow Water Equivalent (SWE) losses by the 2080s projected to reach up to 81% for the Cascades and 76% for the Sierra Nevada mountains. Dead fuel moisture (DFM) content, considered a proxy for the potential for fires to occur, is projected to decrease dramatically in the mountain ranges, which translates to a

high likelihood of increased fire potential under future climate projections. In Chapter 3, I turn to the Arctic and conclude that even under the low emissions scenarios represented by the 1.5°C and 2°C global-mean warming pathways, changes in the timing and amount of SWE will be large, with the majority of the domain projected to experience significant decreases in SWE, with the timing of peak SWE shifting to earlier in the year by 2-3 weeks for most of the domain for RCP 8.5. Parts of Eurasia, namely Siberia, is projected to experience increases in SWE. These changes, in conjunction with warming temperatures, result in large losses of permafrost of up to 11.5 million km^2. Losses of permafrost occur in some of the richest areas in soil organic carbon (SOC) in the world, thus this SOC stock is highly vulnerable. Our work in chapter 3 shows the importance of advancing our ability to model complex interactions in the Arctic climate system, which motivates our development of a new parameter set for standalone land surface modeling and regional climate modeling. In chapter 4, we describe how we developed this new parameter set and explore differences in applying the parameters in standalone VIC-5 simulations versus fully-coupled RASM simulations. We find that RASM-simulated streamflow is much larger than in VIC-5 simulations, and a much closer match to observed streamflow from reanalysis data. Conversely, we find that VIC-5-simulated permafrost extent is closer to observed permafrost extent than that of RASM. We conclude that the performance of a given hydrologic modeling parameter set differs markedly between coupled and uncoupled modeling runs, and that there are key tradeoffs that must be made in terms of optimizing parameter sets.

5.2 Future work recommendations

The work in this dissertation shows that a better understanding of terrestrial processes is necessary given the extensive changes that have already occurred at the mid- and high latitudes due to climate change. Studies of the cryosphere rely heavily on models because of the sparsity

of observations in colder regions, and particularly at higher latitudes, but these models need to be constrained by observations. For further development of Arctic science, available observation-based datasets need to be improved upon so that these datasets can be used in validating and improving the representation of physical processes in the Arctic. Differences between standalone and fully-coupled modeling in the Arctic also warrant further exploration. Given how important the land surface is to the coupled climate system, studies need to improve how land surface model parameters are designed for coupled climate modeling.

Appendix A

Effects of climate change on snowpack and fire potential in the western USA – Supplemental Material

This appendix includes the supplemental materials from chapter 2. This material has been published in its current form in *Climatic Change*. © Springer. Used with permission.

D.R. Gergel, B. Nijssen, J. T. Abatzoglou, D.P. Lettenmaier, M.R. Stumbaugh (2017) Effects of climate change on snowpack and fire potential in the western USA. *Climatic Change* 141: 287-299, doi: 10.1007/s10584-017-1899-y.

A1 Methods

A1.1 Comparison of Simulated to Observed SWE

The VIC model has been widely used to represent hydrological conditions and to study future hydrological change (e.g. Nijssen et al 2001). Mote et al (2005) examined long-term trends in April 1 SWE and found that the fraction of negative trends was nearly identical for observations and VIC output (75% for snow course observations, 73% for VIC). Mao et al (2015) compared elevation profiles of VIC-simulated SWE and observations over California and found good agreement.

To evaluate the performance of the VIC snow model under historic conditions, we performed a limited set of point simulations for comparison with SNOTEL observations. VIC simulations at 1/16º spatial resolution using the Livneh et al (2013) forcing data were run for the period 1987-2005 to provide overlap with the SNOTEL observations. The simulations were run for grid cells that contained SNOTEL sites as well as for the eight surrounding grid cells. Sub-grid cell elevation heterogeneity was accounted for through the use of up to five elevation bands within each grid cell. Using our simulations, we binned simulated SWE and observed SWE by

300 m elevation increments corresponding to the elevation of the SNOTEL site, ranging from 500 m to 3500 m, and the average over each was computed.

Past comparisons of VIC-modeled SWE have been over limited parts of our domain, and the Mote et al. (2005) comparisons are now somewhat out of date (through 1997). Our hydrologic simulations, using historical gridded data (described in Section, 2.3) addressed this by comparing VIC-simulated SWE to observations of SWE from SNOTEL stations, shown in Figure A3.1, temporally averaged over 1987-2005. Although the range of values differs between observed and simulated SWE, with simulated SWE often exhibiting a larger range particularly around 2600 m, the mean, 10^{th} and 90^{th} percentile values are in relatively good agreement. This is particularly the case for middle elevations (2000 m to 3000 m). The White Mountains are the only range that shows little agreement between observed and simulated SWE, particularly in the 10^{th} and 90^{th} percentile values. This is likely due in part to the small number of available observations for this region (the area of the White Mountains is substantially smaller than that of the other ranges, corresponding to a much smaller number of SNOTEL stations, e.g. less than ten versus hundreds). Additionally, some of the lack of agreement in the White Mountains may be due to the large interannual variability in simulated SWE relative to observed.

Comparisons to SNOTEL SWE can be problematic, with SNOTEL SWE being unrepresentative of SWE distribution in the surrounding area due to the majority of SNOTEL stations being located at mid to lower elevations (Nolin 2012). However, Meromy et al (2013) studied the representativeness of SNOTEL-observed SWE to modeled SWE at three resolutions – 1, 4 and 16 km^2 – in California, Idaho, Oregon, Wyoming and Colorado and found that snow depth during the accumulation period was generally less biased, with the ablation period exhibiting greater subgrid variability. At a larger scale over the Colorado Rockies, Chen et al

(2015) compared observed SWE from SNOTEL networks to modeled SWE (using the VIC model) and found relatively good agreement. We are primarily concerned with capturing the interannual variability of April 1 SWE thus catchment-scale issues with the representativeness of SNOTEL SWE are less concerning for our application.

A1.2 Calculation of Dead Fuel Moisture (DFM)

Daily minimum and maximum temperature, relative humidity and precipitation were used to derive Equilibrium Moisture Content (EMC) and calculate 100-hr and 1000-hr DFM as detailed in Section 2.4. We derived minimum and maximum daily relative humidity (RH) from specific humidity (calculated internally by VIC) by assuming that specific humidity is approximately equal to the mixing ratio (w). We then computed minimum and maximum daily RH as $RH = 100 \times w/w_s$, where $w_s = 0.622 \times e_s/p$, e_s is the saturation vapor pressure calculated with the minimum and maximum daily temperatures and p is the atmospheric pressure. We accounted for precipitation duration using an empirical transform that translates daily precipitation amount to precipitation duration (Holden and Jolly 2011) and constrained precipitation duration not to exceed 8 hours.

A2 Results

A2.1 Projected Changes in Snowpack

Most of the differential effects of climate change on SWE can be explained in terms of elevation and thus temperature. Figure A3.5 characterizes changes in the ensemble mean of simulated April 1 SWE between the historical period and the future period for RCP8.5. For this analysis, we applied locally weighted scatterplot smoothing (LOWESS), a method of

nonparametric regression (Cleveland 1981). The curves show the distribution of April 1 SWE for the historical period (1970-1999) and the future climatological periods (2020s, 2050s and 2080s) for RCP8.5. Underlying the SWE curves, we show the distribution of grid cell elevations. In the Sierra Nevada, the largest decrease in SWE occurs at 1500-2000 m, while in the Cascades and Northern Rockies, it occurs around 1500 m. Maximum SWE in the Cascades occurs around 1400 m during the historical period, but it nearly disappears at that elevation by the end of the twenty-first century. Since much of the Cascades is below 1400 m, projected changes in climate will have large impacts on volumetric SWE storage. We also classified grid cells in the five mountain ranges as rain dominant (RD), transient (TR1 or TR2) or snow dominant (SD) (e.g. Elsner et al 2010) by modifying the classification regime of Hamlet and Lettenmaier (2007) to include two transient classifications, corresponding to average winter temperature of between -6°C and 0°C and 0°C and +5°C, respectively (Figure A3.6). By the end of the 21st century for RCP 8.5 projections, the majority of TR1 grid cells in the Cascades and the western part of the Northern and Southern Rockies have transitioned to TR2. The grid cells on the windward slopes of the Cascades and Sierra Nevada that were TR1 in the historical period have almost entirely transitioned to RD. Thus, windward-facing areas and mid- to low-elevation areas such as the White Mountains will be most affected by warming temperatures in western US mountain ranges.

A3 Figures

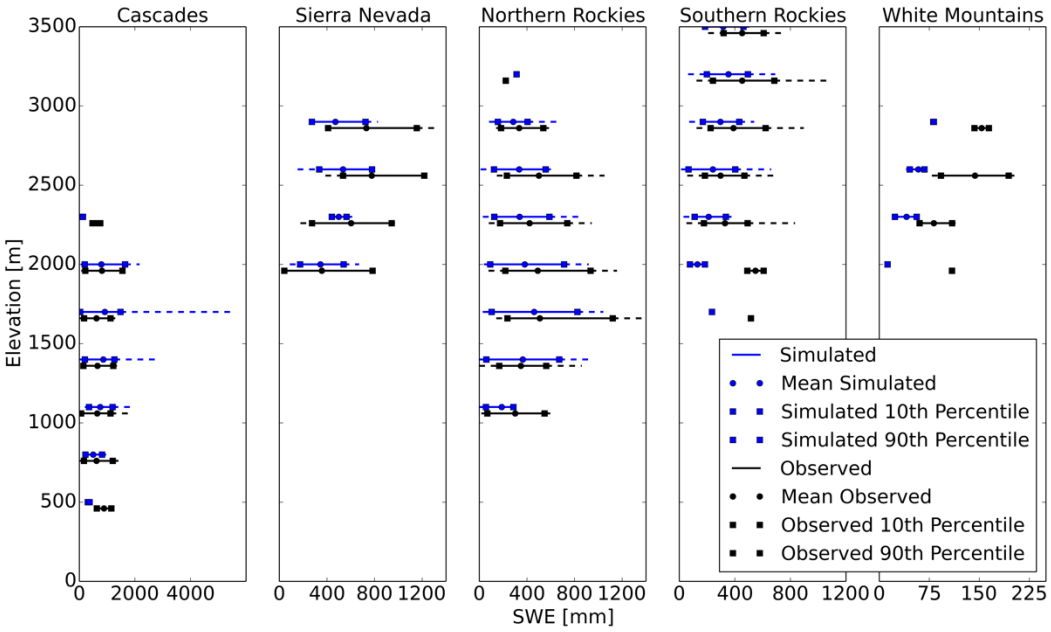

Figure A3.1. Comparison of simulated and observed April 1 SWE (averaged over 1987 – 2005). Observations for April 1 SWE were taken from SNOTEL stations in the five mountain ranges and were compared with VIC-simulated SWE averaged over nine grid cells surrounding the SNOTEL station.

Global Climate Model	Model Source
BCC-CSM1-1-M	Beijing Climate Center- Meteorological Administration, China
CanESM2	Canadian Centre for Climate Modeling and Analysis
CCSM4	National Center of Atmospheric Research, US
CNRM-CM5	National Centre of Meteorological Research, France
CSIRO-Mk3-6-0	Commonwealth Scientific and Industrial Research Organization/Queensland Climate Change Center of Excellence, Australia
HadGEM2-CC	Met office Hadley Center, United Kingdom
HadGEM2-ES	Met Office Hadley Center, United Kingdom
IPSL-CM5A	Institut Pierre Simon Laplace, France
MIROC5	Atmosphere and Ocean Research Institute, University of Tokyo; Japan Agency for Marine-Earth Science and Technology
NorESM1-M	Norwegian Climate Center, Norway

Table A3.1. Selected Global Climate Models (GCMs) from CMIP5 used in this study.

Mountain Range	Historical (1970-1999) °C	RCP 4.5 2010-2039 Increase (°C)	RCP 4.5 2040-2069 Increase (°C)	RCP 4.5 2070-2099 Increase (°C)	RCP 8.5 2010-2039 Increase (°C)	RCP 8.5 2040-2069 Increase (°C)	RCP 8.5 2070-2099 Increase (°C)
Sierra Nevada	-1.06	+1.05	+2.14	+2.79	+1.33	+2.72	+4.55
Cascades	-1.76	+1.06	+2.13	+2.81	+1.32	+2.68	+4.48
Northern Rockies	-6.15	+1.23	+2.50	+3.24	+1.52	+3.16	+5.31
Southern Rockies	-6.20	+1.34	+2.60	+3.30	+1.58	+3.34	+5.61
White Mountains	-0.78	+1.22	+2.29	+2.90	+1.41	+2.97	+4.96

Table A3.2. Average winter (November through March) historical temperature and projections for increases in temperature in western US mountain ranges averaged over the ten GCMs.

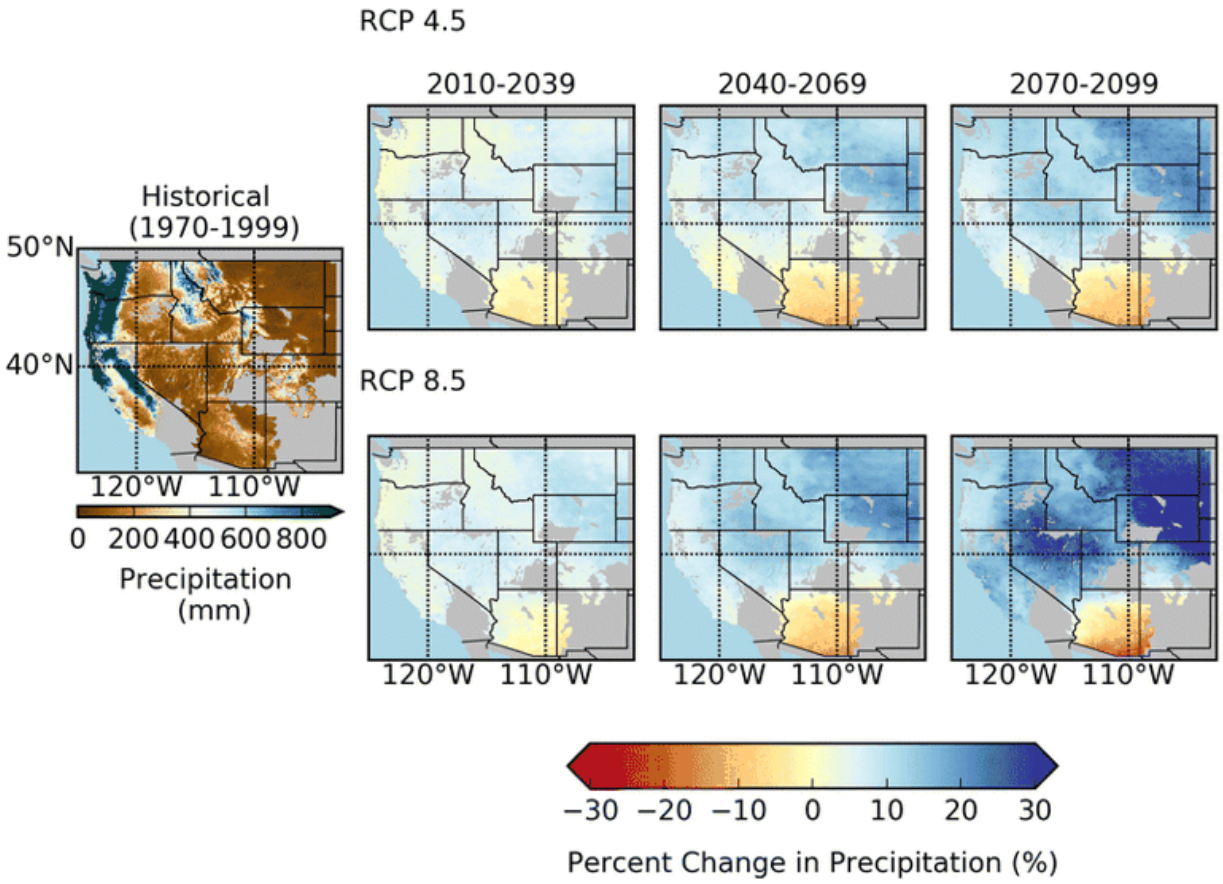

Figure A3.2. Total winter (Nov-March) precipitation projections for mountain ranges and lowland regions from CMIP5.

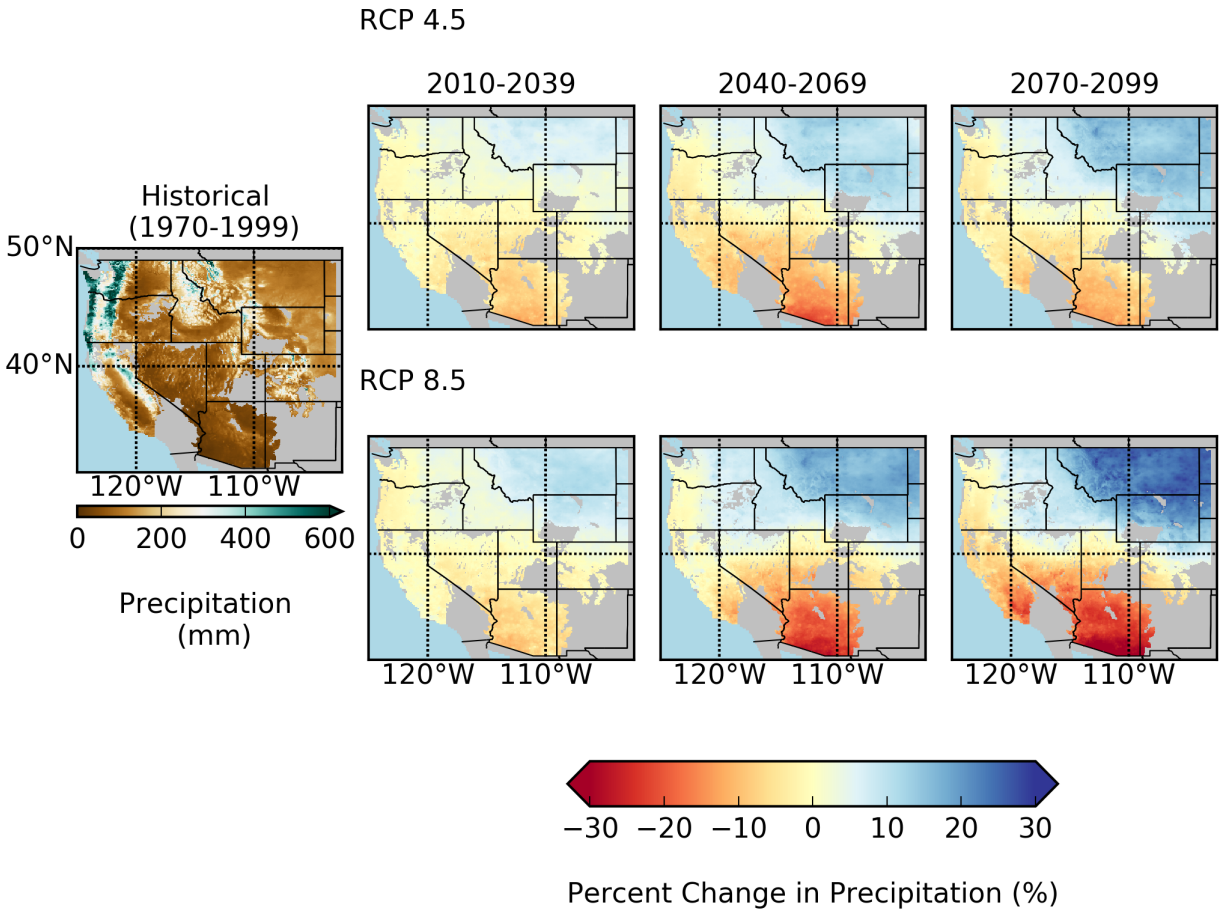

Figure A3.3. Total spring (March-May) precipitation projections for mountain ranges and lowland regions from CMIP5 for RCP 4.5 and 8.5.

Mountain Range	Historical		Average [km³]			Minimum [km³]			Maximum [km³]		
			2020s	2050s	2080s	2020s	2050s	2080s	2020s	2050s	2080s
Sierra Nevada	17.33	RCP 4.5	3.6	7.1	8	1	5.2	5.4	6.1	9.5	10.5
		RCP 8.5	4.1	7.9	11.3	2.1	5.5	9.9	5.7	10.5	13.4
Cascades	58.41	RCP 4.5	11.6	19.6	25.9	7.4	7.6	19	17.4	26.5	35.7
		RCP 8.5	12.6	24.1	37.5	4.9	12.6	25.3	19.1	36.1	47.3
Northern Rockies	103.89	RCP 4.5	9.9	19.2	28.3	1.5	11.5	16.3	16	27.8	40.2
		RCP 8.5	10.8	26.2	50.2	3.3	13.9	33	17.3	38.8	65.7
Southern Rockies	32.18	RCP 4.5	2	5.8	7.4	0.2	2.5	2.4	6.7	10.7	12.3
		RCP 8.5	1.9	7.6	13.6	0.2	4.3	8.6	4.2	12.4	22.8
Whites	0.24	RCP 4.5	0.1	0.2	0.2	0	0.1	0.2	0.2	0.3	0.3
		RCP 8.5	0.1	0.2	0.2	0	0.2	0.2	0.2	0.3	0.3

Table A3.3. Projected losses in April 1 SWE storage (in km3) for five mountain ranges, averaged across the ten GCMs. The maximum and minimum losses denote the largest and smallest SWE storage losses projected by the ten selected GCMs.

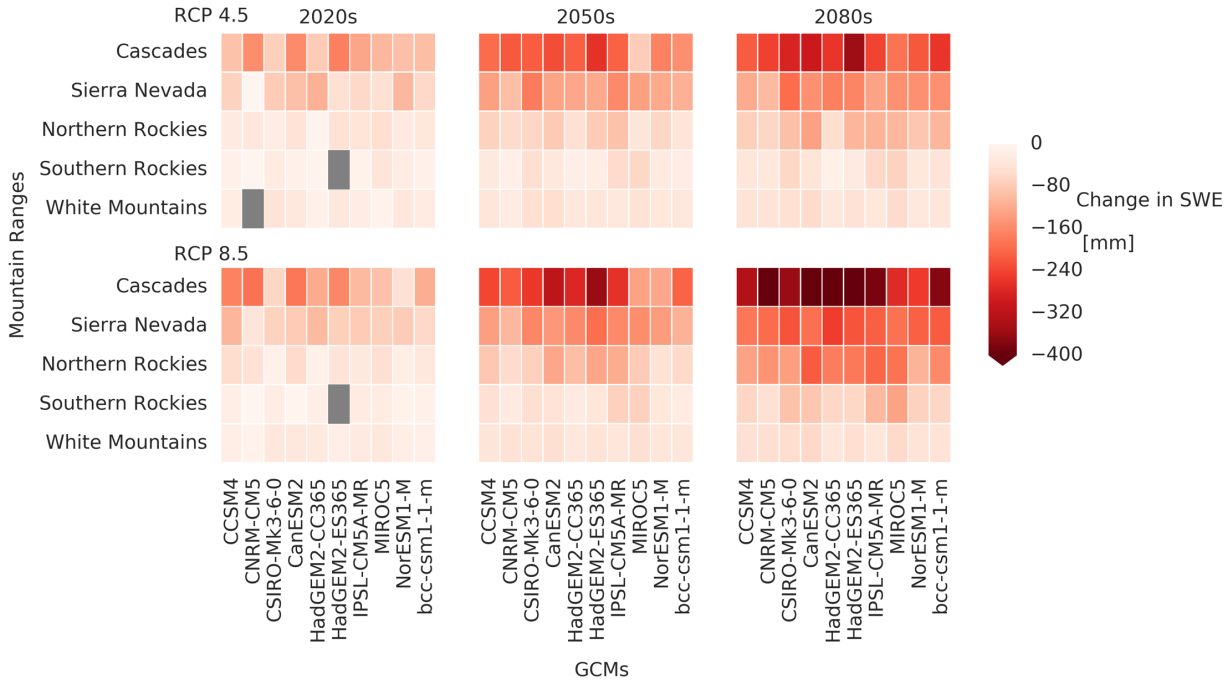

Figure A3.4. Change in mean simulated April 1 SWE between historical and future periods for all GCMs. Changes in grey are not statistically significant.

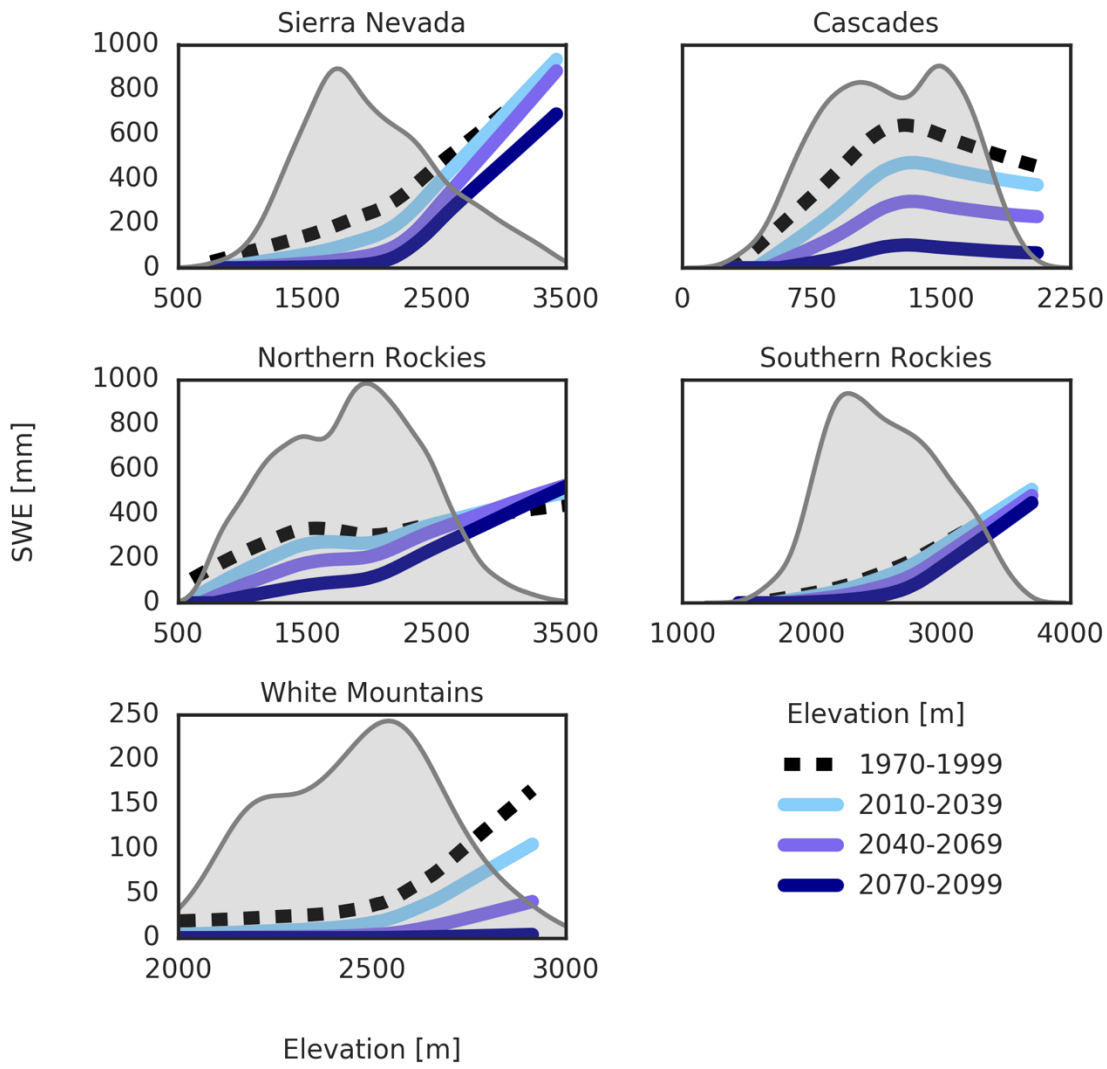

Figure A3.5. Change in ensemble mean simulated April 1 SWE between the historical (1970-1999) period and RCP 8.5. Curves show the distribution of April 1 SWE overlaid on the distribution of grid cell elevations.

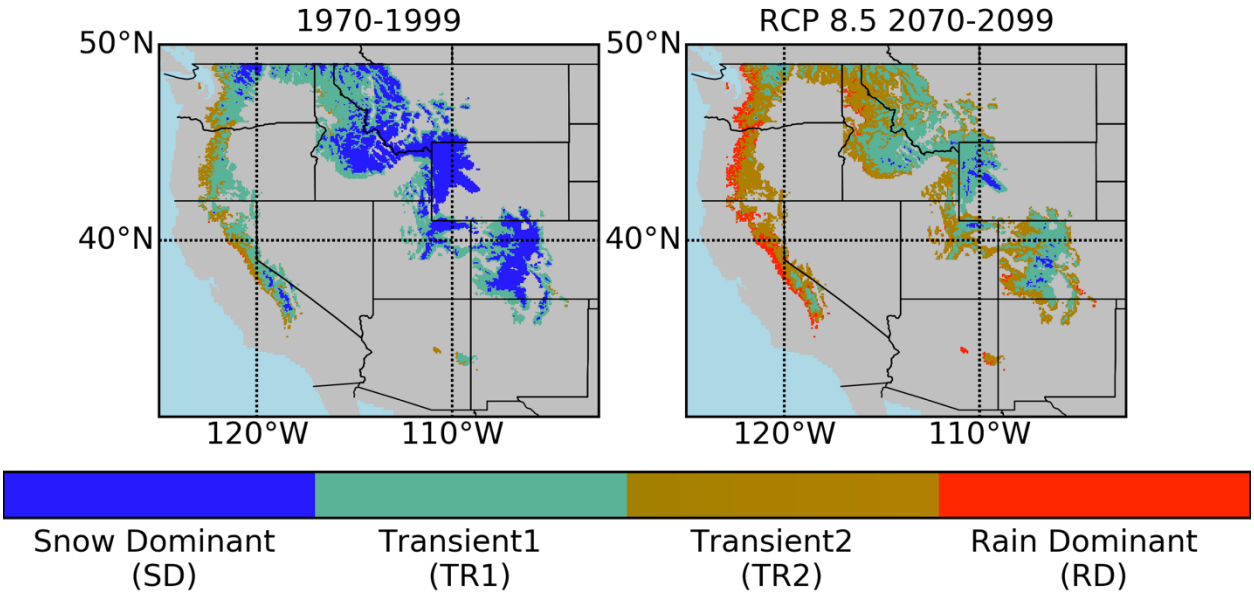

Figure A3.6. Shifts in hydrologic model grid cell classifications based on winter temperature. Classifications are based on Hamlet and Lettenmaier (2007) but modified to include two transient classifications.

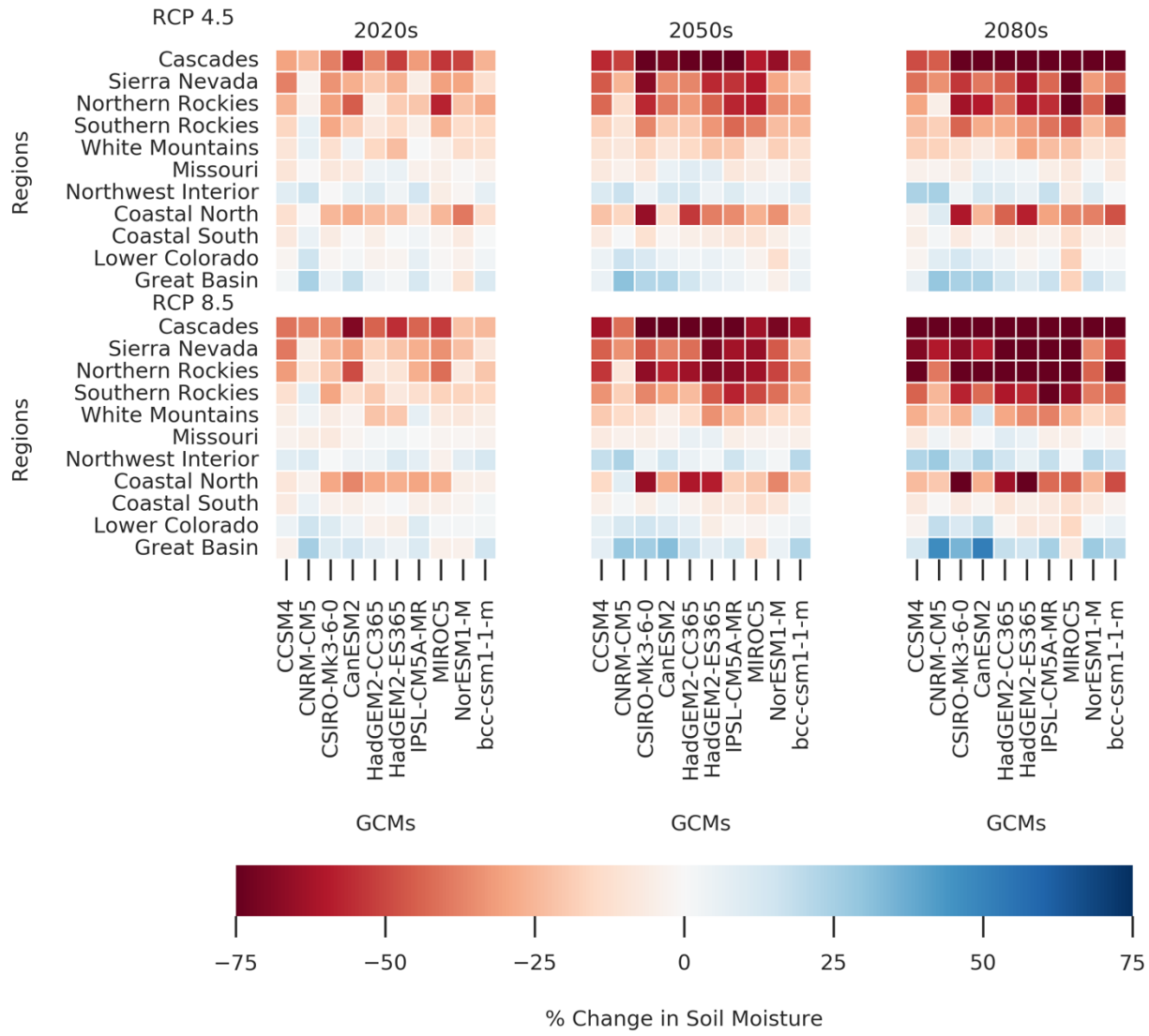

Figure A3.7. Heatmap comparing projected % change in soil moisture between GCMs. Of particular interest are areas where the soil moisture signal differs between models.

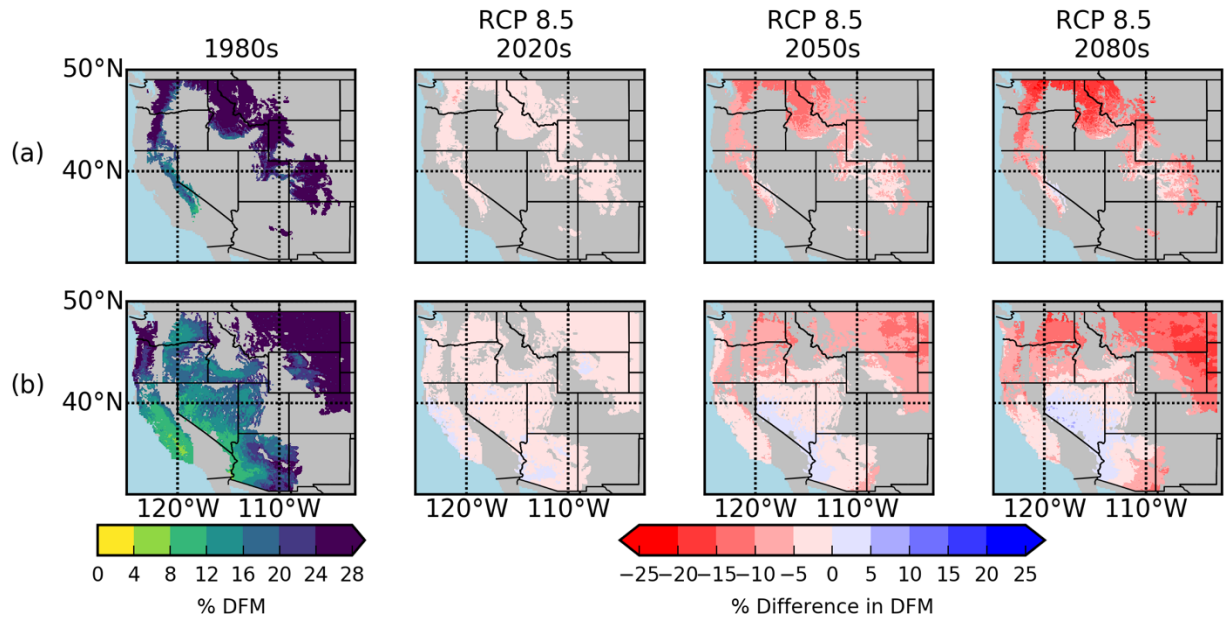

Figure A3.8. Ensemble-mean summer (JJAS) 1000-hr dead fuel moisture (DFM) shown over a) the five mountain ranges, and b) the six lowland regions, for the control period (1970-1999) and RCP 8.5. 2010-2039, 2040-2069, and 2070-2099. For the control period, % DFM is shown, and for the future periods, the % difference in DFM. DFM was calculated using the NFDRS algorithm for fuel moisture.

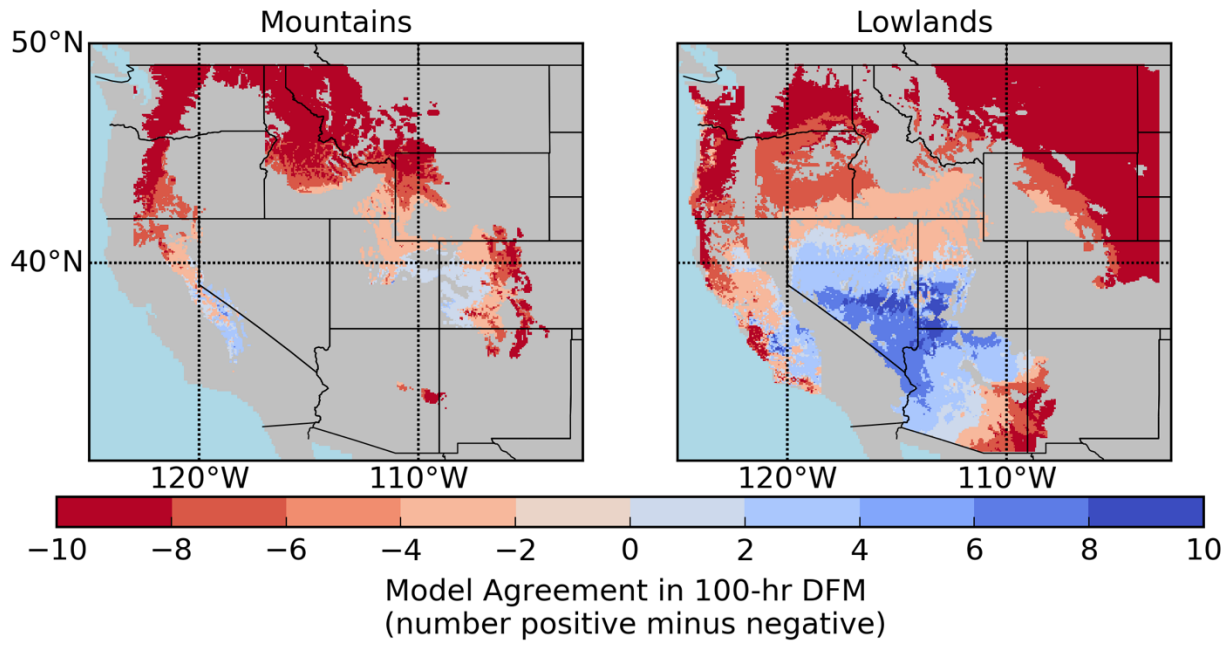

Figure A3.9. Number of models projecting positive changes in 100-hour DFM minus number of models projecting negative changes for the mountain ranges and lowland regions. Consistent agreement between models can be seen in areas in dark blue (positive changes) and dark red (negative changes), whereas lighter colors indicate areas where models do not agree on the sign of change in 100-hr DFM.

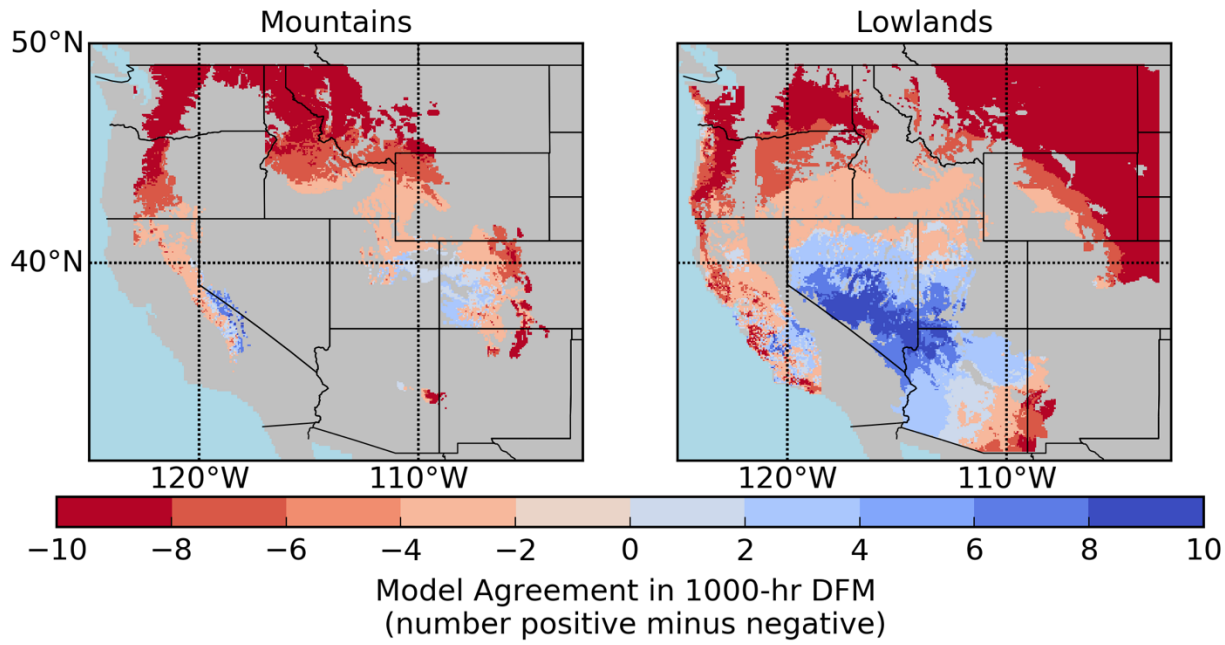

Figure A3.10. Number of models projecting positive changes in 1000-hour DFM minus number of models projecting negative changes for the mountain ranges and lowland regions. Consistent agreement between models can be seen in areas in dark blue (positive changes) and dark red (negative changes), whereas lighter colors indicate areas where models do not agree on the sign on change in 1000-hr DFM.

Region	Area (x 1,000 km^2)
Mountain Ranges	
Sierra Nevada	53.7
Cascades	101
Northern Rockies	304
Southern Rockies	175
White Mountains	4.82
Lowland Regions	
Coastal North	83.7
Coastal South	154
Northwest Interior	289
Lower Colorado	308
Great Basin	287
Missouri	562

Table A3.4. Areas of mountain ranges and lowland regions in study domain.

A4 References

Chen, F., Barlage, M., Tewari, M., Rasmussen, R., Jin, J., Lettenmaier, D., Livneh, B., Lin, C., Miguez-Macho, G., Niu, G-Y., Wen, L., Yang, Z-L. (2015). Modeling Seasonal Snowpack Evolution in the Complex Terrain and Forested Colorado Headwaters Region: A Model Intercomparison Study. *J Geophys. Atmos. 119*: 13795-13819. https://doi.org/10.1002/2014JD022167

Cleveland, W.S. (1981). LOWESS: A program for smoothing scatterplots by robust locally weighted regression. *The American Statistician 35 (1)*: 54. https://doi.org/10.2307/2683591

Elsner, M.M., Cuo, L., Voisin, N., Deems, J.S., Hamlet, A.F., Vano, J.A., Mickelson, K.E.B., Lee, S-Y., Lettenmaier, D.P. (2010). Implications of 21st century climate change for the hydrology of Washington State. *Clim. Change 102***:** 225-260. https://doi.org/10.1007/s10584-010-9855-0

Hamlet, A.F., Mote, P.W., Clark, M.P., Lettenmaier, D.P. (2007). Twentieth-century trends in runoff, evapotranspiration, and soil moisture in the western United States. *J. Climate 20*: 1468-1486. https://doi.org/10.1175/JCLI4051.1

Holden, Z.A. and Jolly, W.M. (2011). Modeling topographic influences on fuel moisture and fire danger in complex terrain to improve wildland fire management decision support. *Forest Ecology and Management 262*, 2133-2141. https://doi.org/10.1016/j.foreco.2011.08.002.

Mao, Y., Nijssen, B., Lettenmaier, D.P. (2015). Is climate change implicated in the 2013-2014 California drought? A hydrologic perspective. *Geophys. Res. Let. 42(8)*: 2805-2813. https://doi.org/10.1002/2015GL063456

Meromy, L., Molotch, N.P., Link, T.E., Fassnacht, S.R., Rice, R. (2013). Subgrid variability of snow water equivalent at operational snow stations in the western USA. *Hydrol. Process. 27*: 2382-2400. https://doi.org/10.1002/hyp.9355

Natural Resources Conservation Service (1997). SNOTEL Data Collection System. Available at: http://www.wcc.nrcs.usda.gov/snow/snotel-wedata.html

Nijssen, B., O'Donnell, G.M., Lettenmaier, D.P., Lohmann, D., Wood, E.F. (2001). Predicting the Discharge of Global Rivers. *J Climate 14*: 3307-3323. https://doi.org/10.1175/1520-0442(2001)014<3307:PTDOGR>2.0.CO;2

Nolin, A.W. (2012). Perspectives on Climate Change, Mountain Hydrology and Water Resources in the Oregon Cascades, USA. *Mountain Res. and Dev. 32(S1)*: S35-S46. https://doi.org/10.1659/MRD-JOURNAL-D-11-00038.S1

VITA

Diana R. Gergel

Education

Ph.D. 2019: Civil and Environmental Engineering, University of Washington, Seattle, Washington, USA. Dissertation title: *Modeling the changing roles of snow and permafrost in mid- and high-latitude climate systems*.

Graduate Certificate in Climate Science 2019: Program on Climate Change, University of Washington, Seattle, Washington, USA. Capstone title: *Mapping climate science information needs and networks in the Pacific Northwest.*

Post-Baccalaureate Studies 2013: Materials Science and Engineering, Boston University College of Engineering, Boston, Massachusetts, USA.

M.A. 2012: History, University of California at Berkeley, Berkeley, California, USA.

B.A. 2009: History and Political Science, University of North Carolina, Chapel Hill, North Carolina, USA. Honors thesis title: *That South Africa Belongs to All Who Live in It: Reifying a Fractured Nation through the South African Truth and Reconciliation Commission.*

Publications

Hamman, J.J., B. Nijssen, T.J. Bohn, **D.R. Gergel,** Y Mao. The Variable Infiltration Capacity (VIC) Model, Version 5 (VIC-5): Infrastructure improvements for new applications and reproducibility. *Geoscientific Model Development* 11: 3481-3496, doi: 10.5194/gmd-11-3481-2018.

Gergel, D.R., B. Nijssen, J.T. Abatzoglou, D.P. Lettenmaier, M.R. Stumbaugh, 2017: Effects of climate change on snowpack and fire potential in the western United States. *Climatic Change 141* (2), 287-299. doi: 10.1007/s10584-017-1899-y

Milshtein, J.D., **D.R. Gergel**, S.N. Basu, U.B. Pal, S. Gopalan, 2015: Mixed ionic electronic conducting powder bed for grid level energy storage and release: A study of tungsten oxide reduction kinetics, *International Journal of Hydrogen Energy* **40:** 9, 3624-3632.

Manuscripts in Preparation

Gergel D.R. and B. Nijssen. Interactions between permafrost and snow cover for limited warming versus RCP 8.5 and their implications for carbon release from permafrost. Manuscript in preparation, to be submitted to *Journal of Geophysical Research Atmospheres*.

Gergel D.R. and B. Nijssen. New land surface parameters for the Variable Infiltration Capacity Model Version 5 for Regional Earth System Modeling in the circumpolar Arctic. Manuscript in preparation, to be submitted to the *Geoscientific Model Development*.

Selected Presentations (°Oral, +Poster)

Gergel D.R., B. Nijssen, 2018: Understanding the impacts of 1.5°C and 2°C warming on the partitioning of runoff and evaporation and active layer depth in the circumpolar Arctic. *American Geophysical Union Fall Meeting*, Washington, DC. °

Mizukami N., A.J. Newman, J. Hamman, A.W. Wood, E.D. Gutmann, **D.R. Gergel**, M.P. Clark, B. Nijssen, J. Arnold, 2018: High-resolution statistically downscaled climate and hydrology projections over Alaska. *American Geophysical Union Fall Meeting*, Washington, D.C. +

Horowitz H.M., **D.R. Gergel,** E.C. Campbell, L. McCullough, L.G. Beckerman, A. Ismael, D. Cuomo, R. Scherrer, 2018: Polar Planetarium Show: a new program connecting local scientists, science center educators, and the public to the poles. *American Geophysical Union Fall Meeting,* Washington, D.C. °

Gergel D.R., J.J. Hamman, B. Nijssen, 2018: Representing the Land Surface in the Regional Arctic System Model (RASM). *Polar CORDEX Conference,* Warsaw, Poland.°

Maslowski W., R. Osinski, Y. Lee, A. Roberts, J.J. Cassano, M.W. Seefeldt, B. Nijssen, **D.R. Gergel**, 2018: On the importance of coupling for modeling and prediction of the Arctic system. *American Geophysical Union Ocean Sciences Meeting*, Portland, OR.°

Gergel, D.R., J.J. Hamman, B. Nijssen, 2017: Improving soil temperature profiles in the Regional Arctic System Model. *American Geophysical Union Fall Meeting,* New Orleans, LA. +

Gergel, D.R., L.S. Hayward, J.D. Mankowski, E.P. Salathe, 2017: Mapping climate science needs and networks in the Pacific Northwest. *American Geophysical Union Fall Meeting,* New Orleans, LA.+

Cao Q., **D.R. Gergel**, A. Mehran, B. Nijssen, W. Petersen, D.P. Lettenmaier, 2017: Evaluation of satellite precipitation products in the Chehalis River Basin during winter 2015-2016 using OLYMPEX data. *American Meteorological Society Annual Conference*, Seattle, WA.°

Gergel, **D.R.,** J.J. Hamman, B. Nijssen, 2016: Modeling the evolution of seasonally frozen soils and permafrost in the Arctic. *American Geophysical Union Fall Meeting,* San Francisco, CA.°

Gergel, D.R., J.J. Hamman, B. Nijssen, 2016. Evaluating the land-surface model treatment of frozen soils in the Arctic. *Graduate Climate Conference*, Pack Forest, WA.°

Gergel, D.R., J.T. Abatzoglou, D.P. Lettenmaier, B. Nijssen, 2016: How does low snowpack affect soil moisture and fire risk? *84th Annual Western Snow Conference*, Seattle, WA.°

Helgason H., M. Baptiste, O. Chegwidden, **D.R. Gergel**, 2016: The 2015 Snow Season in the Pacific Northwest: Will This Be the New Normal? *84th Annual Western Snow Conference*, Seattle, WA.+

Gergel, D.R., Q. Cao, J.J. Hamman, E.A. Clark, D.P. Lettenmaier, B. Nijssen, 2016: Evaluation of satellite precipitation products for hydrologic predictions in topographically complex regions: the Chehalis River Basin as a case study. *Pacific Northwest Weather Workshop*, Seattle, WA.o

Gergel, D.R., M. Stumbaugh, D.P. Lettenmaier, B. Nijssen, 2015: Effects of Climate Change on Snowpack and Fire Risk in the western United States, *Graduate Climate Conference,* Woods Hole, Massachusetts.o

Gergel, D.R., M. Stumbaugh, D.P. Lettenmaier, B. Nijssen, 2015: Effects of Climate Change on Snowpack and Fire Risk in the western United States, *Northwest Climate Conference*, Coeur d'Alene, Idaho.o

Gergel, D.R., M.R. Stumbaugh, S-Y. Lee, B. Nijssen, D.P. Lettenmaier, 2014: Effects of Climate Change on Flood Frequency in the Pacific Northwest, *American Geophysical Union Fall Meeting*, San Francisco, California.o

Dietze, M., H.E. Emery, **D. Gergel,** D. Gianotti, J.A. Mantooth, A.J. Rigden , 2014: Integrating satellite and tower phenology: a case-study in real-time ecological forecasting, *American Geophysical Union Fall Meeting*, San Francisco, California.o

Dietze, M., H.E. Emery, **D. Gergel**, D. Gianotti, J.A. Mantooth, A.J. Rigden, 2014: Predicting phenology: A case-study in real-time ecological forecasting, *Ecological Society of America Annual Meeting*, Sacramento, California.o

Milshtein, J.D., **D.R. Gergel**, S.N. Basu, S. Gopalan, U.B. Pal, 2014: The Role of Mixed Conduction in W-WO3 Redox Kinetics, *Proc. of the 225th ECS Meeting*, Orlando, Florida.o